‘

Characterizing Fractures in Geysers Geothermal Field by Micro-seismic Data, Using Soft Computing, Fractals, and Shear Wave Anisotropy

Topic Area 23: Fracture Characterization Technology

DE-FOA-0000075-23

Final Report

April 30, 2015

Submitted by:

Fred Aminzadeh (PI)

University of Southern California

Center for Geothermal Studies

Table of Contents

1- Summary 4
1.1: Introduction 5
1-2: Data Analysis / Fractal Analysis 5
1-3: Application of Seismic Velocity Tomography in Fracture Characterization 6
1-4: Integrated Evaluation 6
1-5: Autopicker design and implementation 7
1-6: Technology Transfer and Additional Accomplishments 7
1-7: Appendices 7
1-8: Acknowledgements 7
1-9: References 7
2- Fractal Analysis 8
2.1 Background 8
2.2: True Fractal Dimension Analysis 11
2.3: Physical Interpretation of the Results 17
2.4 Concluding Remarks 19
3- *b*-value Analysis 20
3.1: Background and Application of b-value Analysis 20
3.2: b-value Analysis 23
3.3: Result and Discussion 24
3.4: Fractal Dimension versus *b*-value 28
3.5: Conclusion 29
4- Application of Seismic Velocity Tomography in Fracture Characterization 31
4-1: Stress and Rock Property Profiling 31
4-2: Enhancing the Resolution of Seismic Velocity Models 32
4-3: Result and Discussion 34
5- Integrated Evaluation 40
5-1: Tomographic Inversion Versus Fuzzy Clustering 40
5-2: Shear Wave Splitting Versus Tomographic Inversion 41
5-3: 3D Velocity Modelling in NW Geysers 43
5-4 Addition comments 46
5-5 3D Anisotropy Tomography for Microseismic Event Location and Subsurface Physical Characterization 46
6- Phase arrival autopicker design and implementation 49

6-1- Introduction to autopicking 49
6-2: Data Preprocessing 50
6-3: Attribute analysis and ANN design for p phase autopicking 51
6-4: S phase autopicking 53
6-5: Autopicker Results: comparative analysis 56
6-6: Validating improvement using quick inversion for location (hypoinverse) 60
6-7: Future Work 61
7- Technology Transfer and Other Accomplishments 62
7-1: USC-Indonesia geothermal education capacity building project 62
7-2: Distinguished Lecture Program (DLP) 62
7-3: USC Center for Geothermal Studies (CGS) 63
8- External Publications 64
9- Appendices 86
10- Acknowledgements 86
11- References 87

List of Appendices

Appendix 1-1	The Original Proposal Summary
Appendix 1-2	Project Management Plan
Appendix 4-4	Anisotropy Tomography for Micro-earthquake Location and Subsurface Physical Characterization
Appendix 6-1	Abstract for The Integrated Reservoir Characterization for Unconventional Reservoirs Using Seismic, Microseismic and Well Log Data (Maity, 2013; Ph.D. dissertation)
Appendix 6-2	Abstract for Integrated Workflow For Characterizing and Modeling Fracture Network in Unconventional Reservoirs Using Microseismic Data (Tafti, 2013; Ph.D. dissertation)
Appendix 8-1	2011 Geothermal Technologies Peer Review Summary
Appendix 8-2	External Publications

1- Summary

This report summarizes of our accomplishments on the joint technology application collaborative project between the University of Southern California (USC), Geysers Power Company (Calpine), and Lawrence Berkeley National Laboratory (LBNL). The ultimate objective of the project was to develop new methodologies to characterize the northwestern part of The Geysers geothermal reservoir (Sonoma County, California). The goal is to gain a better knowledge of the reservoir porosity, permeability, fracture size, fracture spacing, reservoir discontinuities (leaky barriers) and impermeable boundaries. In this report we relate our accomplishments to the Project Deliverables outlined in the original proposal.

We have implemented advanced technical approach to process and analyze the passive seismic data. The first step was to develop an auto-picker algorithm using neural network and fuzzy logic. We now have a neural network based auto-picker (NNAP) for both P- and S-wave picking. This NNAP took selected seismic attributes that have been used by others in the past for first arrival picking, as its input parameters. NNAP was trained by a number of manual picks. After the training was deemed satisfactory, the first arrival picks for the entire MEQ data volume were generated. The initial results showed the enhancement of first arrival picking in both accuracy and efficiency.

In addition, we have analyzed the fractal pattern of the MEQ events and attempted to relate the fractal behavior of the MEQ events to the fractal dimension of the rocks which could be correlated with the fracturing system and its nature. We have introduced a new method to find the true fractal dimension of the spatial distribution of microseismicity. The results of fractal analysis indicate that induced seismicity is the main source of the fracturing system. In addition, we observed similarity in the patterns of seismicity in different regions. The MEQ pattern is the same as the nucleation and growth of fractures in random media, making MEQ locations a tool to map the fractures at The Geysers geothermal field in northern California.

To obtain characteristics of the fracture network in, we have completed our studies on seismic velocities and estimated elastic properties from them. We have carried out joint interpretation of seismic velocity, Poisson's ratio, extensional stress, and hydrostatic stress to better understand the characteristics of the fracture network. We also have developed (1) algorithms to better understand anisotropic velocity models and their impact the interpretation of the results and (2) a work flow and the accompanying methodology to build anisotropic velocity models from tomographic inversion Aside from several publications, some of which are included in the Appendices, two PhD dissertations have been produced under this program (Maity, 2013 and Tafti, 2013)

1.1: Introduction

The structure of this report will follow that of the original proposal. Appendix 1-1 shows the original proposal summary and its objectives that was approved for funding with its supplementary documents. We will focus on the accomplishments of the project by focusing on the original deliverables. Additionally, the report structure approximately follows the project management plan (PMP) also presented in Appendix 1-2. This Introduction section, briefly summarizes the accomplishments of the project. It will also highlight the key lessons learned and the challenges faced. We will then describe the accomplishments in more detail in:

Section 2- Fractal Analysis

Section 3- *b-value* Analysis

Section 4 - Application of Seismic Velocity Tomography in Fracture Characterization

Section 5- Integrated Evaluation

Section 6- Phase arrival autopicker design and implementation

We will then highlight other accomplishments of the project, including its technology transfer and public outreach accomplishments including the key publications in Sections 7 and 8, respectively, with a list of external publications provided in Appendix 8-1. A brief introduction to the appendices in this report are given in Section 9. Finally, acknowledgements and references are provided in Sections 10 and 11, respectively.

Different sections of this report will capsulate the accomplishments on these deliverables. We will also highlight some of the challenges we faced during the execution of this project. Notably, the original time table as shown in Appendix 1-1 had to be extended through several no cost extensions. After we cover the technical details, which will shed some lights on some of the reasons for delays in the completion of project tasks, we will provide additional details in the Section 4.

1-2: Data Analysis / Fractal Analysis

Our investigation began with a thorough review of the available data. The main data set used for this project was the raw and catalogued MEQ data volume provided by the Lawrence Berkeley National Laboratory (LBNL). The data analysis began with the determination of the fractal pattern of the MEQ events at The Geysers geothermal field in northern California (The Geysers, Section 2) and we:

1. Created distinct seismicity clusters from the original MEQ data volume.
2. Related the fractal behavior of the MEQ events to the fractal dimension of the rocks which could be correlated with the fracturing system and its nature.

3. Introduced a new method to find the true fractal dimension of the spatial distribution of microseismicity. The results of fractal analysis indicate that induced seismicity is the main source of the fracturing system.
4. Observed similarity in the patterns of seismicity in different regions. The MEQ pattern is the same as the nucleation and growth of fractures in random media, making MEQ locations a tool to map the fractures at The Geysers.

1-3: Application of Seismic Velocity Tomography in Fracture Characterization

Based on the catalogued MEQ data volume and the corresponding coarse 3-D P-Wave and S-Wave velocity volumes, we generated set of Krigged (smooth) 3-D velocity models (Section 3). In this work we:

1. Created of different reservoir properties and the characterization of the fracture system.
2. Established of a correspondence between the temporal changes in the velocities and the configuration and timing of the injection and production.
3. Identified the lateral extension of velocity anomalies below injection wells increases up to the middle of normal temperature reservoir (NTR). The same kind of anomalies also could be seen in the high temperature zone (HTZ). Increase in porosity created from fractures is the main cause for decrease in the compressional velocity of the zone of interest.
4. Observed a reduction in velocity and a growth of the region may be indicative of this decrease in different depth of reservoir. In the deeper regions velocity anomalies tend to diminish slightly which may be related to closing fractures with depth or a reduction of the number of cracks or void ratio with depth.
5. Used the effective normal stress as an index for fracture opening. In general, we observed that low Vp and Vs indicate highly fractured regions, while high Vp and Vs may indicate unfractured regions.

1-4: Integrated Evaluation

This section includes different elements of the work that were was performed both at USC and by our project partners at Calpine and Lawrence Berkeley National Laboratories. We demonstrated the best possible solution for describing the microseismicity in The Geysers and cross validated our results to better characterize the fracture network and achieve more reliable results. This included the work on fuzzy clustering and tomography work as well as the GOCAD velocity modeling and anisotropic inversion. We also discuss herein the challenges we faced in integrating our velocity models with those developed as well as the validation and testing of the anisotropy work due to the funding limitations.

1-5: Autopicker design and implementation

We have developed a novel neural networks based approach for first arrival picking of seismic events and demonstrated the superiority of the new method over the existing approached. To validate the usefulness of this new approach, particularly in those scenarios where the number of available recording stations is limited, we extracted data from a minimum number of stations required for running hypoinverse (4 p-wave and 2 shear wave picks) to find out how the results vary with the contemporary autopicker and the ANN autopicking workflow. A sample set was selected from the Geysers dataset and from each of the event files, a smaller subset of stations was selected to validate the possible improvements with the new approach. The files were run through a contemporary autopicker first followed by the ANN autopicker and respective phase files were generated for use with hypo-inverse algorithm. We show the hypocenters obtained for each of these individual events (a total of 8 event files were used). It is clear that with limited station coverage, the differences in the results observed are appreciable.

1-6: Technology Transfer and Additional Accomplishments

We provide a brief review of many other accomplishments of the project, not directly specified in the original proposal such as a new USAID supported geothermal capacity building, and distinguished lecture program (DLP). We also highlight some of the technology transfer accomplishments of the project as well as many public outreach activities such development Center for Geothermal Studies and the associated websites, (http://cgs.usc.edu/).

1-7: Appendices

We provide a brief overview of all the appendices to the report. It includes both the original research proposal, more technical details on the accomplishments and subsequent publications, description of some of the software developed and links to the PhD dissertations.

1-8: Acknowledgements

Many individuals contributed to the successful completion of this project. The acknowledgement section describes those individuals, both the faculty members, past graduate students and others at USC, Calpine and LBNL who contributed to the project.

1-9: References

Some of the key references are included here. For a more comprehensive list references on each main body of work see the full references in the respective appendices.

2- Fractal Analysis

We show that microseismic events (earthquakes with small magnitudes, generally defined as less than magnitude 3 [3M]) can be fruitfully used to gain insight into the properties of the fracture network of large-scale porous media, such as oil, gas, and geothermal reservoirs. As an example, we analyze extensive data derived from the GGF in northeast California. Injection of cold water into the reservoir to produce steam leads to microseismic events. We also demonstrate that analysis can provide insight into whether the fractures are of tectonic type, or are induced by injection of cold water. As such, using the catalogue of the microseismic events, we estimate the fractal dimension D_f of the spatial distribution of hypocenters of the events in three seismic clusters associated with the injection of cold water into the field. The fractal dimensions are all in a narrow range centered around, $D_f \approx 2.57 \pm 0.06$, comparable to the measured fractal dimension of fracture sets in the greywacke reservoir rock. Our results imply that the stress regime in the reservoir allows the activation of less favorably-oriented fractures that produce an increase in D_f. The estimate $D_f \approx 2$ for tectonic seismicity has been interpreted as indicating that most tectonic events occur either on the subset of near-vertical faults, because they have lower normal stress, or on the backbone of the fracture and fault network, the multiply-connected part of the net- work that enables finite shear strain. Our results lend support to the latter. The results that the entire fracture network, and not just its backbone, is active at The Geysers indicate that the seismicity is not a result of the triggered release of tectonic stress, but rather is induced by the release of local stress concentrations, driven by thermal contraction that is not constrained by friction. The possible implication for hydraulic fracturing, so-called fracking, is also briefly discussed.

2.1 Background

The Geysers geothermal field (GGF) is located about 150 km north of San Francisco, California (Figure 2.1). The field contains a large number of wells, some of which are used for injecting cold water into the porous formation. When water comes into contact with the hot matrix, it evaporates, generating steam that is produced from a network of fractures in the crystalline rock. Some of the fractures are of natural tectonic type associated with the nearby boundary of the San Andreas fault. On the other hand, when a fluid (such as cold water) is injected into the (hot) rock (free water falls), it induces nucleation and propagation of some fracture, and also activates the less favorably-oriented fractures. Due to very low permeability of the formation matrix of the GGF, the steam production depends on the presence of natural or induced fractures. Cost-effective production of the steam requires that the trajectories of the wells intersect the densely-fractured regions. Hence, locating such regions is vital to the economics of power generation from the GGF. Injection of a fluid, such as cold water, into a porous formation also induces microseismic events (Wyss, 1973)-earthquakes with small magnitudes and the purpose of this paper is to show that such events can help one to map out the fracture network of the GGF, or any other large-scale porous formation in which such events occur. Various approaches have been already used to characterize the fracture network of the GGF, including geologic mapping (Hebein, 1986; Sternfeld, 1989), outcrop analysis (Sammis et al., 1991), core analysis (Nielson et al., 1991), and shearwave splitting (Lou et al., 1997; Malin and Shalev, 1999; Erten et al., 2001; Elkibbi et al., 2004).

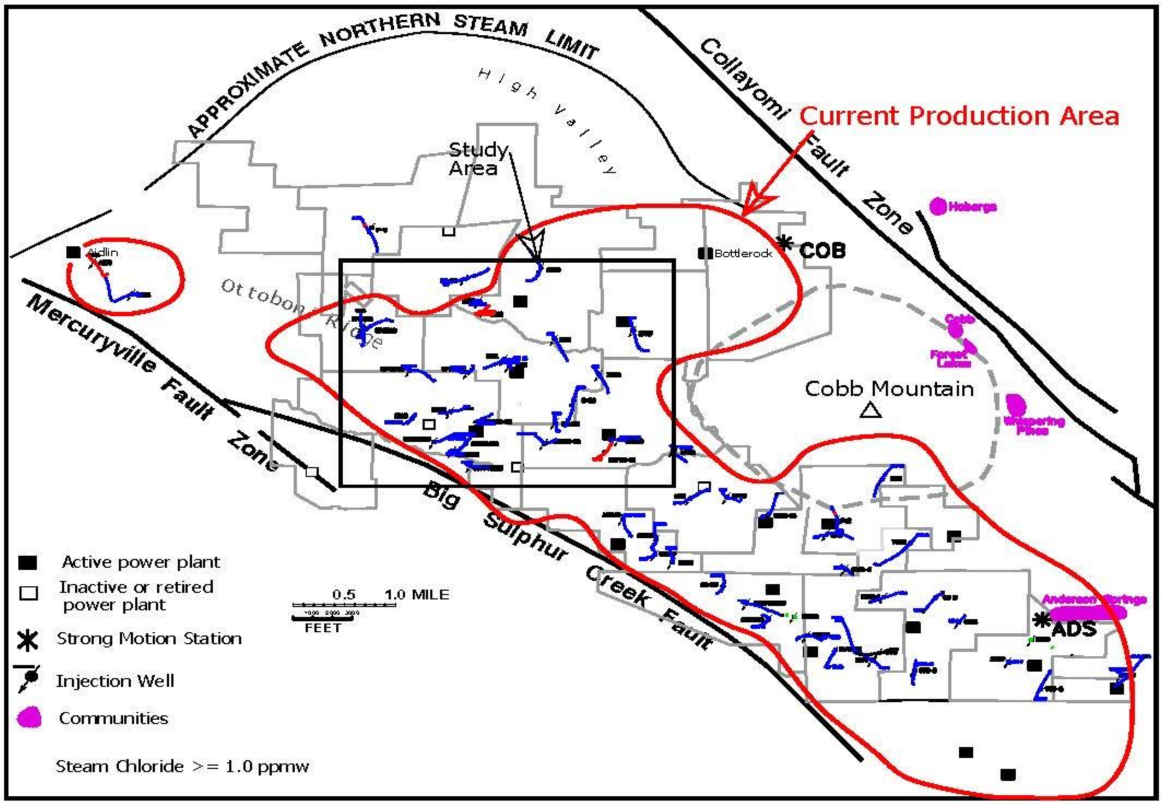

Figure 2.1: Map of The Geysers geothermal field, the area under study (black rectangle), and the location of the injection wells and seismic activities. Figure provided by Joseph Beall of Geysers Geothermal Company.

Fractal geometry is expected for the tectonic fractures and many tectonic fault net- works have been shown to have a fractal structure. Hirata et al. (1987) mapped the fault patterns, demonstrating that fractal structure could be anticipated from the fracture process generated by small or large earthquakes and that this type of rock fracturing from the macroscopic to the microscopic level is a scale-dependent process. Sammis et al. (1992) used fractal geometry to analyze the fracture pattern at The Geysers over a wide range of scales including regional maps, outcrops, and drill-cores. They concluded that the fracture network in the greywacke reservoir rock is fractal, with a dimension between 1.6 and 1.9 in 2-D planar section. Sahimi et al. (1993) reported fractal dimensions of 1.9 and 2.5 in 2D and 3D, respectively, for the fracture patterns in heterogeneous rocks. Studies by several groups have suggested that the fracture network of rock formations may be self-similar and scale-invariant (for a comprehensive recent review, see Sahimi (2011) and Bonnet et al. (2001), implying that, statistically, the fracture network appears the same over a range of length scales, and that long-range correlations, which are a fundamental feature of fractal structures, affect any phenomenon that may occur in the network. Such studies began in 1985, when the geologic and hydrologic framework at Yucca Mountain in Nevada was being studied. Barton (1985); Barton et al. (1987); Barton and Hsieh (1989) developed the so-called pavement method, whereby one clears a subplanar surface and maps the fracture surface, in order to measure its connectivity, trace length, density, and scaling, in addition to its orientation, surface roughness, and aperture. An important finding from the Yucca Mountain study was that the fractured pavements had a scale-invariant structure, characterized by a fractal dimension fractal dimension D_f, defined by

$$n(\pounds) \propto \pounds^{-D_f}, \tag{2.1}$$

where $n(\pounds)$ is the number of fractures of length £, and D_f is the fractal dimension of the network, which is less than the Euclidean dimension of space in which the network is embedded. The Yucca Mountain study indicated that it is possible to represent the distribution of fractures ranging from 20 cm to 20 m by a single parameter, D_f. For the fracture surfaces analyzed by Barton and co-workers, $D_f \approx 1.6 - 1.7$. La Pointe (1988) carried out a careful reanalysis of three fracture-trace maps of Barton (1985) estimating that the corresponding three-dimensional (3D) fracture networks are also fractal with $D_f \approx$ 2.37, 2.52, and 2.68. Velde et al. (1991) analyzed the structure of fracture patterns in granites, while Vignes-Adler et al. (1991) carried out the same type analysis for fracturing in two African regions, reporting strong evidence for the fractality of the fracture patterns, while 2D maps of fracture traces spanning nearly ten orders of magnitude, ranging from microfractures in Archean albites to large fractures in South Atlantic seafloors, were analyzed by Barton and LaPointe (1992), who reported that $D_f \approx 1.3 - 1.7$. Sammis et al. (1992) analyzed the fracture pattern in the GGF over a wide range of scales, including regional maps, outcrops, and drill-cores, concluding that the fracture network in the greywacke reservoir rock has a fractal structure with a fractal dimension, $1.6 \leq D_f \leq 1.9$, in 2D (planar) sections. Sahimi et al. (1993) suggested that the fractal dimensions of the fracture patterns in heterogeneous rocks should be around 1.9 and 2.53 in two and three dimensions, respectively (see below). See also Hatton et al. (1993) for further discussion of the issue of 2D and 3D sampling in laboratory tests. The results of such tests may depend on the heterogeneity and the anisotropy of the fracture set.

On the other hand, Hirata et al. (1987) mapped the fault patterns in a certain rock formation demonstrating that a fractal pattern should be expected from the fracturing process, generated by earthquakes of various sizes, and that the fractures generated are scale-invariant over multiple length scales, ranging from the macroscopic to the field scale. Computer simulations (Sahimi and Goddard, 1986; Sahimi and Arbabi, 1992, 1996) as well as the simulation of hydraulic fracturing in which water is injected into a heterogeneous solid to generate fracture (Herrmann et al., 1993), indicated that the resulting fracture networks are self-similar fractals.

Since earthquakes usually occur on existing faults, the spatial pattern of their hypocenters is often used to reveal the structure of their underlying fault network. Hirata (1989) estimated the fractal dimension of the spatial distribution of seismic events hypocenters in the Tohoku region, based on a correlation function (Equation 1.2). He reported fractal dimensions between 1.34 and 1.79 in 2D sections. Robertson et al. (1995) estimated the fractal dimension of the spatial distribution of the hypocenters of several aftershock sequences in south and central California, reporting D_f to be between 1.82 and 2.07 in three dimensions, with an average of about 1.95.

2.2: True Fractal Dimension Analysis

Microseismic events can be characterized by the fractal dimension D_f of hypocenters. The fractal dimensions are estimated based on a correlation function defined by (Hirata et al., 1987; Wiemer, 2001).

$$C(r) = \frac{2}{N_t(N_t - 1)} N_r(R < r) \tag{2.2}$$

where Nr(R < r) is the number of pairs of events that have a spacing R less than r, and Nt is the total number of events within the region of interest. As pointed out earlier, injecting of cold water into a geothermal reservoir or hydraulic fracturing job induces microseismic events; thus, if the spatial distribution of such microseismic events has a fractal structure, C(r) should follow a power law,

$$C(r) \propto r^{D_f} \tag{2.3}$$

The fractal dimension D_f [1] defined by Equation 1.3 is also called the correlation dimension, and denoted sometimes by D_c. Throughout this thesis, whenever we refer to the fractal dimension of our own data, we mean D_f, as defined by Equation 1.3.

We used catalogs provided by the Lawrence Berkeley National Laboratory and the online data set from Northern California Earthquake Data Center[2]. The area covered by our study was the northwest (NW) region of the GGF, indicated by rectangle in Figure 2.1. As mentioned earlier, injecting cold water into the GGF induces microseismic events-earthquakes of small magnitudes. Their hypocenters and the locations of injection wells are shown in Figure 2.2. Beall et al. (2010) reported a strong correlation between seismic activity and the rate of injection of cold water into the NW region of the GGF. Based on the area's seismic activity and the location of injection wells, we initially defined three clusters consisting of the spatial distributions of the

[1] D is equal to 0 for a point, 1 for a line, 2 for a plane, and 3 for a sphere. Non-integer values reveal a clustering of the events closest to the shape described by the nearest integer value.

[2] http://www.ncedc.org/SeismiQuery/events_f.html

hypocenters of the microseismic events; see Figure 2.3. Cluster number 2, shown in Figure 2.3, was then divided into four subclusters, each of which was also analyzed to delineate possible size effects. As Figures 2.2 and 2.3 indicate, some clusters and subclusters are denser than others. We deliberately selected such clusters in order to also understand the effect of the events density on the properties computed.

The spatial distribution of the hypocenters of the seismic events in the clusters that are shown Figure 2.3 was characterized by the fractal dimension D_f. The fractal dimensions were computed using the Zmap program (Wiemer, 2001) which determines D_f using Equations 1.2 and 1.3. As an example, Figure 2.4 presents a plot of log C(r) for the entire spatial distribution of the hypocenters in region 2 of Figure 2.3. The linear portion of the curve yields a fractal dimension, $D_f \approx 2{:}59$. The interpretation of such values of D_f will be given shortly.

We should point out that the fractal dimension estimated from the data presented in Figure 2.4 is for a bit less than two orders of magnitude variations in the distance r. In principle, the distance r over which the correlation function C(r) is varied and used to estimate D_f must vary by about four orders of magnitude (Grassberger and Procaccia, 1983). If the range of variations of r is not broad enough, then one must consider an alternative interpretation of the data (Sahimi, 2011; Bonnet et al., 2001). Unfortunately, however, the range of length scales that can be explored in seismicity distributions is severely limited by the accuracy with which the individual events can be located, which itself is limited by the heterogeneity of the crust. At the same time, however, our data are

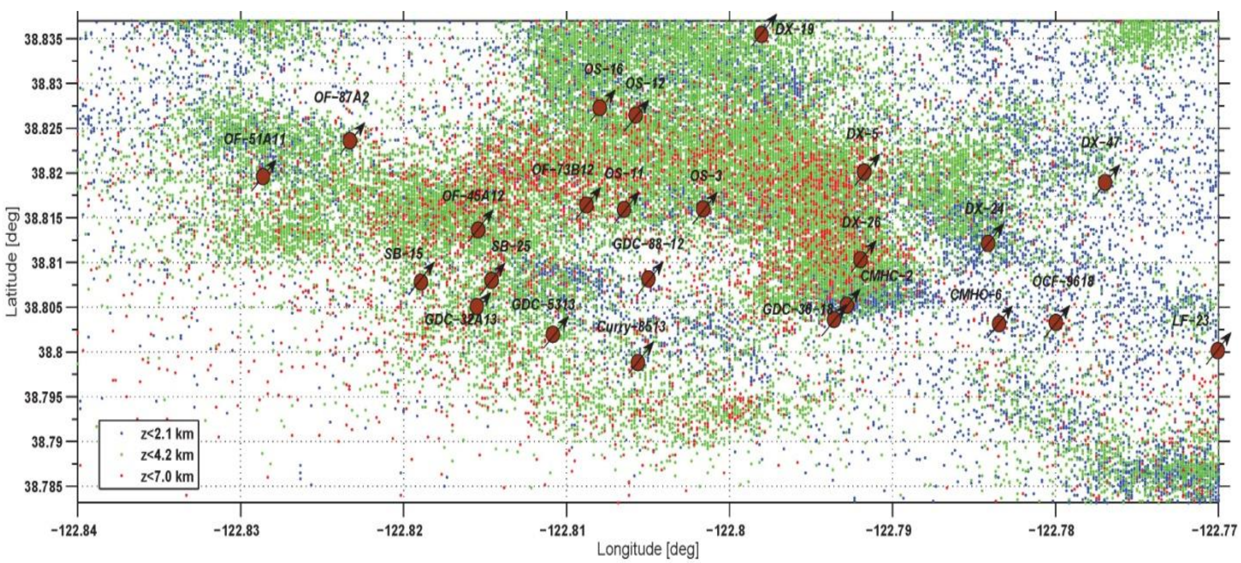

Figure 2.2 Clusters of the earthquakes hypocenters and the locations of active injection wells from 2006 to 2011. Each point represents one event.

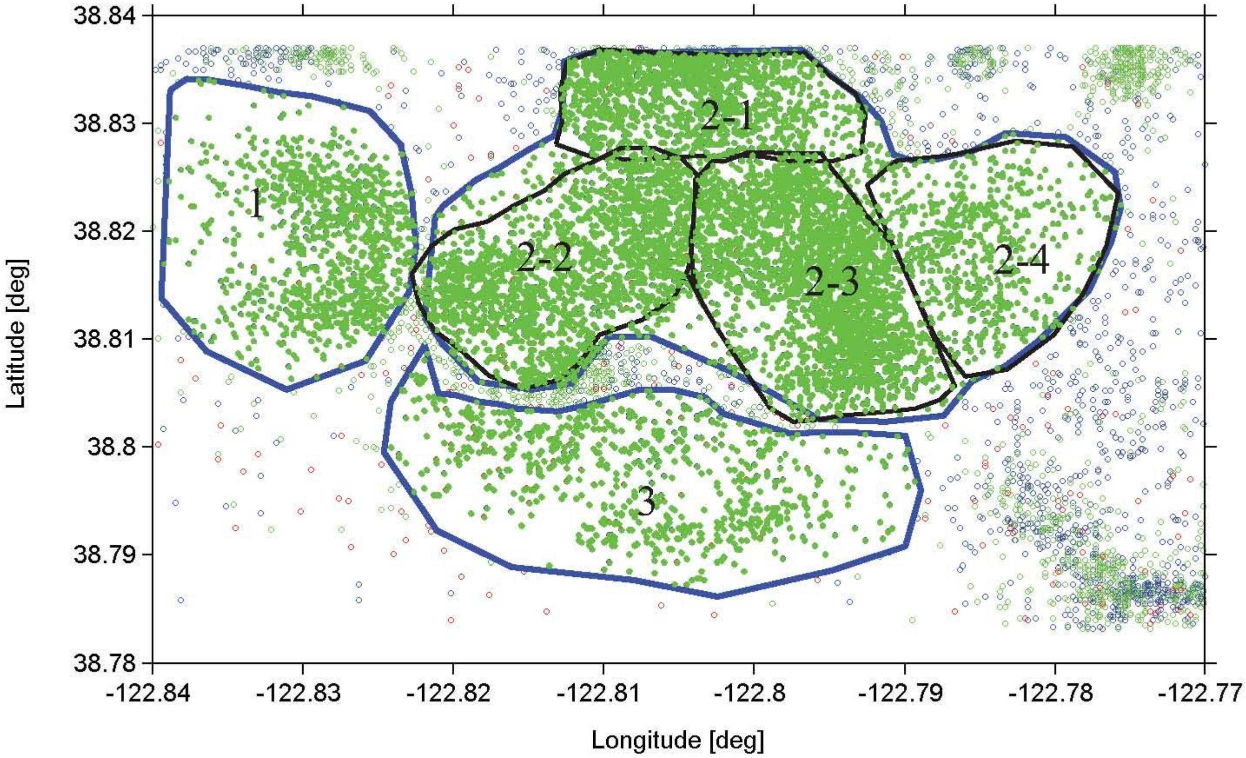

Figure 2.3 The four regions studied, as well as the four subregions. Each point represents the location of an event.

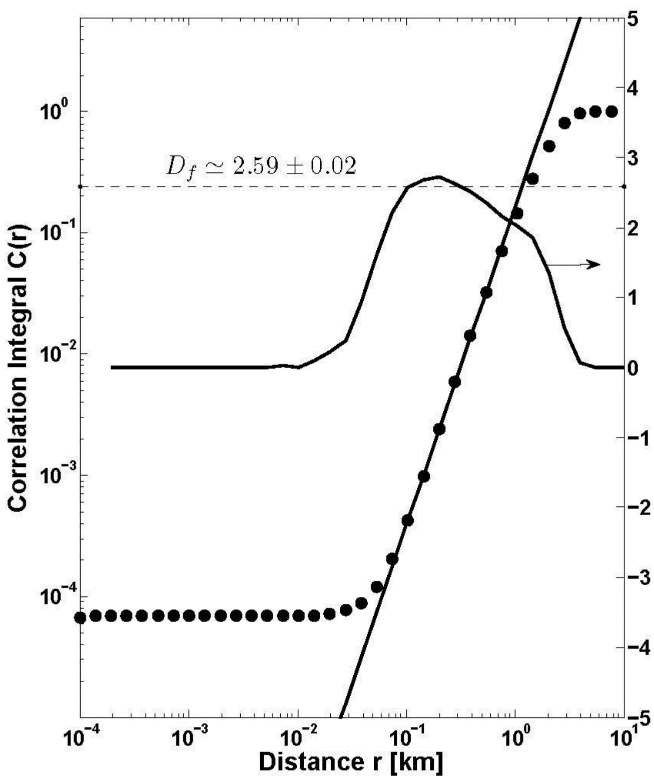

Figure 2.4: The logarithmic plot of the correlation function C(r) vs distance in region 2 of The Geysers geothermal field. Also shown are the variations of the local slopes around a constant value, indicating the accuracy of the data and the overall slope of the plot.

not indicative of other interpretations and spatial distributions of the events. Thus, although one must, in principle, be cautious about attributing fractal characteristics to the data set and consider other possibilities, our results are completely consistent with such characteristics. Moreover, when the variations of local slopes are well-behaved and indicate a plateau, we may obtain a reliable estimate of the fractal dimension D_f. In Figure 2.4, we also show the variations of the local slope; it is zero over the tail region of C(r) and rises where the power law region begins. The scaling region where the power law is observed begins at r _ 0:04 km. The local slope at that point is about 2.3. The maximum of the local slope is about 2.7, only 17% larger. At r ≈ 2 km where the power-law region ends and C(r) reaches a plateau, the local slope is about 2:1. The average of all the local slopes is 2.59. Hence, we conclude that the estimate of D_f from Figure 2.4 is reliable. Figure 2.5 shows the dependence of the fractal dimension Df on the density of the microseismic events in region 1 from 2006 to 2010.

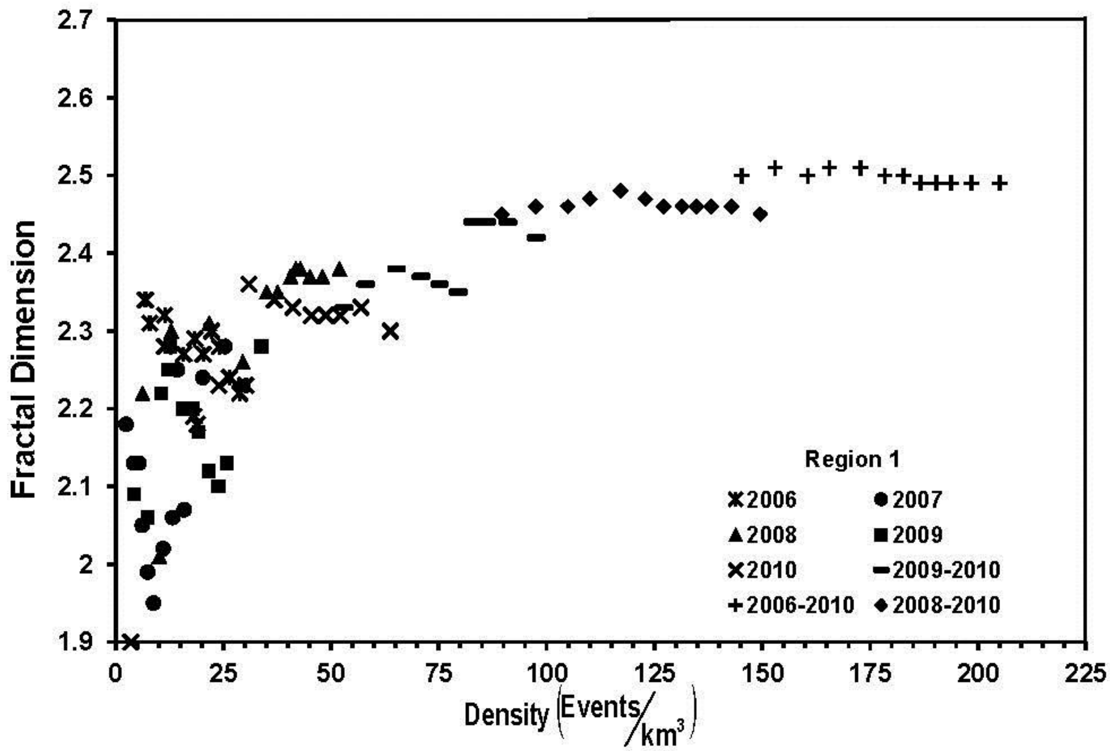

Figure 2.5: Dependence of the fractal dimension D_f on the density of the microseismic events in region 1 from 2006 to 2010.

Care must be applied in using seismicity to estimate the fractal dimension of a fracture network. Smith (1988) and Robertson et al. (1995) illustrated that a minimum number of data points exists for estimating the true fractal dimension of the underlying fracture network. Eneva (1996) also illustrated that the number of data points, the size of the region under study, and the measurements' errors can significantly affect the estimate of the fractal dimension, and that assigning a specific physical meaning to the fractal dimension associated with a limited data set might be problematic. Thus, to ensure that we sampled a large enough number of data points to compute the true fractal dimension of the underlying fracture-fault network, the effective values of D_f were plotted as a function of the density of the events in a given cluster. Figure 2.6 indicates the same trends for the fractal structure of the spatial distributions of the hypocenters in the four subregions carved out of region 2. For all of the subregions, the fractal dimensions associated with the spatial distribution of the hypocenters converge to values that vary in a very narrow range. As a further test, the northwest region of the GGF was analyzed separately, with the results shown in Figure 2.7, indicating again that the spatial distribution of the hypocenters in this region forms a fractal cluster. All of the estimated fractal dimensions are listed in Table 2.1.

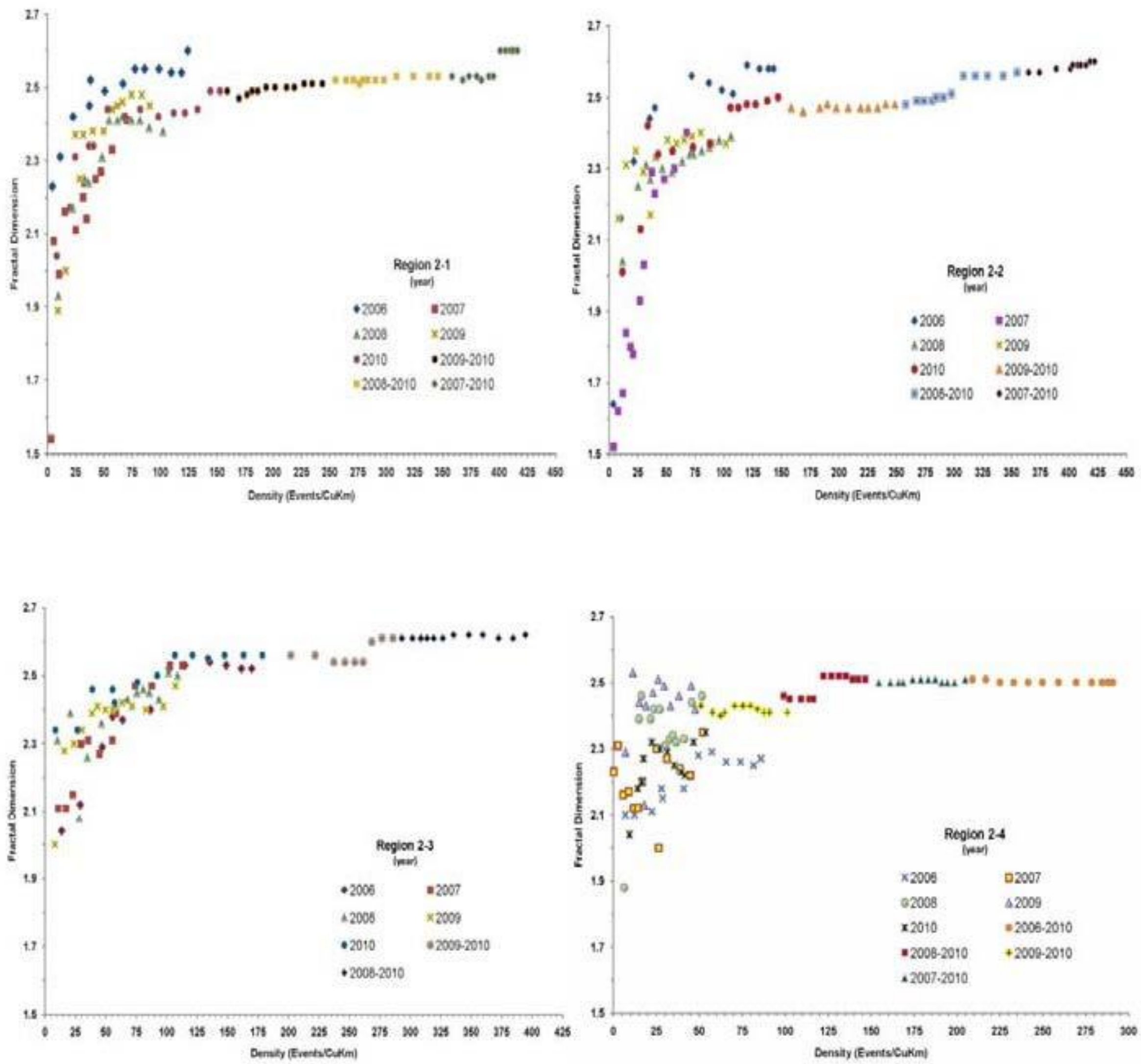

Figure 2.6: Fractal dimension versus density of events at the NW Geysers (Region 2) from 2006 to 2011 (top left) Region 2-1, (top right) Region 2-2 (bottom left) Region 2-3 (bottom right) Region 2-4.

When earthquakes are not induced, for example, by the injection of cold water into a rock formation, and are of tectonic type, the value of D_f is always close to 2 (Sahimi et al., 1993).

Such a value of D_f has been interpreted in two different ways (1) it indicates that most tectonic events occur on a subset of near-vertical faults, because they have lower normal stress and (2) the second interpretation (Sahimi et al., 1993) is that the events occurring on the fault networks, referred to as *backbone*, with multiple connected part, enables finite shear strain. The latter proposal is supported by the recent work of Pasten et al. (2011), who analyzed the spatial distributions of hypo-centers and epicenters of earthquakes in central Chile and reported estimates of D_f, which are consistent with this hypothesis. We shall come back to this point shortly.

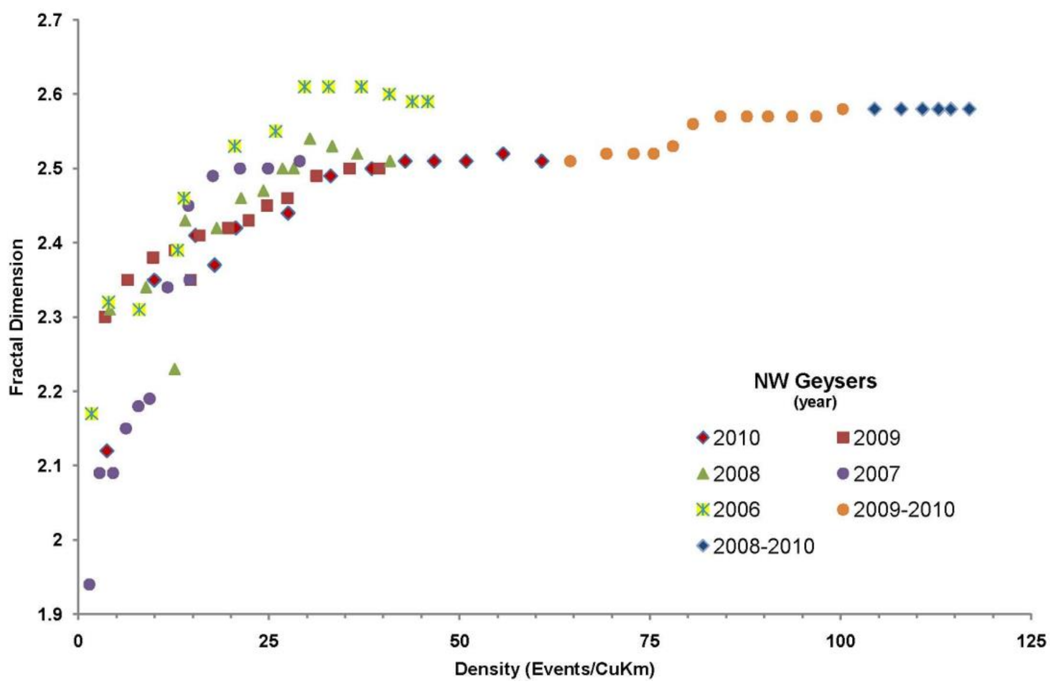

Figure 2.7: Same as in Figure 2.5, but for the northwest region, from 2006 to 2010.

Table 2.1: Estimates of the fractal dimensions for the individual regions.

Region	Measured Fractal Dimension D_C
NW Geysers	2.58 ± 0.03
Region 1	2.50 ± 0.03
Region 2	2.63 ± 0.06
Region 3	2.58 ± 0.03
Region 2-1	2.60 ± 0.04
Region 2-2	2.60 ± 0.04
Region 2-3	2.62 ± 0.06
Region 2-4	2.51 ± 0.03

In any case, estimates of D_f reported here are significantly larger than 2, thus confirming that seismic activity in the GGF is more likely to have been induced by the injection of cold water into the formation, rather than being of tectonic type. Therefore, the estimates of D_f provide significant insight into the structure of the fracture networks, as well as into their origin. It is, therefore, possible to directly use the spatial distribution of microseismic events to map out the fracture network of a large-scale porous medium, such as a geothermal reservoir. Also, the pattern of microseismic events is the same as the nucleation and growth of fractures in random media Sahimi et al. (1993). In addition, the fact that computed D_f is significantly smaller than 3– the spatial dimension of the region in which the hypocenters are embedded– implies that only a small part of the overall structure contributes to distributing the strains.

2.3: Physical Interpretation of the Results

If fractures nucleate and grow more or less at random in a highly heterogeneous medium, such as large-scale porous formations, then they should form a network of interconnected fractures that resembles what is called a percolation cluster (Stauffer and Aharony, 1994; Sahimi, 1994), i.e. a cluster of (more or less) randomly distributed inter- connected fractures that percolates between two widely-separated planes. To describe this phenomenon in more intuitive but physically understandable basis, we appeal to the critical path analysis (CPA) first developed by Ambegaokar et al. (1971) and confirmed by many sets of simulations. They argued that transport processes in a highly heterogeneous medium can be reduced to one in a percolation system at or very near the percolation threshold. The idea is that in a medium with broadly distributed heterogeneities, a finite portion of the system possesses a very small conductivity, hence making a negligible contribution to the overall conductivity or other effective flow or transport properties. Therefore, zones of low conductivity may be eliminated from the medium, which would then reduce it to a percolation system. Ambegaokar et al. (1971) described a procedure by which the equivalent percolation network, called the critical path, is built up. They showed that the resulting percolation system is at or very near its percolation threshold. When applied to heterogeneous fractured rock (Sahimi, 2011), CPA suggests that the fracture network must have the connectivity of a percolation cluster because, for example, the fractures are the main conduits for fluid flow in rock as their permeabilities or hydraulic conductances are much larger than those of the matrix in which they are embedded. Using the procedure of Ambegaokar et al. (1971), one finds that the fracture network of rock must be at, or very near, its percolation threshold.

The relationship among percolation theory, the spatial distribution of earthquakes hypo- and epicenters, and fault-fracture networks was first explored by Stark and Stark (1991); Trifu and Radulian (1989) in a qualitative manner, but was configured in a quantitative foundation by Sahimi et al. (1993). The utility of identifying the fracture network of large-scale porous media with the sample-spanning percolation cluster is that the latter has been studied extensively (Stauffer and Aharony, 1994; Sahimi, 1994). In particular, it is well known that the sample-spanning percolation cluster at or very near the percolation threshold is a self-similar fractal object with a fractal dimension, D_f ' 1:9 and 2:53, in two and three dimensions, respectively. Moreover, the multiply connected part of the cluster, which allows various phenomena such as fluid flow and stress transport to occur in the network, is the aforementioned backbone, which is also a fractal object with fractal dimensions of 1.64 and 1.9 in two and three dimensions, respectively. Indeed, as mentioned earlier, the recent work of Pasten et al. (2011), who analyzed the spatial distributions of hypo- and epicenters of earthquakes in central Chile, yielded D_f ' 2:02 _ 0:05 and 1:73 _ 0:02, respectively, which are within 5% of the fractal dimensions of 3D and 2D percolation backbones.

We must point out that a network of interconnected fractures and/or faults with irregular shapes and sizes resembles what is usually referred to as continuum percolation (Balberg, 2009), which differs from the better known and more studied lattice percolation, which deals with networks of bonds and sites. All numerical and analytical works have indicated (Balberg, 2009), however, that the fractal dimensions of the sample-spanning clusters and their backbones are the same for lattice and continuum percolation.

The estimates of the fractal dimensions listed in Table 2.1 deviate from that of the sample-spanning percolation cluster by, at most, 4%, well within the estimated errors, but not close to that of the percolation backbone. Thus, the seismicity induced by the injection of cold water happens on a fracture network that is similar to the 3D samples panning percolation cluster, whereas the tectonic events occur on the backbone of the fault network. The reason is that when cold water is injected into the GGF, the path the fluid takes within the porous formation and the fractures that it generates within the rock are, due to the heterogeneity of the formation, random. Even if the path is not random but contains extended correlations, the structure of the cluster at the largest length scale should still resemble that of a percolation cluster. The high-pressure cold water generates some fractures that are dead-ends, because the growth of such fractures stops only when the pressure of the water cannot overcome the resistance offered by the rock. As a result, the network generated by the injection contains both dead-end as well as multiply connected fractures, i.e., the sample-spanning percolation cluster.

On the other hand, for earthquakes of tectonic origin to occur, finite strains and deformations must occur on the fault or fracture network. But that is possible only on the multiply connected part of the cluster, as the singly connected faults or fractures are dead-ends and cannot contribute to strain release. Therefore, such earthquakes should occur on the backbone of the fault-fracture network, which has a much lower fractal dimension close to 2.

The significance of the link between the structure of a fracture network and those of percolation clusters and their backbones is that the latter have been studied extensively, and deep insights into their structural properties have been gained (Stauffer and Aharony, 1994; Sahimi, 1994). This knowledge can, therefore, be used for realistically modeling a fracture network of the GGF or that of any other rock formation, for that matter.

2.4 Concluding Remarks

In this chapter, we analyzed the structure of the spatial distribution of hypocenters of microseismic events in the GGF. The results indicate that the distribution forms a fractal cluster with a fractal dimension very close to that of a 3D sample-spanning percolation cluster. The results also indicate that the spatial locations of microearthquakes hypocenters provide deeper insight into the structure of the fracture network of large-scale porous media.

The dimension D = 2 for tectonic seismicity has been interpreted as an indication that most tectonic events occur on the subset of near-vertical faults (because they have lower normal stress), or occur on the percolation[3] 3 backbone of the fracture network which enables finite shear strain. The fractal dimension of about 2.6 is identical to the fractal dimension of nucleation and growth of fractures in random media. Hence, microseismic locations with a fractal dimension of 2.6 may reveal the connected fracture network and the reservoir heterogeneity.

In addition, the results indicate that by calculating the fractal dimension of a microseismic cloud we may identify whether stimulated microseismic data are triggered (tectonic) or induced. Hence, we may find an explanation for changes in observed fracture behavior or determine if those changes might be caused by the presence of nearby faults (tectonic) or by contact with the fracturing treatment (induced).

Finally, determining the fractal behavior of microseismic event clouds in different stages of stimulation and their dimensions, allows us to assume that the fracture network at the underlying unconventional reservoir is self-similar (scale independent), and thus that its structure, mechanical, and transport properties are best described by using fractal geometry.

[3] Percolation theory is a mathematical theory that examines the likelihood of connectivity, through a generated fracture network.

3- *b*-value Analysis

This chapter discusses the impact of considering *b*-value analysis in microseismic distribution. We will discuss how this critical insight can lead to characterize a fracture network created from fluid injection. As an example, we analyze extensive data for the GGF in northeast California. This type of analysis can also lead to insight into whether the fractures are of tectonic type, or induced by the injection of cold water. To demonstrate this phenomenon, we estimate the b values in the Gutenberg-Richter frequency- magnitude distribution using the catalogue of the microseismic events. For most cases, the *b*-values are about b ~ 1.3 ± 0.1. The *b* are significantly higher than those commonly observed for regional tectonic seismicity or aftershock sequences for which b ≈ 1 are typical. Our results indicates that the seismicity is not a result of the triggered release of tectonic stress, but is induced by the release of local stress concentrations, driven by thermal contraction that is not constrained by friction in the GGF.

3.1: Background and Application of b-value Analysis

Some authors reported b = 1 as a universal constant for earthquakes in general (Frohlich, 1993; Kagan, 1999). Consequently, Schorlemmer et al. (2005); Zoback, 2007) and Gulia et al. (2010) showed how the type of fault / fracture mechanism can affect b values. Typical b-values for normal, strike-slip, and thrust events and the average b-value with the associated standard error are shown in Figure 3.1.

They concluded that a normal fault has a greater b-value than a strike-slip one, and that a strike-slip has a greater b-value than a thrust one. Wessels et al. (2011) said that this behavior is inversely related to the stress regime, which means that where we have higher b-value, we expect a lower stress regime (Table 3.1). The b-value may be proportional to vertical stress minus horizontal stress, because normal faults tend to happen under lower horizontal stresses than thrust faults do (Grob and van der Baan, 2011).

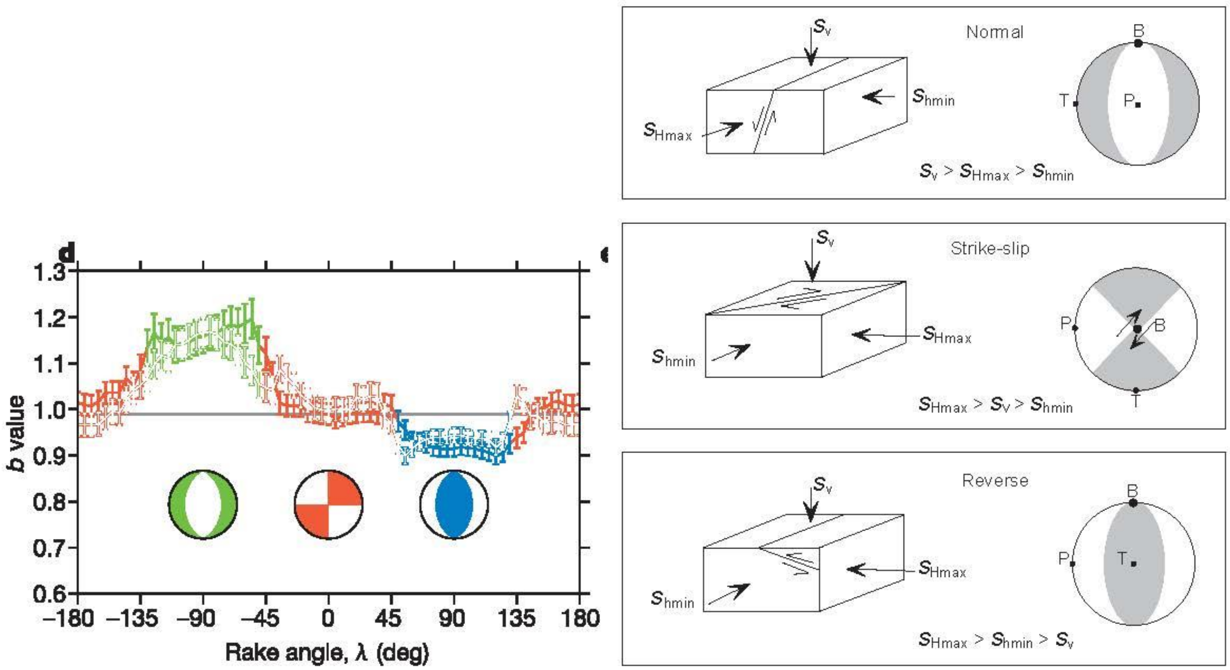

(a) (b)

Figure 3.1. b-values of normal (green), strike-slip (red) and thrust events (blue)[4]; average b-value (grey line); standard error (vertical bars) (Schorlemmer et al. 2005; Zoback, 2007).

Table 3.1: b-values versus stress regime and dominant faulting mechanism, based on work by Schorlemmer et al. (2005)

b-value	*Stress regime*	*Fault type*
$b < 1$	$S_H > S_h > S_v{}^1$	Reverse(compressive)
$b\ 1$	$S_H > S_v > S_h$	Strike-slip
$b > 1$	$S_v > S_H > S_h$	Normal(extensional)

In recent years, *b*-value analysis has found application in monitoring and characterizing the fracturing process. For instance, Downie et al. (2010); Maxwell et al. (2010); Wessels et al. (2011) distinguished the fault movement from fracture stimulation by comparing the b-values for various distributions of microseismic events. Figure 3.2 demonstrates *b*-value of ~ 2 for fracture related events and ~ 1 for associated fault events. Figure 3.3 shows the application of *b*-value map on the same dataset to differentiate fault (dark blue) from fracture areas (green). Downie et al. (2010) also used the same concept to evaluate the efficiency of different stimulation stages. Figure 3.4 demonstrates that microseismic events in stage 7 of stimulation are fault related which can affect the oil production by water invasion or other factors.

[4] SH: maximum horizontal stress, Sh: minimum horizontal stress, Sv: vertical stress

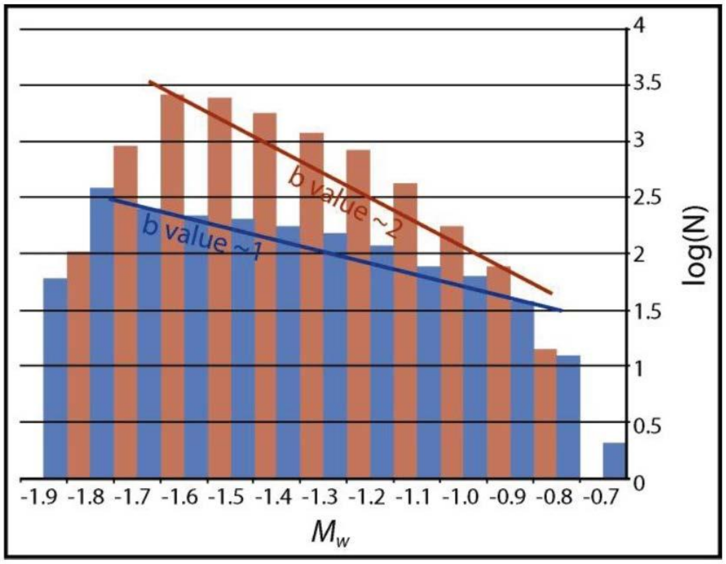

Figure 3.2 Microseismic histogram of fault (blue) and fracture related events (red) (Wessels et al., 2011).

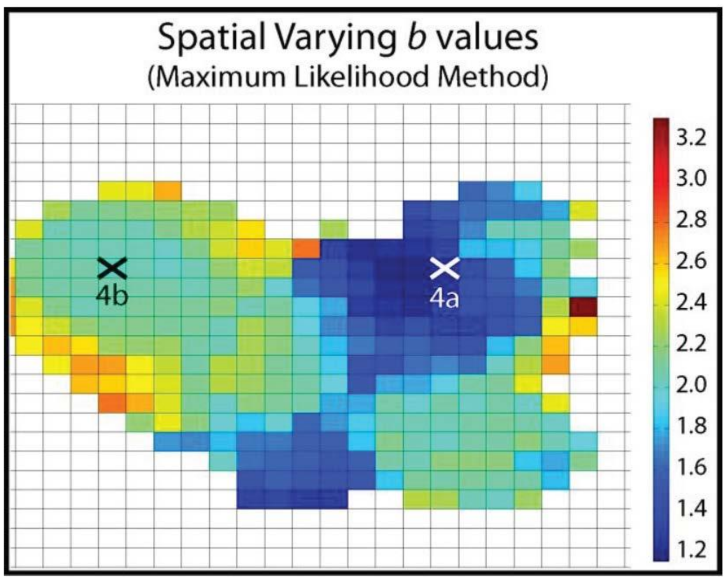

Figure 3.3. b-value map within the fracture treatment area. Lower values are associated with fault activity whereas higher b-values are indicative of more fracture event creation (Wessels et al., 2011).

Furthermore, Grob and van der Baan (2011) demonstrate how the temporal evolution of b-values in steam flooding a heavy-oil reservoir may indicate the opening or closing fractures. Figure 3.5 demonstrates three regimes in their observation with relation to Schorlemmer et al. (2005) work: b-values larger than 1.1 (extensional faulting [normal] or opening of fractures), b-values around 1.0 (a strike-slip regime) and a final regime with values around 0.65 (closing of fractures or compressive faulting [reverse]).

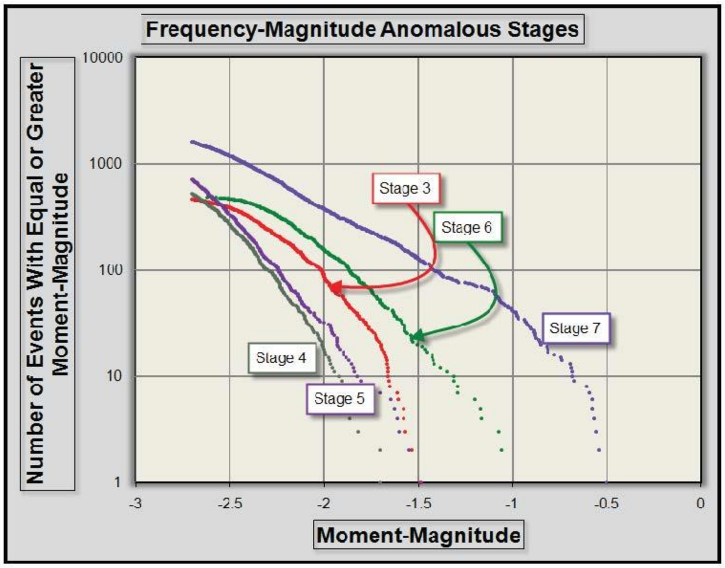

Figure 3.4: Comparison of b-value analysis for different stages of stimulation in horizontal Barnett Shale well (Downie et al., 2010)

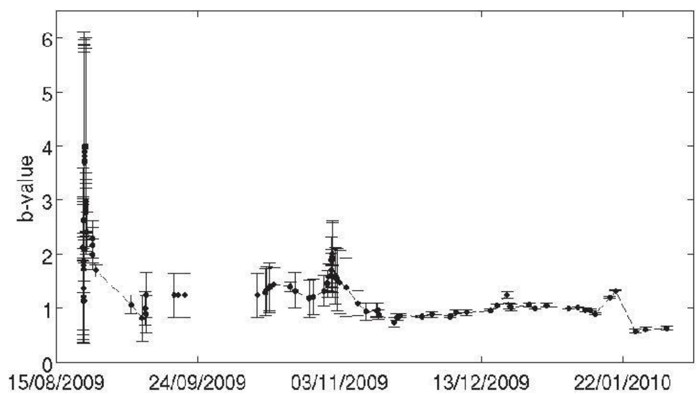

Figure 3.5: Temporal evolution of b-values for a heavy-oil dataset to characterize opening or closing phase of fractures.), (Grob and van der Baan, 2011).

3.2: b-value Analysis

Microseismic events can be characterized by the b-value of their frequency-magnitude distribution in the Gutenberg-Richter relationship (3.1)

$$logN(m > M) = a - bM \tag{3.1}$$

According to Eq. 2.1, *b* is the slope of the linear portion of the plot of log *N* versus *M*. The plot has negative curvature for small earthquakes, due to undersampling caused by the detection threshold. The break from negative curvature represents the so-called minimum magnitude of completeness, M_c. There is also deviation from linearity for large values of *M*, due to the limited observation times for properly sampling much-less frequent larger events. In most cases, *Mc* may be estimated by the maximum curvature method (Wyss, 2000). But, when we used it, the method did not yield physical estimates of b in some cases, in which case manual curve fitting or the least-squares method was utilized for estimating the *b*-values. If *Mc* is determined by the maximum curvature method, then the *b* is estimated using the maximum likelihood method, according to which (3.2)

$$b = \frac{0.433}{\langle M \rangle - M_c}\,, \qquad (3.2)$$

where (*M*) is the average magnitude of the earthquakes. A typical plot is shown in Figure 3.6 for the northwestern region of the GGF during 2006, illustrating the application of the maximum likelihood method for estimating b.

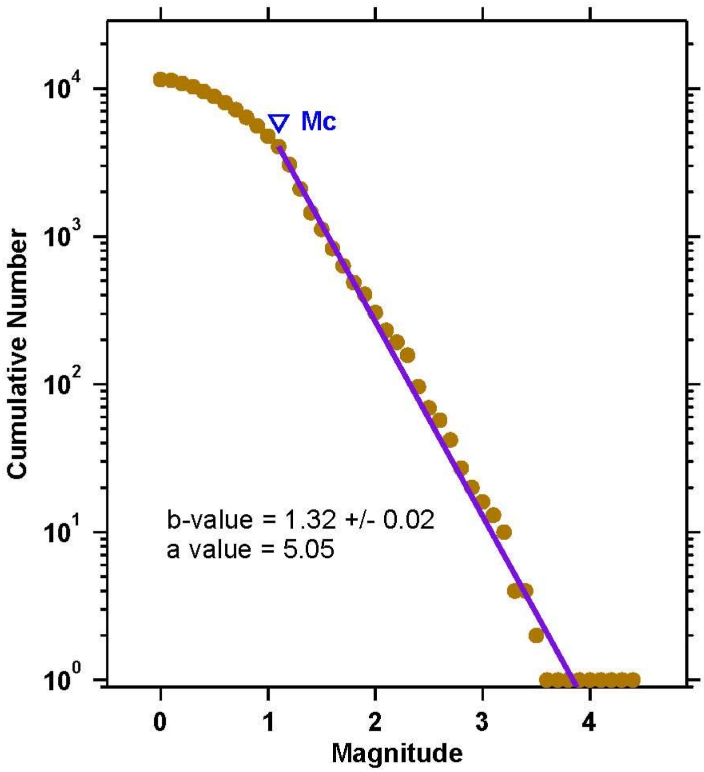

Figure 3.6: Magnitude distributions of The Geysers seismicity in 2006

3.3: Result and Discussion

We analyzed seismicity for the NW GGF using the NCEDC catalogues. We determined the *b-value* by measuring the slope frequency-magnitude distribution for magnitudes above a common *Mc* where most seismic activities greater than this magnitude have been recorded. This value is also near to the mode of magnitudes. The distribution of magnitudes for microseismic events are interesting and important. For example, Figure 3.7 presents the distribution for the northwestern region of the GGF from 2006 to 2011. It peaks at *M* ~ 1 but is not Gaussian (symmetric), as it has a relatively long tail for larger earthquakes. This peak (mode) can be used as *Mc* for estimating *b-value*. We used *Mc* ~ 1:1 at The Geysers for events in the year 2006, which can also be obtained through the Maximum Curvature Method (Figure 3.6).

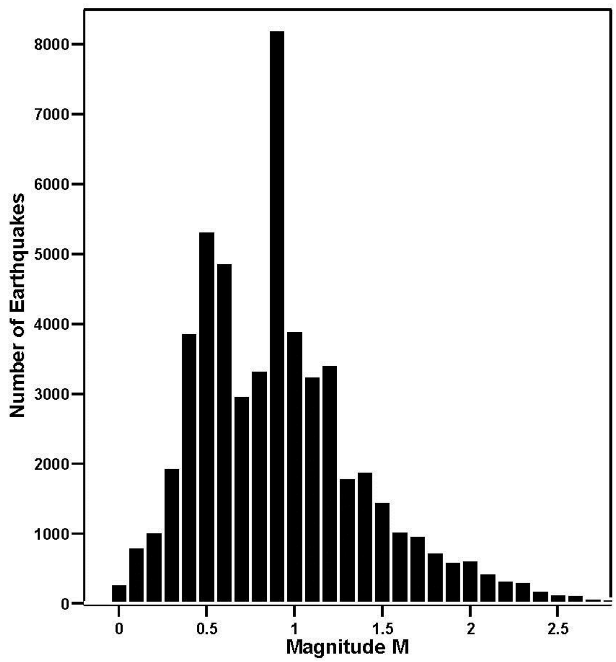

Figure 3.7: Distribution of earthquakes magnitudes in The Geysers

Figure 3.8 presents the variations of *b* over the time period in which we studied the microseismic events at the GGF for the four subregions. Except for region 3, the b values are all larger than 1.3, indicating a very large number of very small seismic events, as larger values of *b* correspond to smaller earthquakes, which explains why the *b* values we obtained are all larger than 1, the typical value for large earthquakes with a tectonic origin. More interestingly, the b values for the same three regions approach 1.2 nature of the events was still more likely to be of the induced type ($b > 1$) rather than the tectonic type ($b \sim 1$). These findings are all consistent with the catalog of events that we studied. Wyss (2000) emphasized the significance of studying the time variations of the b values.

Estimates of the *b*-values at the GGF vary from 1.11 to 1.32, and are all listed in Table 3.2. They represent estimates for the entire 2006 to 2010 period.

b-values from GGF are more than 1.2 consistent for an induced event. These values are significantly higher than those commonly observed for regional tectonic seismicity or aftershock sequences, in which $b = 1$ are typical. Therefore, seismicity is probably not the triggered release of tectonic stress, but is induced seismicity releasing local stress concentrations most likely driven by thermal contraction at the GGF.

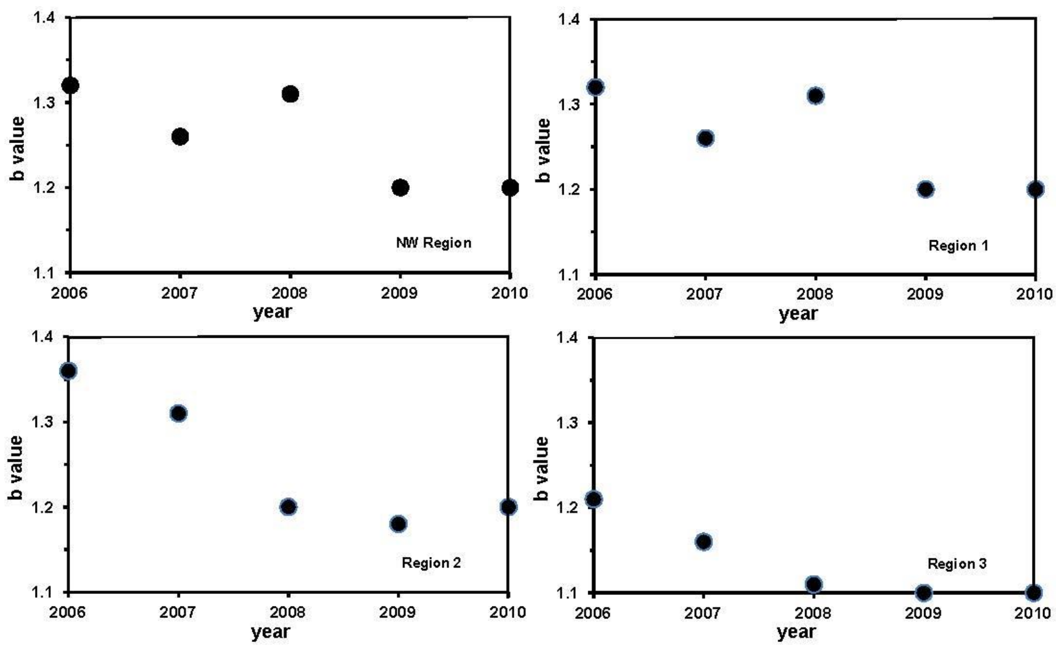

Figure 3.8: Time dependence of the b values in the four regions of The Geysers

Table 3.2: Estimates of the *b*-values for the individual regions. Estimates of *b* are for the 2006 to 2010 period.

Region	b-value
NW Geysers	1.27 ± 0.02
Region 1	1.33 ± 0.02
Region 2	1.36 ± 0.02
Region 3	1.28 ± 0.02
Region 2-1	1.20 ± 0.05
Region 2-2	1.10 ± 0.02
Region 2-3	1.20 ± 0.03
Region 2-4	1.17 ± 0.03

Table 3.3: Observation of large earthquakes in seismicity history of The GGF, 1990 to 2013 between 0 to 7 km depth, from NCEDC catalog.

1980-2013 (33 years of seismicity)		
Magnitude	> 4	> 5
Number	12	none

Moreover, the frequency-magnitude distribution can be used to make probabilistic hazard forecasts for the discussed areas, by simply rewriting the equation 2.1 in terms of the annual probability of a target magnitude *M*

$$P(M > M_{target}) = \frac{10^{a-bM}}{T} \tag{3.3}$$

where T is the observation period, recurrence time is inverse of this annual probability. We have used this analysis to show how an accurate b value is critical to hazard analysis and physical understanding. We show how small changes in b value result in large changes in projected numbers of larger seismicity. Calculated Probability of more than 1 is considered 1 in the final results which means that an earthquake of this magnitude will probably happen each year.

Figure 3.9 shows that an earthquake greater than 4.7 is not probable at The GGF, a conclusion that can be validated by both the history and the nature of seismicity there. But, using b-value of 1 results in a misleading forecast for the probability of an earthquake at The GGF. A thorough investigation of seismicity from 1990 to 2013 validated such a probabilistic model using b value of 1.32 at The GGF. During 33 years of production at The GGF, no earthquake with a magnitude greater than 5 was reported, and only 12 events with magnitude greater than 4 were reported– findings that are compatible with the forecast we have made in Figure 3.9. Hence, large earthquake cannot be triggered from both of case studies and we are in a safe production zone, away from causing any possible hazard in nearby urban areas.

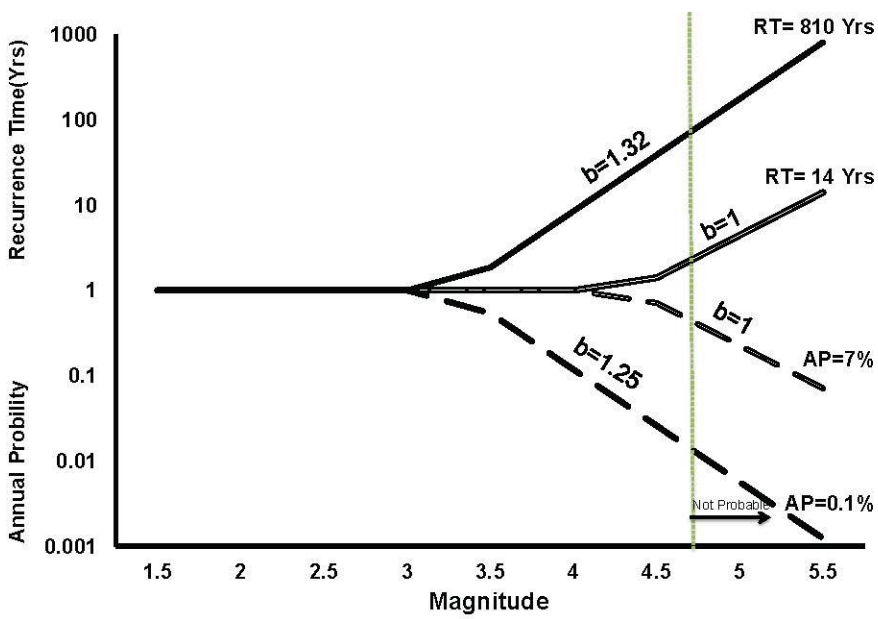

Figure 3.9: Annual probability and recurrence time for seismicity at The GGF

3.4: Fractal Dimension versus *b*-value

In chapter 2 we reported that the fractal dimensions are all in a narrow range centered around, D_f ~ 2:57 ±0:06, and that in most cases the *b* values are about *b* ~ 1:3 ± 0:1, consistent with the Aki relation, D_f = 2*b*. Both D_f and *b* are significantly higher than those commonly observed for regional tectonic seismicity or aftershock sequences for which D_f ~ 2 and b ~ 1 are typical. Our results indicate that the activation of less favorably-oriented fractures produce an increase in both *b* and D_f. This result further validate that the seismicity is not a result of the triggered release of tectonic stress, but is induced by the release of local stress concentrations, driven by thermal contraction unconstrained by friction.

Aki (1981) proposed an important relation between the fractal dimension D_f of a fault network and the *b*-value in the Gutenberg-Richter (GR) law (Equation 2.1)–magnitude-frequency distribution of seismicity that develops on that network. If during an earthquake slip scales with the area of the active fault plane, then the Aki relation is given by, D_f = 3*b*/c, where *c* is a scaling constant between moment and magnitude relationship, which has a world-wide average of about 1.5 Kanamori and Anderson (1975). But, whereas Hirata et al. (1987) did not observe a correlation between the two for acoustic emissions in laboratory experiments, Hirata (1989) reported the approximate relation, D_f ~ 2:3 - 0:73*b*, for seismicity in the Tohoku region in Japan. Comprehensive discussions of the relation between D_f and the *b*-values are offered by Wyss and Sammis (2004); Chen et al. (2006).

Main (1992) conducted a very notable work in an effort to find the origin of the positive/negative correlation between the fractal dimensions and b-values. Figure 3.10 demonstrates his results. He assumed two different models; model A with the alignment of uniformly distributed events along a plane, and model B where earthquakes around potential nucleation points clustered on an existing failure plane such as a fault or fracture. He reported that model A has interaction and weakening potential, with more concentrated deformation of cracks where energy release potential is high, and that positive correlation exists between the two values. On the other hand, model B has a negative correlation between *b* and *D*, whereby mechanical hardening of the system forces a reduction in the potential energy release rate associated with distributed damage to decrease the local stresses on a crack.

In this section, we address whether the Aki relation between D_f and *b* holds for the GGF. The b-value and stable fractal dimension in the 3 regions and 4 sub-regions in Figure 1.3 are given in Table 2.4. As Table 2.4 indicates, values of b are more scattered than those of the fractal dimension D_f . This finding is, in fact, not surprising because although each hypocenter is on a fault, it is not obvious that each earthquake fully activates a fracture in the network, hence more uncertainty results in the *b* values.

Note that, according to Table 3.4, values of D_f and *b* for the three regions roughly follow the Aki relation, D_f ~ *2b*, whereas those for the sub-regions do not. This finding is presumably due to the higher sensitivity of the b values to the size of the area in which seismic activity and microearthquakes occur. Note also that the estimates $b > 1$ confirm that the seismicity at the GGF is induced and does not have tectonic origin because, as pointed out earlier, the fractal dimension of the spatial distribution of earthquakes' hypocenters with a tectonic origin is usually close to 2 with a b value of about 1 (Frohlich, 1993). Some researchers have suggested (Wiemer et al., 1998) that high b values are a necessary, but not sufficient, condition for earthquakes to occur near an active magmatic body– but that hypothesis is not applicable to the GGF. We would like to emphasize that, at this point, we are only documenting our findings for the GGF and providing a plausible explanation. Clearly, much work needs to be done to check the generality of the proposal. See Refs. (Main, 1992; Henderson and Main, 1994; Oncel et al., 1996) for alternative interpretations and discussions.

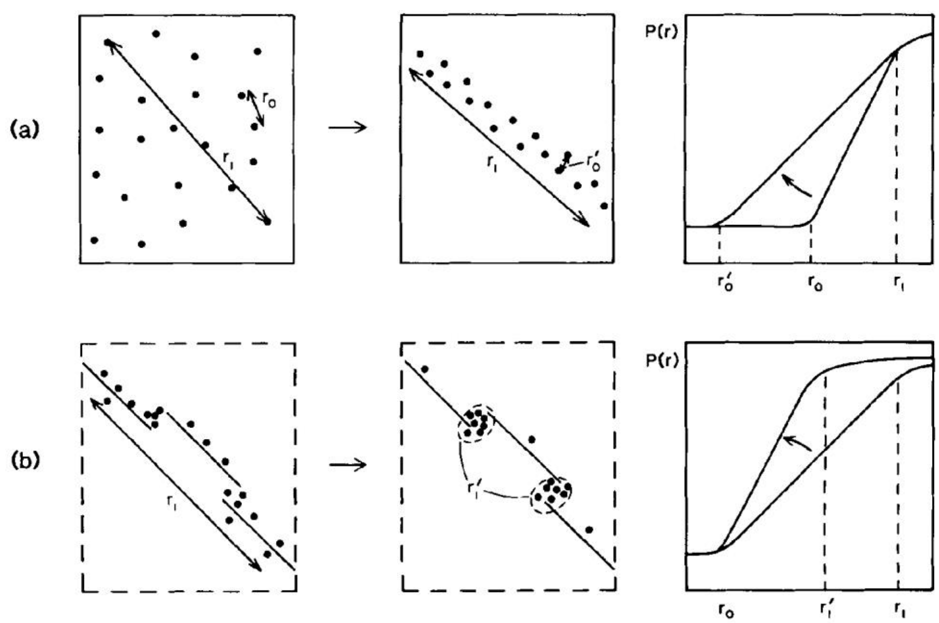

Figure 3.10: Schematic diagram showing two different types of damage localization: (a) Model A, (b) Model B. The left diagrams show the initial seismicity distribution; the middle diagrams show the evolution toward more concentrated activity; and the right diagrams show the correlation plot Pr(Cr) associated with this change.(Main, 1992).

3.5: Conclusion

It is possible to use microseismic moment-magnitude values from selected time periods to determine the b-values of those events, and to ascertain if the microseismic events that are stimulated have been triggered or induced. In other words, we can differentiate fracture-related events from fault-related ones in real-time; a microseismic cloud with b-value larger than 1.2 is induced and not tectonic, and higher b-values mean lower stress.

Furthermore, *b*-value evaluation helps us identify areas in which we have a fracture opening process or closing one. Whereas increase in b-value means an opening fracture, a decrease means a closing fracture.

With this kind of calculation in real-time microseismic monitoring, we will be able to avoid triggering larger earthquakes, distinguish triggered microseismic events (not connected to fracture network) from induced ones (has permeability and is connected to the network), and optimize the stimulation cost and time by screening the nearby fault. Hitting the nearby fault through stimulation can create a channel for excess water production[5], results in extra time and expense for completion, and cause a deviation of fracturing materials and fluids from their designed path.

In addition, the probabilistic forecast and physical understanding of the seismicity at the GGF indicates that large earthquake cannot be triggered from it, and that we are in a safe production zone, away from geohazards.

Finally, the relationship between D_f and the b values opens up another path for the characterization of a fracture network of highly heterogeneous rock with higher confidence compare to analyzing them individually.

Table 3.4: Estimates of the fractal dimensions and the b values for the individual regions. Estimates of b are for the period 2006 to 2010.

Region	Measured Fractal Dimension D-C	b-value
NW Geysers	2.58 ± 0.03	1.27 ± 0.02
Region 1	2.50 ± 0.03	1.33 ± 0.02
Region 2	2.63 ± 0.06	1.36 ± 0.02
Region 3	2.58 ± 0.03	1.28 ± 0.02
Region 2-1	2.60 ± 0.04	1.20 ± 0.05
Region 2-2	2.60 ± 0.04	1.10 ± 0.02
Region 2-3	2.62 ± 0.06	1.20 ± 0.03
Region 2-4	2.51 ± 0.03	1.17 ± 0.03

[5] Water production increases costs, and necessitates separation, storage, transportation, and disposal facilities for the produced water.

4- Application of Seismic Velocity Tomography in Fracture Characterization

After obtaining the seismic velocity models from microseismic data using tomographic inversion, we used these models to characterize the fracture network at The Geysers both for improving the production in current NTR or creating the new reservoir conditions in the HTZ. We attempted to obtain a fundamental understanding of the relationship between seismic velocity models (both shear and compressional wave) and fracture properties to accomplish this task.

Effective, reliable, and accurate characterization of The Geysers specially their complex fracture system necessitate fundamental understanding of the geophysical and geomechanical properties of the reservoir rocks and fracture systems. Geophysical and geomechanical anomalies in the reservoirs can be associated to various features of the reservoir such as porosity, fracture density, salinity, saturation, tectonic stress, fluid pressures, and lithology. Therefore, comprehensive treatment of these various factors should be considered to accurately interpret these anomalies.

We will rely on realistic assumptions and data such as lithology logs, laboratory measurement of rock properties and other information about microseismic data to find the best possible solution to characterize the fracture network. The goal is to create the rock porosity and fracture density map of the reservoir based on velocity models developed from microseismic data which will be accomplished in the final report.

4-1: Stress and Rock Property Profiling

Having both compressional and shear wave velocity models, it is possible to define most of the elastic rock properties uniquely (Tokosoz & Johnson, 1981). In particular, we can calculate the extensional stress, hydrostatic stress, Poisson's ratio, Bulk modulus, Young modulus, and shear modulus volume to characterize the fracture network at The Geysers.

Compressional waves (primary or P-waves) propagate by alternating compression and dilation in the direction of the waves. Shear waves (secondary or S-waves) propagate by a sinusoidal pure shear strain in a direction perpendicular to the direction of the waves. These velocities are approximately related to the square root of its elastic properties and inversely related to its inertial properties:

$$V(approx.) = \sqrt{\frac{\text{elastic property}}{\text{inertial property}}}$$

For instance in rock materials, Vp and Vs are defined in the following equation:

$$V_P = \sqrt{\frac{B + \frac{4\mu}{3}}{\rho}} \qquad V_S = \sqrt{\frac{\mu}{\rho}}$$

where ρ is density (an inertial property), μ is shear modulus and B is bulk modulus . Extensional stress (VE), hydrostatic stress (VK), Poisson's ratio, bulk modulus, Young's modulus, and shear modulus can be described in term of these seismic velocities (modulus are in GPa =1.45 × 10^5psi and velocities are in km/s):

$$V_E^2 = \frac{V_S^2\left(3V_P^2 - 4V_S^2\right)}{\left(V_P^2 - V_S^2\right)} \qquad V_K^2 = V_P^2 - \frac{4}{3}V_S^2 \qquad \nu = \frac{V_P^2 - 2V_S^2}{2\left(V_P^2 - V_S^2\right)}$$

$$B = \rho V_P^2 - \frac{4\mu}{3} \qquad \mu = \rho V_S^2 \qquad E = 2\rho V_S^2(\nu - 1)$$

4-2: Enhancing the Resolution of Seismic Velocity Models

For estimating the properties from the velocity models extracted from tomographic inversion, integrating them with other data, or interpreting the possible temporal changes of them, a finer grid size seems essential. Therefore, we recommend using kriging (a geostatistical tool to estimate the value of a missing points (e.g., velocity values in fine grid mesh) from the known values (the initial velocity field) to generate the high resolution velocity models. Kriging allows us to have the velocity models which are reliable for characterizing the fractures at The Geysers. We begin with the initial velocity model provided by LBNL (Boyle et al., 2011). Figure 4.1 shows the initial compressional velocity model with 4950 points and spacing of about 600m. We perform the kriging analysis using the software in SGeMS and Gslib environment.

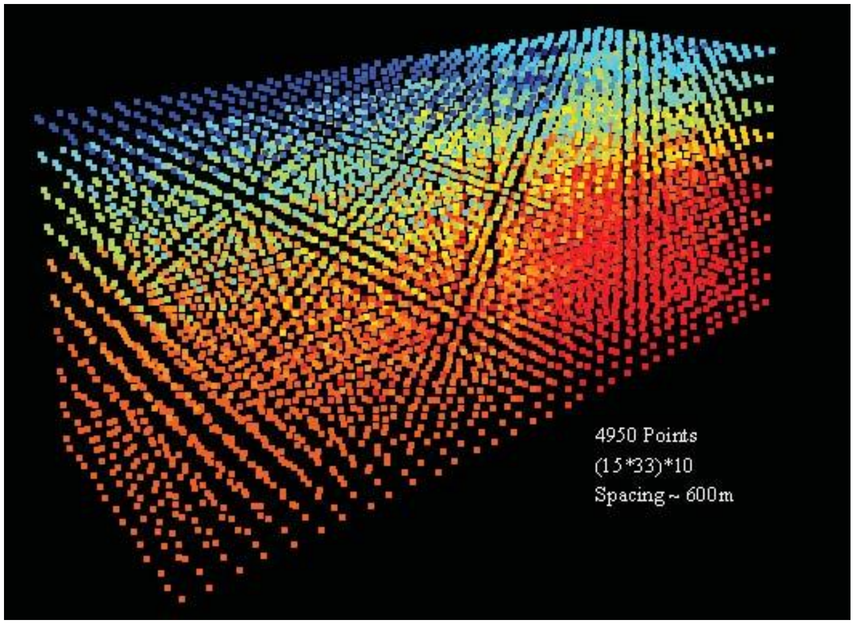

Figure 4.1: The initial velocity model provided by LBNL- The dots show the color coded velocity values associated with the MEQ event location

To create a higher resolution velocity model, we calculate variogram values for different lag separations from 500m to 10km. Then, we use the Gaussian model with a practical range of 57 and sill of 0.4 to fit the data ($\gamma(h) = 0.4\left[1 - \exp\left(\frac{-3h^2}{a^2}\right)\right]$) for the kriging analysis (Figure 4.2:). We implement ordinary kriging on 1,395,360 points in a Cartesian grid. Figure 4.3: shows the final compressional velocity model on a fine grid size volume with spacing of less than 100m. We apply the same procedure for the shear wave velocity model. Although the created velocity models have inherent uncertainty associated with velocity estimates from tomographic inversion, they could be a powerful tool in characterizing The Geysers.

Based on experimental analysis (Boitnott, 2003) and an analytical calculation using effective medium theories (Berge et al., 2001), we know that seismic velocities may increase with depth due to closing of small cracks due to reservoir pressure, overburden pressure, cementation. Decrease in velocity can also be observed due to fracturing, chemical alteration, extreme temperature gradient with depth, pore pressure, porosity. In addition fluid saturation has different effects but overall, has no effect on Vp, decreases Vs, or increases in Vp/Vs and Poisson's ratio. Decrease of Poisson's ratio may be observed due to compaction and lithification of sediments and rock. Furthermore, we can use effective normal stress as an index for fracture opening. In general, low Vp and low Vs indicate highly fractured regions, while high Vp and high Vs may indicate unfractured regions.

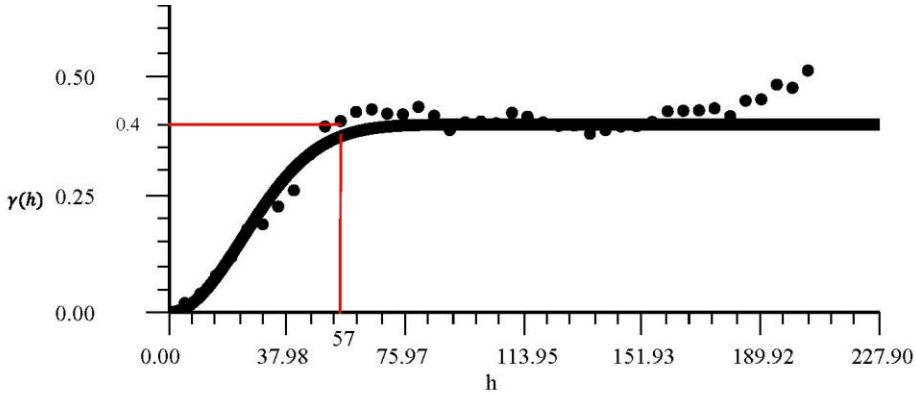

Figure 4.2: Variogram model based on initial velocity model for The Geysers

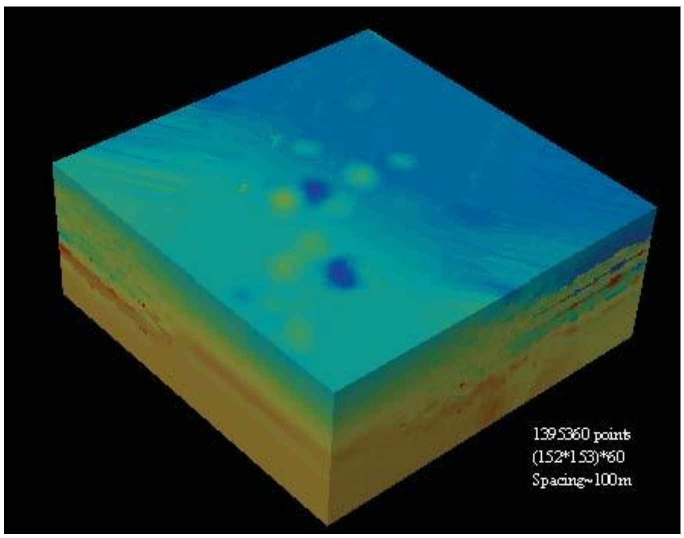

Figure 4.3: The final kriged velocity model for The Geysers

4-3: Result and Discussion

Using the smoothed velocity models (i.e., kriged models) as discussed above, **Error! Reference ource not found.** shows selected the injection wells and corresponding velocity anomalies. **Error! Reference source not found.** Figure 4.5 shows that the lateral and depth extension of elocity anomalies below the injection wells where the velocity anomalies extend to the middle of NTR where most of production wells are completed and then decrease with depth. The same kind of anomalies also could be seen in the HTZ. Increases in porosity created from fractures is the main cause for decrease in the compressional velocity of the zone of interest. Hence, the low velocity anomalies may be correlated with fracture network densities and fracture spacing in the system. Thus, changes in the velocities may serve as another indicator of the evolution of fracture network in HTZ.

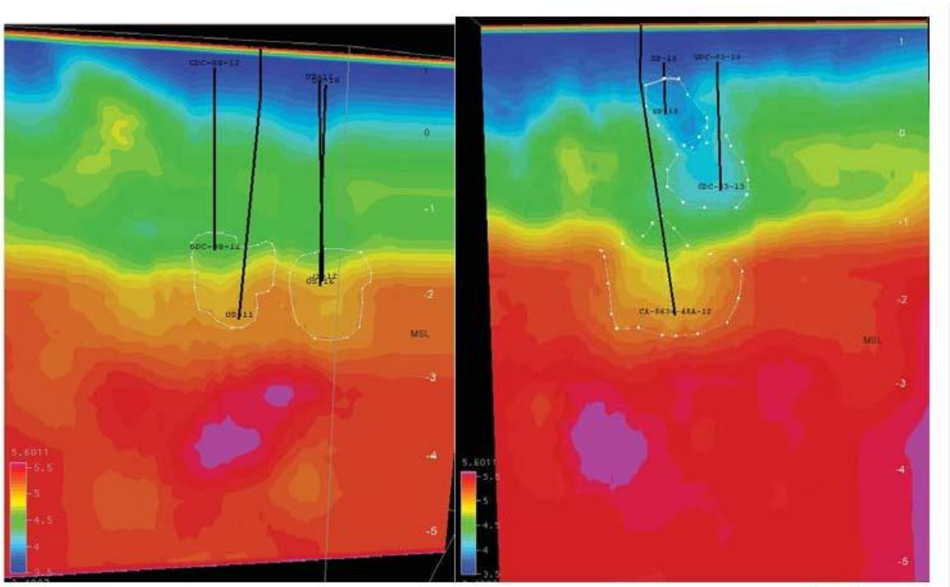

Figure 4.4: Velocity anomalies around select active injection wells at The Geysers, Inline view

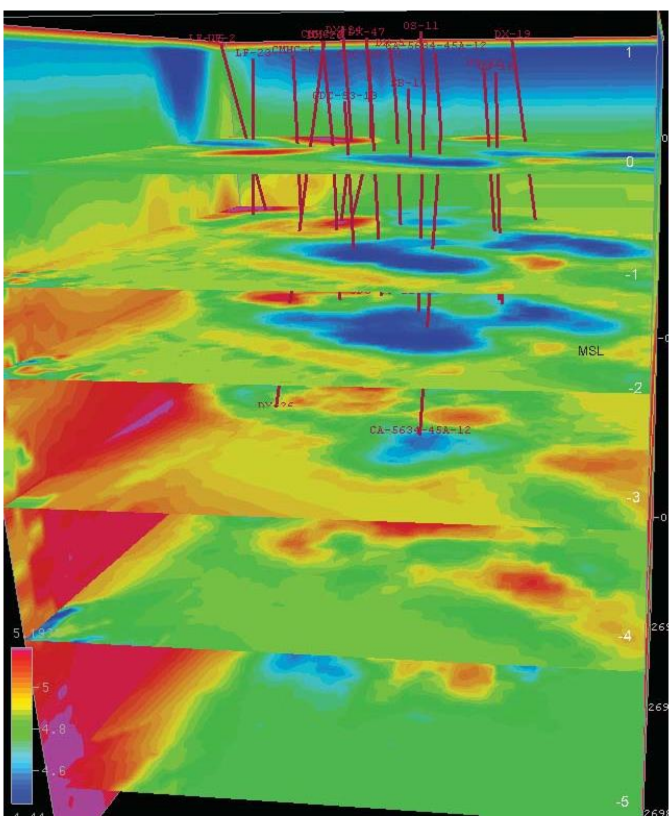

Figure 4.5: Example of the schematic view of the Neural Network

We observed a reduction in velocity and a growth of the region that are indicative of this decrease in different depth of reservoir (Figure 4**Error! Reference source not found.**.5). In the eeper regions velocity anomalies tends to diminish slightly. They can be related to closing fracture with depth or reduce the number of cracks or void ratio with depth (This is consistent with observation made by Berge et al. (2001) at The Geysers. It is also notable that there is no clear separation between lithologies and no apparent signature with depth for seismic velocities in core analysis where we do not have overburden pressure to close the fractures (Boitnott, 2003). These observations lead to an expected distribution of the velocity with depth at The Geysers. The area where we have both low Vp and Vs indicate highly fractured regions, while both high Vp and Vs may delineate unfractured regions.

We also consider two different horizons in The Geysers for investigating more about our methodology. The first horizon is located in the NTR where the injection and production wells has been completed. Existing fracture network there has the main role in production of steam. Our aim in this horizon is locating and characterizing the fracture network. The second horizon is the area 1500 ft beyond the completion points in HTZ where no production occurs. A good assumption with respect to rock type is we have dominantly graywacke in NTR and felsite in HTZ. Our goal here is to find zones where fractures propagate during field development phase and creation of the enhanced geothermal systems. Figure 4.6 shows Vp, Vs, and Vp/Vs for these two horizons. High Vp/Vs anomalies associated with low VS anomalies are saturation anomalies. In the other hand, high Vp/Vs anomalies associated with high Vp are caused from another phenomena such as lithology. Finally, low Vp/Vs anomalies associated with low Vp anomalies are reasonably interpreted as fracture anomalies. Figure 4.7 clearly shows the velocity anomalies related to fractures in NW Geysers and areas with denser fracture network can be identified easily. As shown in these figures we can successfully locate the propagated fracture network in the HTZ which is shown with white circle. Furthermore, according to the equations in the last section, we estimate the volumes of the Poisson’s ratio, extensional stress, and hydrostatic stress (pore pressure) to further investigate the fracturing phenomenon in the reservoir. Figure 1.8 and Figure 4.9: clearly show that Poisson’s ratio anomalies are very similar to Vp/Vs which is good indicator for fluid saturation. Reduction in extensional stress indicate the open fracture areas in the same areas as shown in white circle in velocity anomalies and it is further validation that those anomalies are fracture related not lithology or other phenomenon.

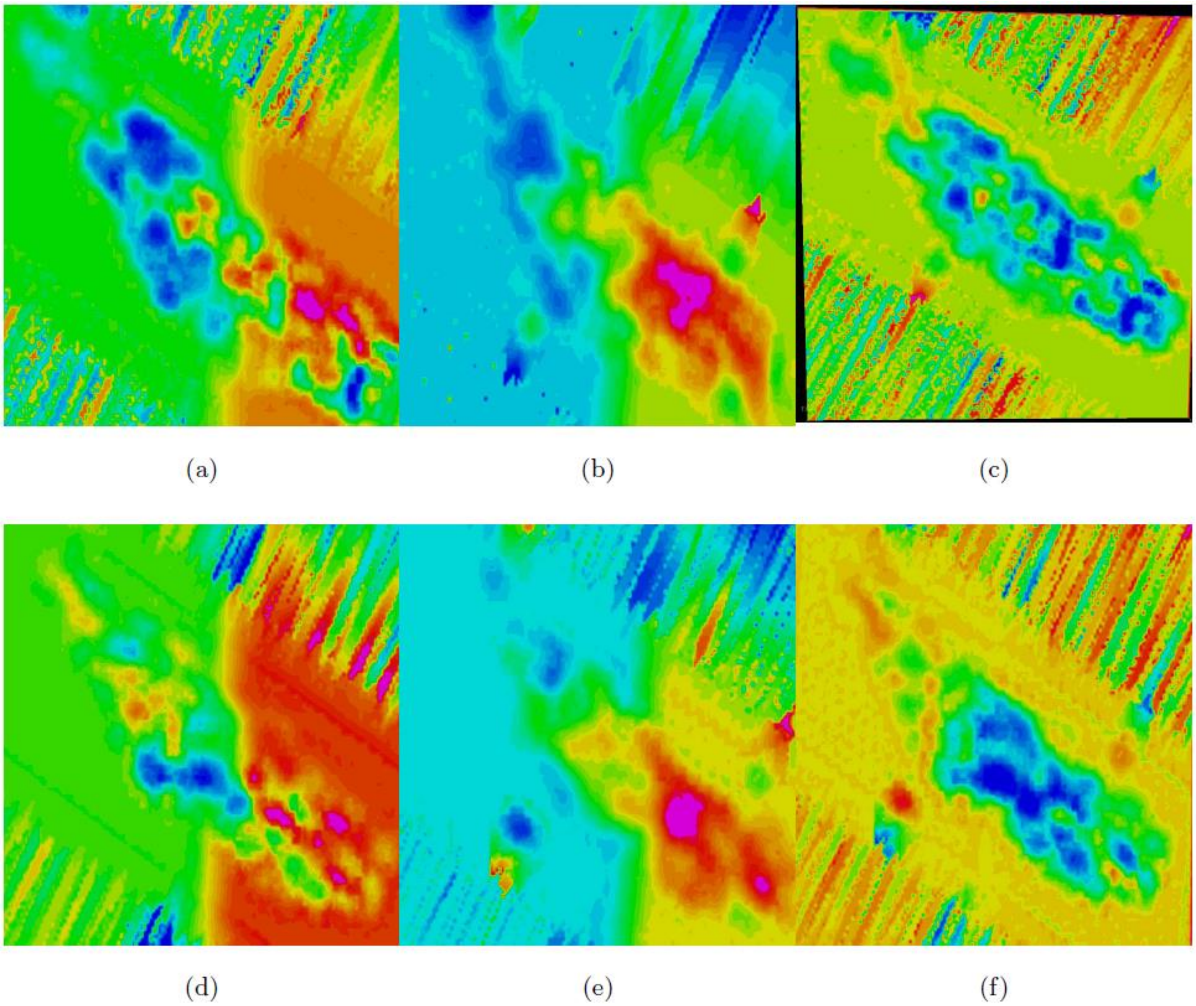

Figure 4.6: NTR horizon at The Geyser (a) Vp , (b) Vs, (c)Vp/Vs, HTZ horizon (d) Vp , (e) Vs, (f) Vp/Vs

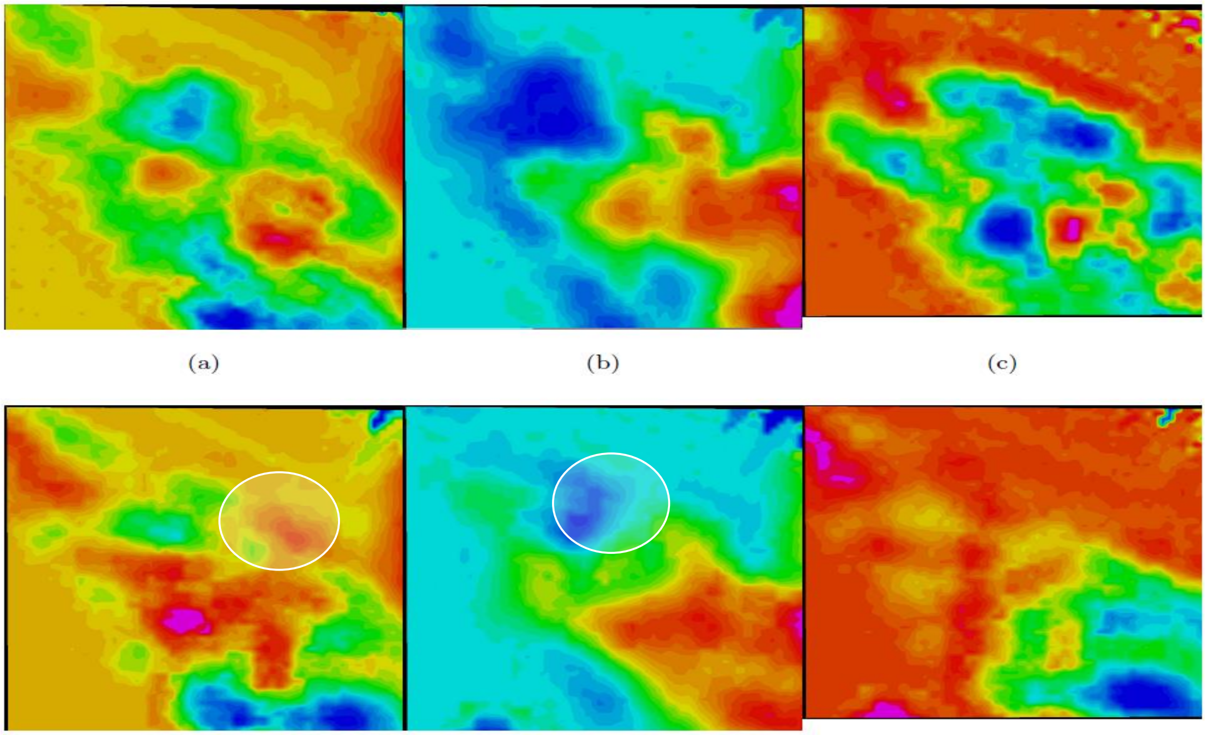

(d) (e) (f)

Figure 4.7: NTR horizon at The NW Geysers (a) Vp, (b) Vs, (c) Vp /Vs, HTZ horizon, (d)Vp , (e) Vs, (f) Vp /Vs. The white circle indicates the area of the propagated fracture network in the NW Geysers Area.

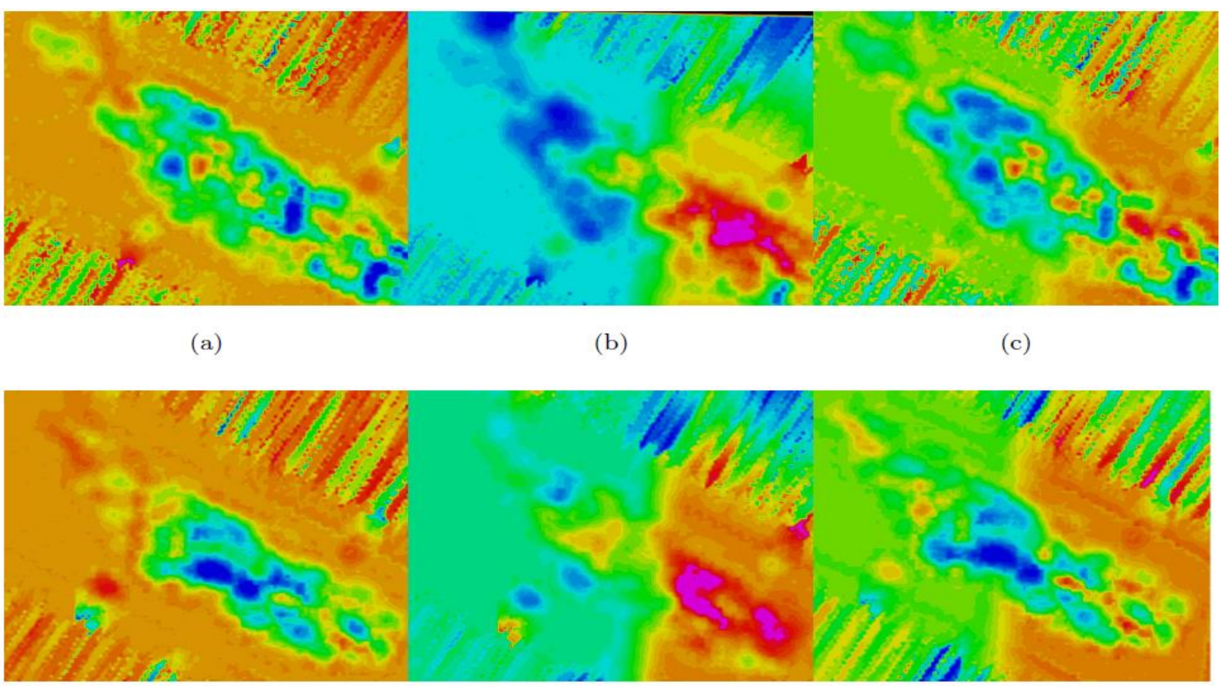

(d) (e) (f)

Figure 1.8: NTR horizon at The Geyser (a) Poisson's ratio, (b) Extensional stress, (c) Hydrostatic stress; HTZ horizon at The Geyser (d) Poisson's ratio, (e) Extensional stress, (f) Hydrostatic stress

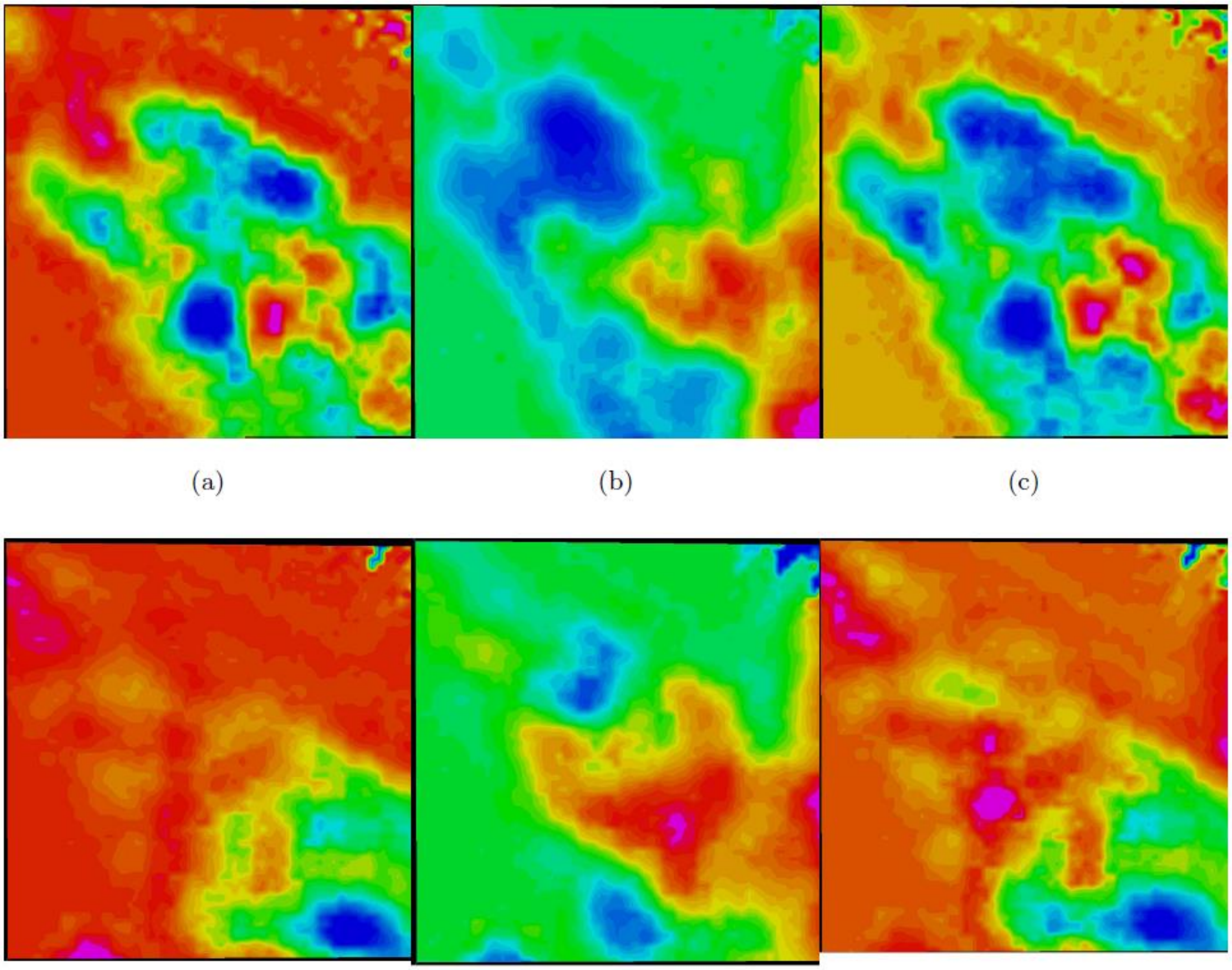

(a) (b) (c)

(d) (e) (f)

Figure 4.9: NTR horizon at The NW Geysers (a) Poisson's ratio, (b) Extensional stress, (c) Hydrostatic stress, HTZ horizon at The NW Geysers (d) Poisson's ratio, (e) Extensional stress, (f) Hydrostatic stress

5- Integrated Evaluation

In this section, we will show how each part of our work can be integrated with those carried out by our project partners at Calpine and LBNL to further enhance their value. We demonstrate the best possible solution for describing the microseismicity in The Geysers and cross validate our results to better characterize the fracture network and achieve more reliable results.

We also discuss the challenges we faced in integrating our velocity models with those developed at Calpine. Several no cost extensions were granted to us by the DOE, in part with the objective of resolving some of the inconsistencies in the velocity models. Although we made some progress in the integration of the two sets of velocity models we were not fully successful. This was in part due to the fact that different software platforms were used as well as the associated issues in connection with graduation of the students involved in the project and exhaustion funds to engage new students to fully resolve the problems.

The same is true in connection with the anisotropic tomographic inversion. Although excellent preliminary results were generated by LBNL which led to the completion of much of the project goal of developing a new approach for anisotropic tomography (Appendix 4-4). Testing and validation of the results were not completed due to the funding limitations.

5-1: Tomographic Inversion Versus Fuzzy Clustering

To accurately locate the boundaries of the connected fracture network, hypocenters of microseismic events were analyzed to examine the possible correlation between MEQ events and the fracture network. Fuzzy clustering technique was used to investigate the movement of microseismic events in the HTZ (Aminzadeh et al., 2010), and velocity models are created to find the fracture related anomalies. We could overlay the cluster centers on kriged compressional velocity model to validate the result from each of them individually. To validate the result from each of the cluster centers, we could overlay the cluster centers on kriged compressional velocity model. However, funding was not available to accomplish this.

We explored this kind of relationship between microseismic cluster center changes and the temporal change of the compressional velocity model at The Geysers. Figure demonstrates that these anomalies are correlated with microseismic events cluster movement. Fracture propagation or fluid movement within the fracture network clearly can be identified by considering the contribution of fractured area on velocity model anomalies and movement of microseismic events fuzzy clusters.

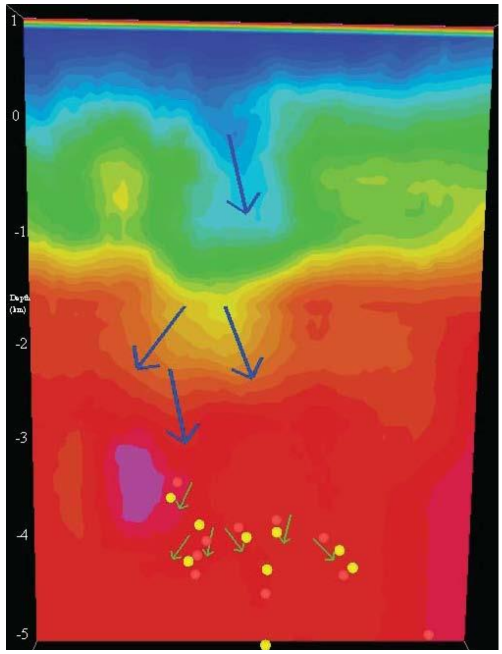

Figure 5.1: Correlation between microseismic cluster movement and velocity anomaly direction, pink circles is microseismic cluster center in 2006 and yellow circles are the microseismic cluster center for 2009

5-2: Shear Wave Splitting Versus Tomographic Inversion

In this section, we will show how shear wave splitting result and tomographic inversion methodology, that we described, can cross-validate each other or eliminate the errors in analyzing them individually. This work accomplish our integration with results from Elkibbi and Rial (2005) with ours described in the previous section.

Elkibbi and Rial (2005) stated that the dominant polarization direction observed in NW Geysers is between N-S and N60E. They also indicated that time delays observed between the slow and fast shear waves at The NW Geysers is from 8 to 40 ms/km. As seen in the Figure 5.2: , cross-plotting their result with ours can help us to spatially interpret the orientation and density of fractured area better. Where we have both low Vp and Vp/Vs along with high time delays, these areas have identified higher fracture density with more confidence.

According to Figure 5.2, it is clear that the interpreted denser area from both methods are consistent in most parts of the reservoir.

In addition, Figure Figure 5.3: demonstrates stations near Squaw Creek Fault Zone (S4, S5, S6, and S11) have higher fracture density than other. This is consistent with extensional stress distribution which indicates open fractures. On the other hand, high time delays occur in stations S1, S2, S3, and S8 which indicate that this area also may have higher fracture intensity than western stations but they have consistency with Poisson’s ratio distribution not with extensional stress. Hence, it is possible that the time delays there are because of degree of fluid saturation or fluid type.

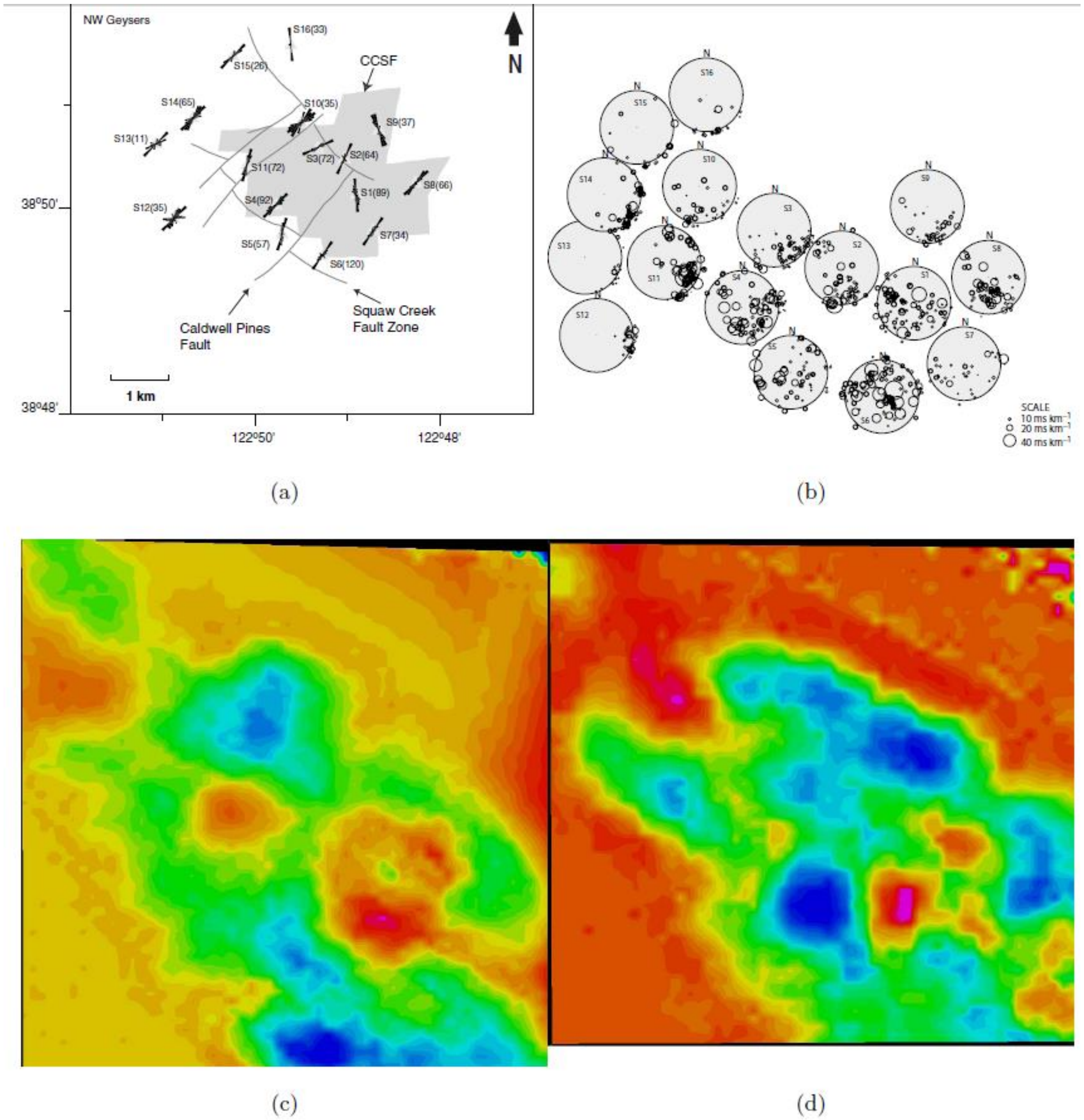

Figure 5.2: (a) Fracture orientation result from shear wave splitting analysis, (b) fracture density result from shear wave splitting (Elkibbi & Rial, 2005), (c) Vp, (d) Vp/Vs in the NW Geysers.

This additional successful integration between shear wave splitting and velocity modeling validate our hypothesis about velocity or stress anomalies.

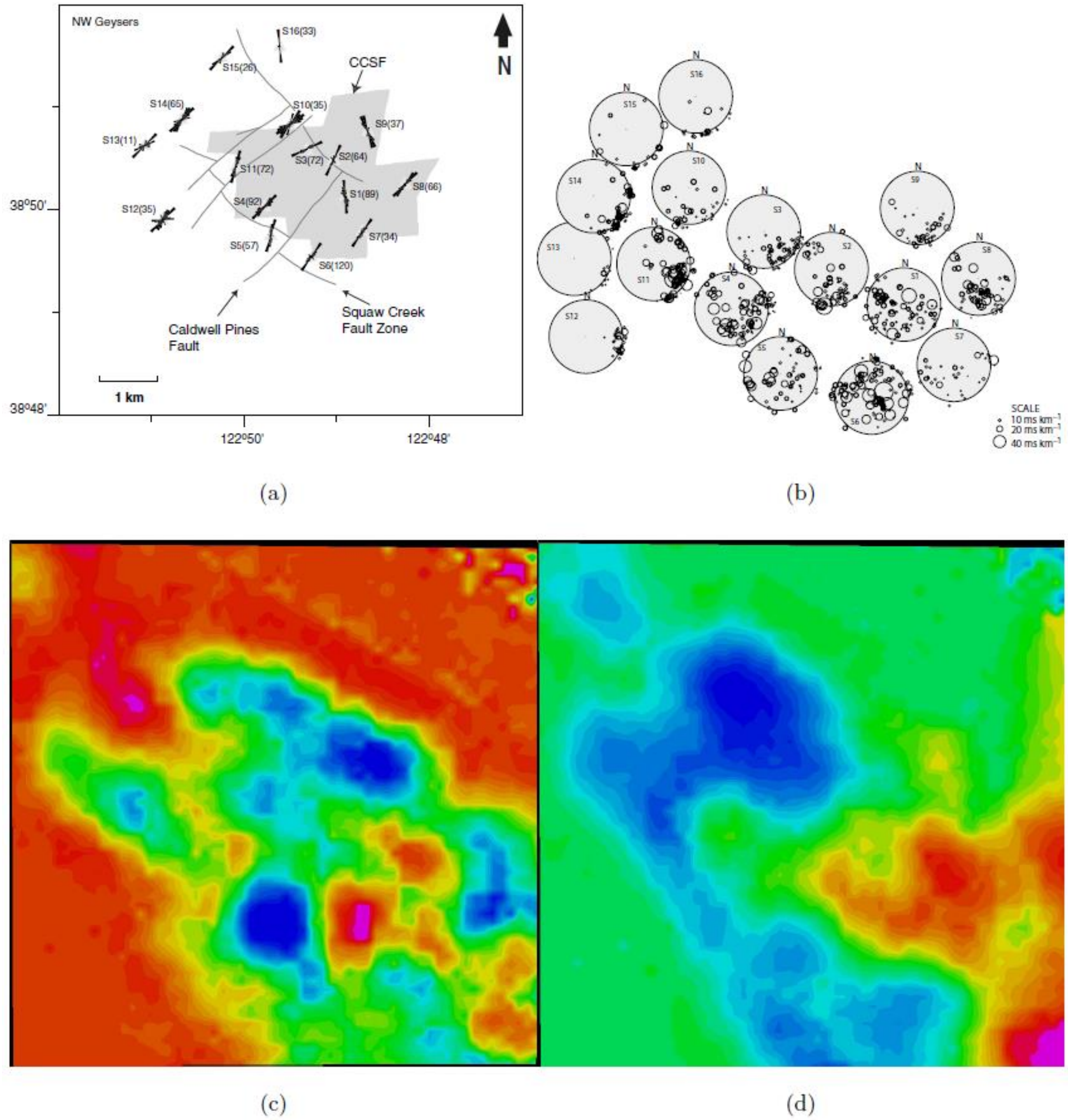

Figure 5.3: (a) Fracture orientation result from shear wave splitting analysis, (b) fracture density result from shear wave splitting (Elkibbi and Rial, 2005), (c) Poisson's ratio, (d) Extensional stress in the NW Geysers.

5-3: 3D Velocity Modelling in NW Geysers

The aim of the study was to use the velocity model created earlier by USC, described in section 4, and validate those results against the structural model created by Calpine. The USC velocity model was created earlier using the OpendTect software based on the seismic data provided by LBNL.

GOCAD software was used to develop the geological model by Calpine and USC tried to import the model into Petrel as well as an older version of GOCAD but due to compatibility issues, USC was unable to import the model in GOCAD. Importing of the model into Petrel was tried and due to the complexities involved in transfer from one platform to another it was mutually decided that Calpine would use the velocity model created by USC and refine it based on the their geologic model shown in Figure 5.4.

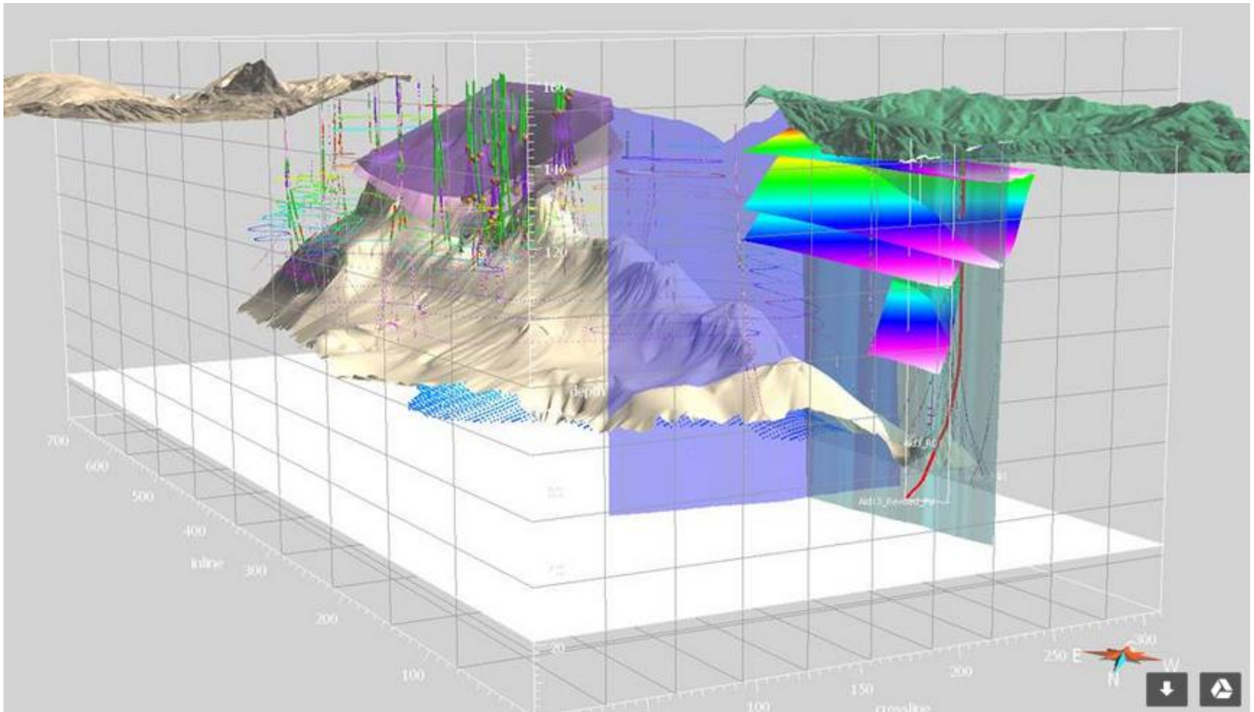

Figure 5.4: GOCAD model of the NW Geyser Area

The seismic data processed for velocity modelling was in Lambert conformal co-ordinates, CA State Plane II-402 NAD 27 datum, which was converted to Cartesian co-ordinate system in order to make it compatible with OpendTect software import format. The velocity model thus created and extracted is in Cartesian co-ordinate system. When the velocity model is extracted it gives X and Y values and also gives the velocity values at different depths at uniform intervals.

USC converted the model as per the requirement of the GOCAD software and as desired by Calpine using Matlab and the model was sent to Calpine which did not match the area of study due to mismatched co-ordinate system. After the discussion with Calpine it was decided to convert the co-ordinate system using few reference wells which were present both in the seismic data as well as the Calpine geological model. USC generated an algorithm to use the reference wells and revise the co-ordinates of the entire velocity model but the results were not in congruence as checked by Calpine and shown in Figure 5.5.

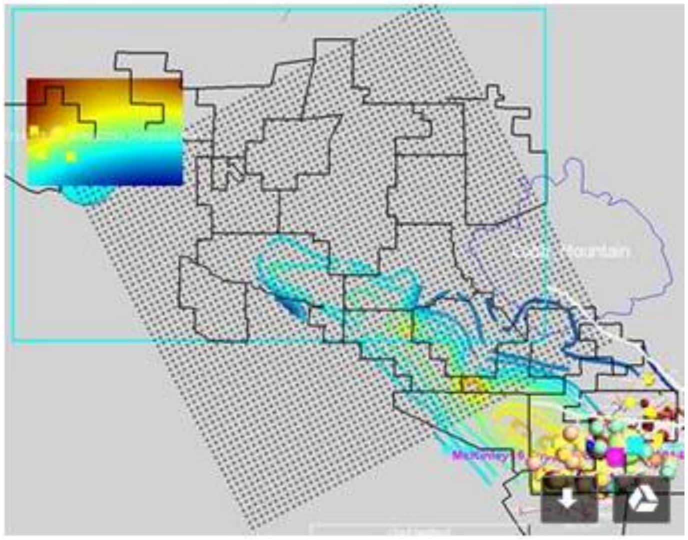

Figure 5.5: 2D map of the entire area, our NW Geysers study area being part of this.

It should be noted our NW Geysers study area is a subset of what is reported here as Calpine study area. The blue polygon shown in Figure 5.5 is the area of the velocity model generated as per the conversion system whereas black boundaries represent the area of study. After following several iterations and various algorithms to match the study area with the velocity model co-ordinates no good match was obtained by USC.

Figure 5.6 shows the location of the wells used for the referencing between USC and Calpine.

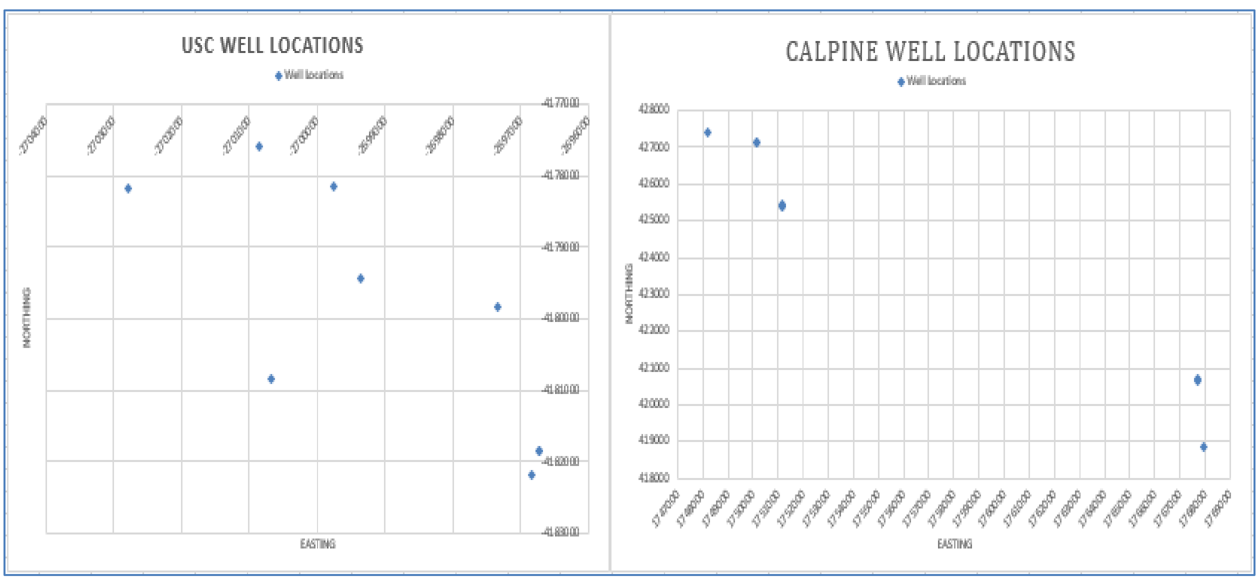

Figure 5.5: Wells used for cross-referencing of the coordinates.

5-4 Addition Comments

It was found that since Lambert is a spherical projection system, whereas the conversion algorithm used before velocity modelling was possibly for Latitude –Longitude data to Cartesian coordinate system and thus the values obtained are not appropriate. On processing the old coordinate system conversion algorithm it was found that it provides a z-value which was ignored in velocity modelling. In absence of the z-value in the velocity model, it is not possible to achieve the real coordinates.

Thus it can be suggested that one way to use the velocity model could be to use the initially used seismic data and back track the coordinate system based on that. It would involve writing an algorithm to compare the initial available coordinates from seismic data to that of the velocity model and revise the final velocity model coordinates accordingly. This step needs availability of the initial seismic data which is currently unavailable.

5-5 3D Anisotropy Tomography for Microseismic Event Location and Subsurface Physical Characterization

In this section we report on the work done by our CO-PIs at LBNL, Drs. Lawrence Hutchings and Leon Thomsen. The more detailed discussion and mathematical details are given in Appendix 4-4. The purpose of this work was to apply the theory of anisotropic wave propagation to tomographic inversion of MEQ arrival times, in the context of a complex subsurface and complex surface topography. The result of this analysis is the development of three-dimensional models of anisotropic structure, P and S-wave anisotropic velocity models, and identification and characterization of subsurface fractures. We worked with the assumption that locally (within each elemental volume, voxel), the anisotropy is uniform polar anisotropy, and of course we recommended our approach only for situations where this assumption is plausible. We did not specify the local orientation of the pole of symmetry, rather we solved for it, finding two Euler angles as well as five elastic parameters in each voxel.

Anisotropy can be due to thin-layer bedding, mineral or pore alignments, or fractures and faults. In our model, these are the planes of symmetry that we identified with polar anisotropy. We used the terms "fractures" and "faults" to mean planar discontinuities in the rock mass, affecting wave propagation and possibly fluid flow, without implication regarding physical causes. In addition to the tomographic inversion for anisotropy, we identified faults from the location of MEQs and their focal mechanism solutions. The orientation of fractures and faults, can also be obtained from standard shear-wave splitting interpretations (Lou and Rial, 1997)[6]. This, and focal-mechanism solutions are applied in our inversion program as constraints when available. Generally, however, we relied on the plane of symmetry solved in the tomographic inversion as

[6] All the references sited in this section are included in Appendix 4-4.

indicating the orientation and location of anisotropic geology. Further interpretation is required to characterize the permeability.

Travel time tomography from MEQ recordings is more difficult than the corresponding problem from controlled-source surveys, since it includes the complication of locating MEQs. This is a difficult task, as we need to know the velocity of the subsurface in order to locate the MEQs accurately, which is what we are solving for. It also adds four unknowns (3 spatial source coordinates, plus origin time) for every MEQ event, adding to the 7 unknowns previously mentioned for each voxel. Further, MEQ events generally are at depths of 1 – 5 km in geothermal or hydroshearing environments, so that obtaining physical parameters at depths can be difficult.

We modified the computer program simulPS (Thurber, 1983; Eberhard-Phillips, 1992) to include inversion for anisotropic parameters, double difference seismic event locations (Waldhauser and Ellsworth, 2000), and added common ray path inversion (discussed below). The program applies standard linearized least squares inversion to minimize the residual between observed arrival times and those calculated from tracing rays though the volume. We used this application to obtain absolute MEQ locations and initial geologic velocity structure. We added double difference calculations to the program as herein described. The double-difference seismic locations takes advantage of the travel time difference between closely located events to get accurate relative locations. This is applied in the location loop of the program. In the tomography loop for anisotropic parameters, we common ray paths by identifying overlapping ray paths to common stations and localize the inversion to the portions of the path between two events. In this application the two events do not need to be closely located (common source location), rather have overlapping ray paths to a common station (common ray path approach). The new program is called SimulAD (anisotropic and double-difference). We applied our inversion to data from The Geysers. The lithology of The Geysers geothermal reservoir is dominated by low-grade metamorphism of fractured greywackes that commonly lack schistosity, warranting the general assumption that it is composed of stress-aligned fracturing in an otherwise isotropic medium.

The Geysers geothermal field located in the Coastal Ranges, just north of Napa Valley. The region is dominated by the plate boundary motion along the San Andreas Fault (Figure 1 in Appendix 4-4). The Geysers is nested between the southwest-bounding Maacama Fault and the northeast-bounding Collayami Fault, and includes a mixture of strike-slip and thrust faults [McLaughlin, 1981]. The subduction of the Farallon plate beneath the North American plate led to Pliocene-Holocene volcanism, which left enough heat to metamorphose the greywacke of the overlying Franciscan mélange to biotite [Moore and Gunderson, 1995].

The Geysers geothermal reservoir is the world's largest generator of electricity from geothermal energy since 1970. It is a vapor-dominated geothermal reservoir with temperatures reaching 400°C between 2 and 5 km depth, and where significant volumes of waste water are injected in order to fully exploit the resources [Majer et al., 2007]. The reservoir is thought to be created by percolating groundwater through the natively low-permeability Franciscan mélange and along fractures opened due to local faulting, and heated by a large, silicic magma body just north of the steam field [Stimac et al., 1992]. The Geysers was historically fluid-dominated [Sternfeld, 1989; Moore and Gunderson, 1995], but increased fracture volume due to crustal extension has been implicated in the formation and sustained presence of the vapor-dominated conditions that exist today [Allis and Shook, 1999]. A number of steam production wells were drilled into the northwest Geysers in the 1980's, but later abandoned because of the poor economics caused by low natural steam production as well as problems with corrosive non-condensable gases (NCG). Figure 5.7 shows the study area (blue outline) and the instrument locations.

scale |__|__| 2 km

Figure 5.7: The study area (blue outline) and instrument locations as indicated by Hutchings and Thomsen (see Appendix 4-4 for the reference). "White" symbols are permanent LBNL network stations; "yellow" are temporary DOE monitoring sites; and "red" are supplementary instruments installed by LBNL for the Prati-32 test. Only instruments located within the study area were used for the tomography, except C08 which was also used.

6- Phase arrival autopicker design and implementation

6-1- Introduction to autopicking

Passive seismic as a tool for monitoring reservoirs has become fairly common in recent years. Some of the more common uses include development of unconventional reservoirs such as geothermal reservoirs, tight gas or oil reservoir systems which require hydrofracing, monitoring of injection wells (CO_2 injection, steam flooding, etc) among others. Autopickers provide an automated method to detect energy arrivals in the seismic signals that are collected continuously during a passive seismic survey. With large arrays and huge amounts of data being collected, traditional autopickers are increasingly facing issues with run times as well as in high SNR (signal to noise ratio) environments.

One of the older and commonly used method for phase arrival detections is the Short term averaging / Long term averaging (STA/LTA) algorithm (Allen, 1978) and its modification as suggested by Baer et al. (1987). Methods based on abrupt changes in attributes of the seismic coda such as energy change as used in Coppens method (Coppens, 1985) and modified Coppens method (Sabbione, et al., 2010), statistical attributes such as frequency and higher order statistics (skewness& kurtosis by Saragiotis, et al., 2002) have all been proposed over time. Modern autopickers using fairly advanced algorithms such as cross-correlation attribute analysis or statistical techniques have been used in specific scenarios and have been improving the accuracy and validity of the picks being made.

Our work involved developing an advanced artificial intelligence (AI) based autopicker using an integrated automatic neural network (ANN) approach aimed at providing accurate picking of both p and s phases in a rapid fashion and to obtain the usable results in situations where traditional autopickers show a relatively high failure rate. Such a technique becomes particularly useful in situations where high degree of non-uniqueness is involved. The AI based approach used provides the "best possible" pick detection (based on selected parameters and expert picks) within an environment of appreciable uncertainty created by the non-uniqueness of the problem in hand. Some effort has already been made on various applications of ANN in autopicking and seismic prediction (McCormack, 1990; Veezhinathan, 1992; Aminzadeh et al, 1994, Zhao, 1999; Aminzadeh, et al, 2011). This work extends the previous work incorporating many seismic attributes and other new methods to further enhance the quality and efficiency of the picking process. This hybrid autopicking workflow as depicted in Figure 6.1 has been tested extensively on LBNL's Geysers passive seismic monitoring array. This method should be useful where the data poses considerable challenge with very low SNR levels and high percentage of unusable data due to various factors including ambient noise as well as lower average MEQ magnitudes. We also compare the results obtained from the hybrid autopicker with more traditional autopickers in use, to validate the advantages of the new method. As discussed before, **Error! eference source not found.** provides the basic workflow used in the autopicker implementation.

Individual sections describing each part of the workflow along with results have been discussed hereafter.

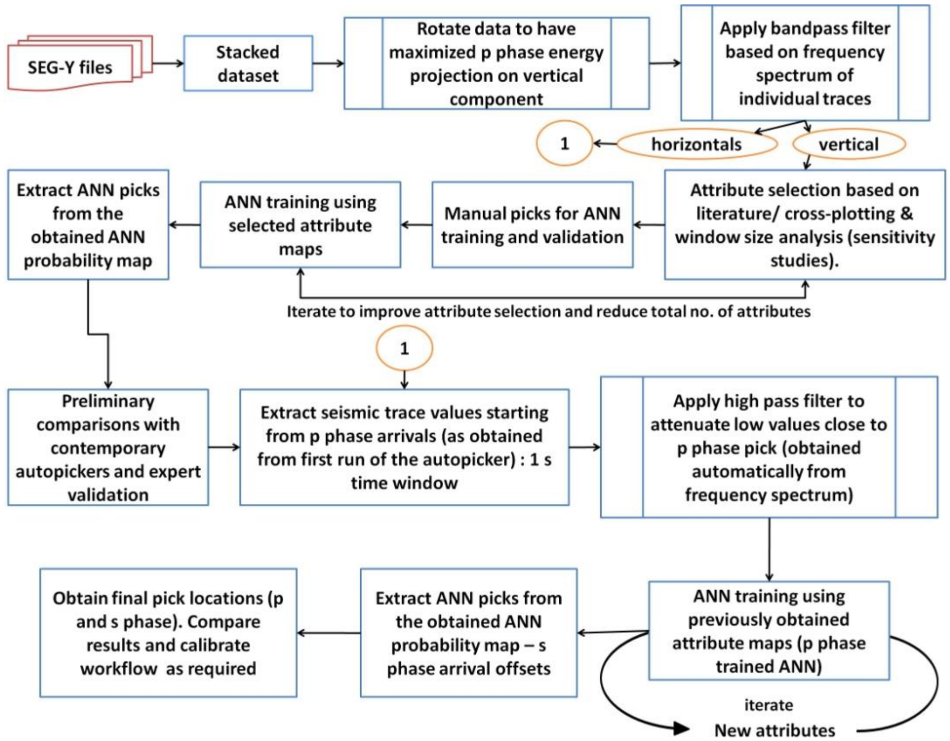

Figure 6.1 - Workflow

6-2: Data Preprocessing

The raw windowed data around detected events was obtained from the recording stations based on threshold noise using a triggering algorithm developed by the contractors. For this project, we have 3C data from each of the 5 recording stations in the vicinity of the monitored reservoir. Once the events were detected, the next step was to obtain accurate phase arrivals from data collected at different stations to be used for further analysis. A small subset was selected from the available dataset for the autopicker development. Before running any picking algorithms, it was necessary to remove noise from the collected data and this was done by using a bandpass filter designed with cut-off frequency automatically selected based on the frequency spectrum of the seismic trace. Since the best results for p phase arrival are expected from the vertical component and the s phase arrival from the horizontals, the dataset is divided based on the component type and fed through a rotation algorithm to maximize the p phase energy on the vertical component and the s phase energy on the horizontals. It is important to note that based on the data quality, additional data conditioning steps may be necessary and is decided on a case–by–case basis.

6-3: Attribute analysis and ANN design for p phase autopicking

To test different attributes/ properties to be used for the ANN autopicker design, a literature review was carried out to understand the attributes in use and these attributes were computed on a trial basis to select useful attributes for use in the training of the ANN. The selection was criteria based with maximum emphasis given to sharp transitions near arrivals as per manual (expert) picks. The aim here was to minimize the number of attributes to be used in the training process to reduce run times and to increase the accuracy without dilution in results due to too many attributes. Figure Figure 6.2: shows sample attribute maps computed from seismic trace data stacked together for easier computation. Many of these were tested as possible input nodes before deciding on the final inputs for testing and validation on an independent dataset.

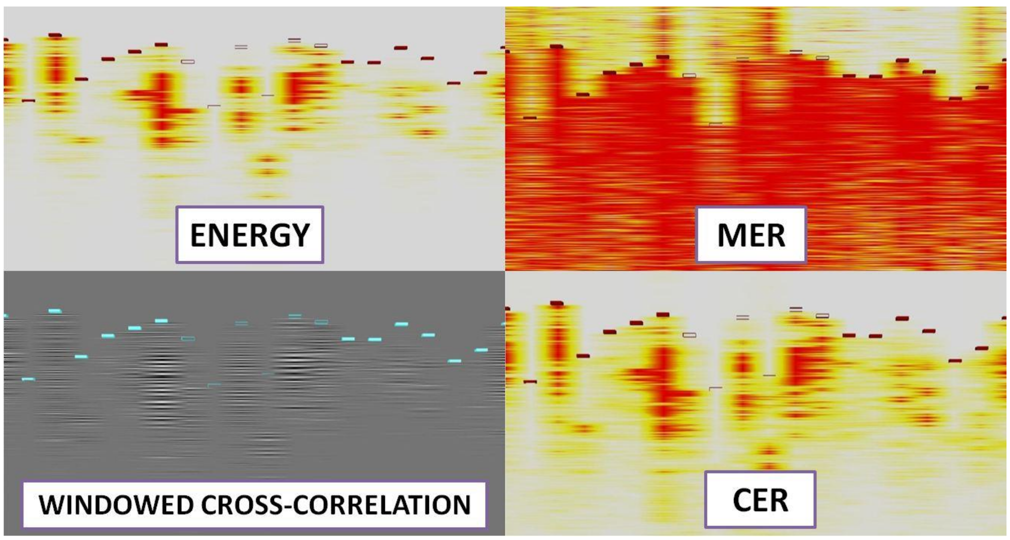

Figure 6.2: Sample attribute maps to choose ANN input nodes

Figure 6.3: shows blow up of a sample seismic trace (at arrival) along with some of the sample attributes we worked with as inputs to the ANN. This comparative framework allows pruning of those attributes which either fail in high SNR environments (such as STA/LTA ratio) or those which are too computationally expensive. This was also necessary to check how computation windows impact the said transitions in attribute trends and what the best possible computation windows were for good ANN design. The best possible attribute combination was selected based on this analysis and **Error! Reference source not found.** gives a listing of the attributes used for he final ANN implementation in an unsupervised neural network approach for both p and s phase autopickers. Figure shows the trained ANN output maps (both supervised and unsupervised networks for comparison) superimposed on expert picks made for the training and testing datasets. This provided an indication of the picking efficiency and the improved ANN match "transitions" seen with the unsupervised network and the acceptable transitions seen with the supervised network design which uses a back propagation algorithm. The unsupervised neural network design was chosen for p phase picking as the run times associated with unsupervised

network design are appreciably faster (order of 10) and is used as the final pick in this study for further analysis.

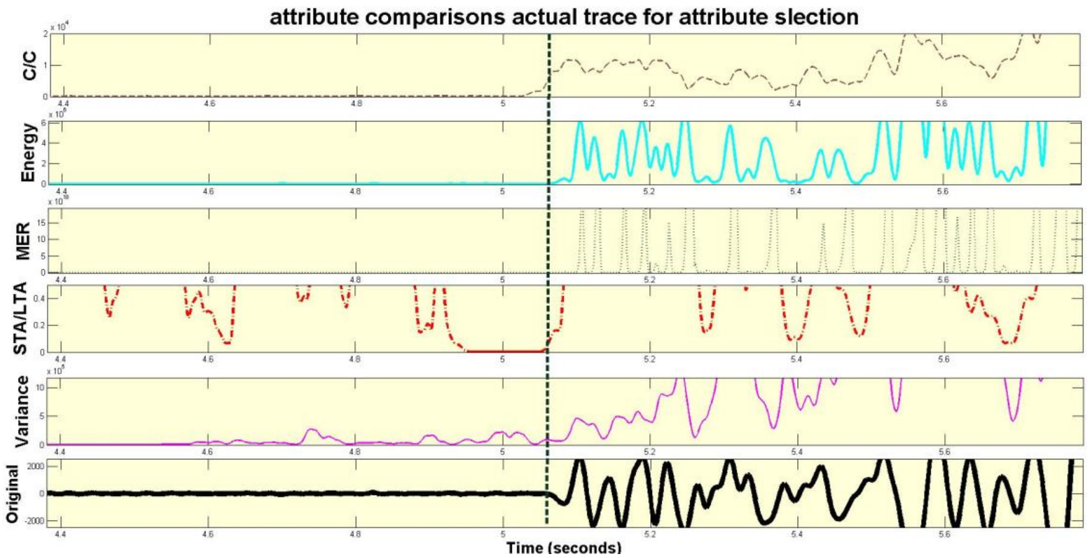

Figure 6.3: Comparative analysis of actual trace with evaluated attributes for improved attribute design and selection

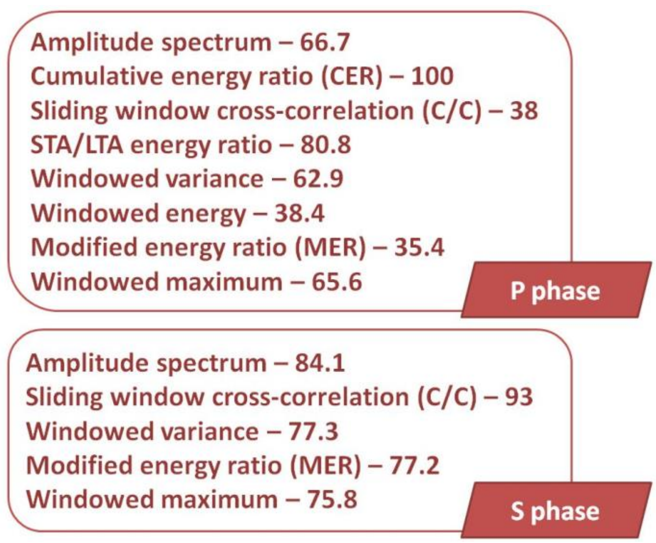

Figure 2: ANN inputs (both supervised and unsupervised networks) used in training. The values enclosed in brackets indicated trained weights associated with ANN training

The ANN output was fed through a post processing algorithm which was designed to extract the p phase picks based on the matching probability (output) as well as final pruning of the output location based on a selected attribute (modified energy) showing sharpest transition. The p phase picks were important to extract the localized time window for possible s phase arrival detection as explained later. In this part of the workflow, a small time window of 1 second was chosen starting from the p phase arrival at each station and the data is extracted from within this window from the two horizontal components for use in the s phase autopicker design and implementation.

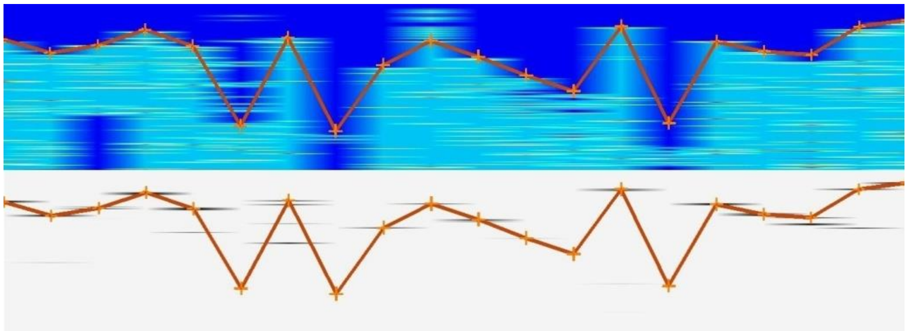

Figure 6.5: ANN output probability maps (background) with expert picks (cross-hairs). The top map is a sample from unsupervised ANN output volume while the bottom map is from a supervised ANN learning scheme

6-4: S phase autopicking

Once the necessary data for s phase picking has been extracted as described in the previous section, a new stacked volume was obtained which was expected to include the distinctive s phase arrival. Manual picks were then made in order to create a sample set for ANN training. Since the distinctive signal response for s phase arrival was difficult to detect in many scenarios, the ANN output was used to make a preliminary arrival estimate and the final pick was made by pruning the location based on the observed variation of a chosen attribute (sliding waveform cross-correlation). **Error! Reference source not found.** lists the attributes used in the ANN raining and as can be seen, most of these attributes are either same as those used for the p phase autopicker or are derivatives of those attributes. This enables faster computation of s phase picks due to lower computation times for ANN node inputs.

The mathematical description of these attributes is detailed below:

STA/LTA: The ratio of short window average and long window average energy values over the entire seismic trace under study.

$$\frac{STA}{LTA} = \frac{\sum_{i=SWL}^{i=SWU} {X_i}^2}{\sum_{i=LWL}^{i=LWU} {X_i}^2}$$

Where we have, S: small, L: large, U: upper, L: lower, W: window

Cumulative energy ratio (CER): The ratio of cumulative energy over two windows (one before and one after) about the point of evaluation with the same window size. If point of evaluation is j then we have,

$$CER_j = \frac{E_1}{E_2} = \frac{\sum_{j-ws}^{j} X_i^{\ 2}}{\sum_{j}^{j+ws} X_i^{\ 2}}$$

Where 'ws' is the window size as per predefined evaluation criteria.

Modified energy ratio (MER): This attribute is evaluated using the cumulative energy ratio and is a derivative of the short and long window averaging method discussed before. This attribute has seen use in the past with microseismic data involving appreciable noise levels.

$$MER_j = \{CER_j \times |X_j|\}^3$$

Windowed maximum: The ratio of the maximum about short windows at the point of evaluation.

$$WMR_i = \frac{\max\limits_{ll:j}|X_i|}{\max\limits_{j:ul}|X_i|}$$

Where 'll' is the lower limit and 'ul' is the upper limit of evaluation window.

Windowed variance: Calculated in similar fashion as the WMR attribute but with variance as the evaluated property in the ratio instead of the maxima.

Sliding window cross-correlation: About the evaluation point j, two small sections are extracted as per the window size. These two sections are cross-correlated and a threshold value is set for attribute extraction (normalization based on 0 (no match) to 1(perfect match) with a limiting value set for better isolation of transition phase, i.e. phase arrival).

$$W1 = X_i, i = j - ws{:}\, j$$

$$W2 = X_i, i = j{:}\, j + ws$$

$$CV_i = E[(W1 - \mu_{W1})(W2 - \mu_{W2})]$$

Where μ_{W1} and μ_{W2} are the mean values for W1 and W2 windowed data series.

Based on a limiting value (statistically evaluated from the obtained correlation values over the trace data), the lower values are further reduced and the higher values are increased using power function

$$if\, CV_i < LV, CV_i = CV_i^{\ 0.5}$$

$$else\ CV_i = CV_i^{\ 2}$$

Figure 6.6**Error! Reference source not found.** shows the ANN output (variable density plot) uperimposed on the pruned (windowed) seismic sections used in s phase picking as well as one of the ANN inputs superimposed on the corresponding seismic section. The high ANN output probability values and phase arrivals (from seismic trace) were observed which indicated the applicability of the trained ANN for s phase arrival detection. The corresponding sample attribute values indicated the usability of the selected attribute. The ANN output match was used to obtain a preliminary arrival time which was refined further based on localized information around this initial pick. Figure 3 shows two samples from the validation dataset showing one vertical and two horizontal components (from same station) along with identified p and s phase arrival locations. The validation set over which both the p and s phase arrival workflows were implemented included 12 event files with a total of approximately 720 seismic traces.

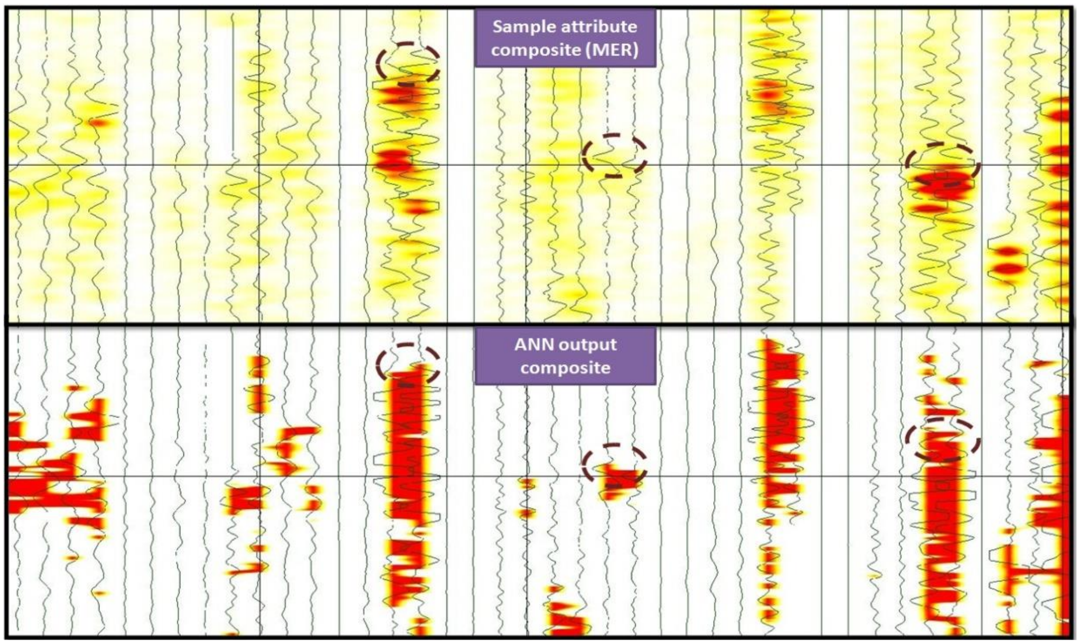

Figure 6.6: Seismic stacked section overlaid on training attribute (cross-correlation) and ANN output probability map (bottom section) highlighting some successful s phase detections

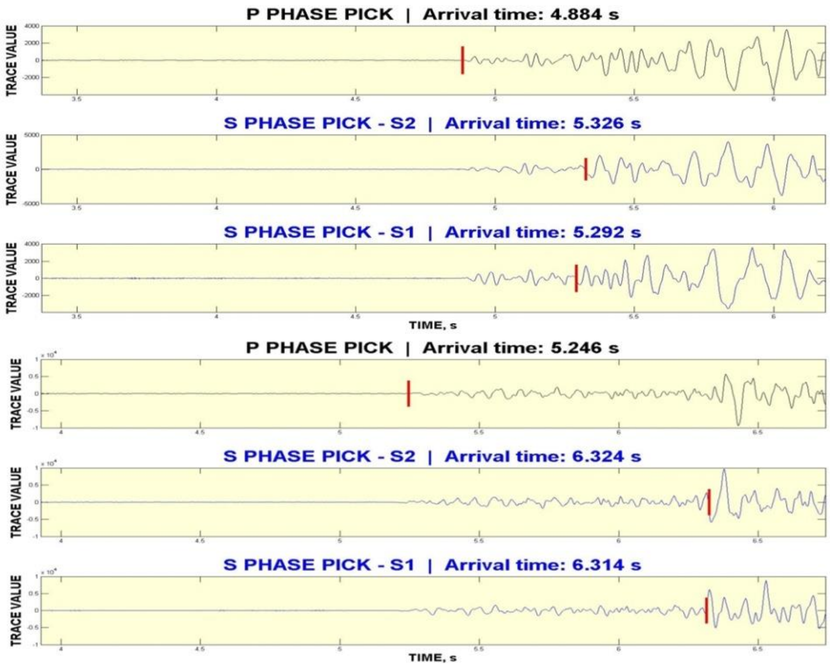

Figure 3 Two sample event windows from station AL3 with p and s phase arrivals as detected by the autopicker

6-5: Autopicker Results: comparative analysis

The validation dataset was run through an independent in house (USC) p phase autopicker as well as an advanced autopicker used by LBNL. The LBNL autopicker is designed to make p and s picks (from vertical and horizontal components respectively) and then store the best p phase and s phase picks for additional processing schemes such as inversion. The integrated autopicker developed at USC also scores the p phase and s phase picks made (Figure 6.8:) and the soundness of the scoring and selection criteria has been tested using an independent dataset used for the autopicker validation. Based on the devised selection criteria, the total number of usable p phase and s phase picks from the validation dataset have been obtained (Figure) which also shows the variation of the quality control factors obtained during independent p and s phase autopicking workflows over the entire validation dataset.

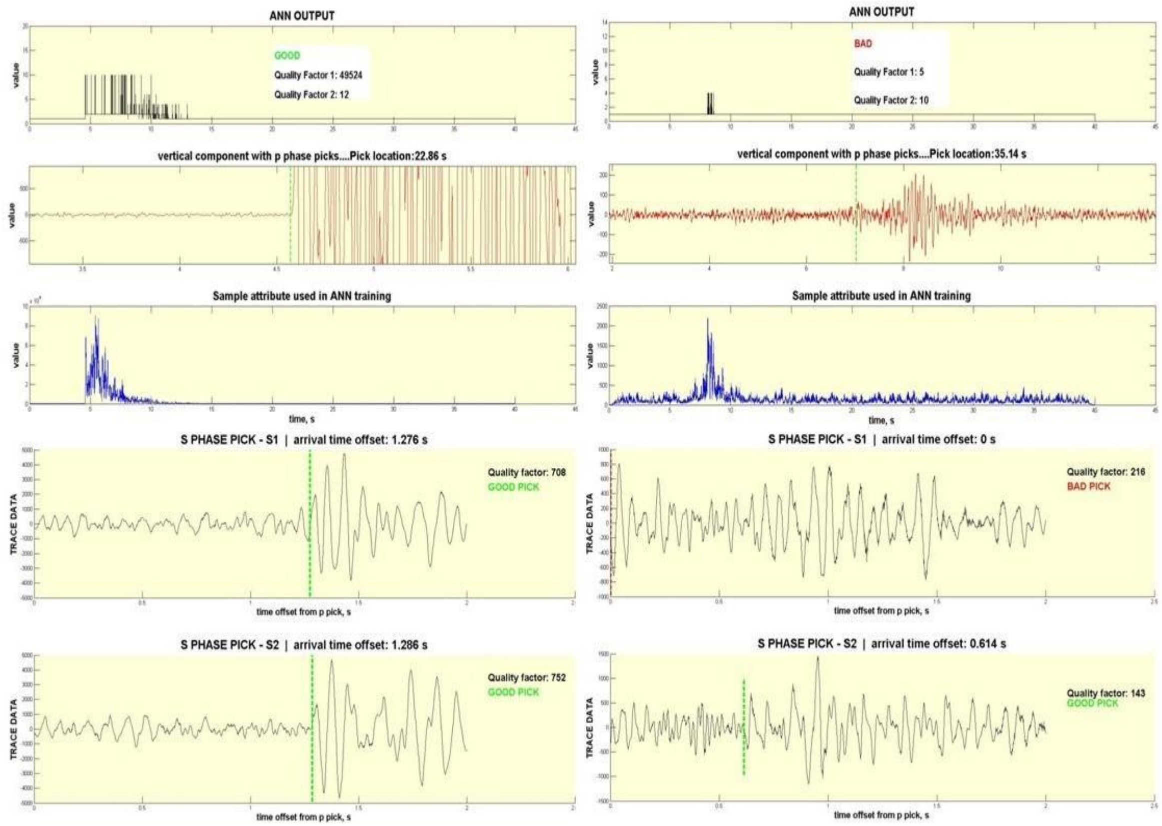

Figure 6.8: Sample p and s phase picks with quality control to remove unusable picks (both p and s phase)

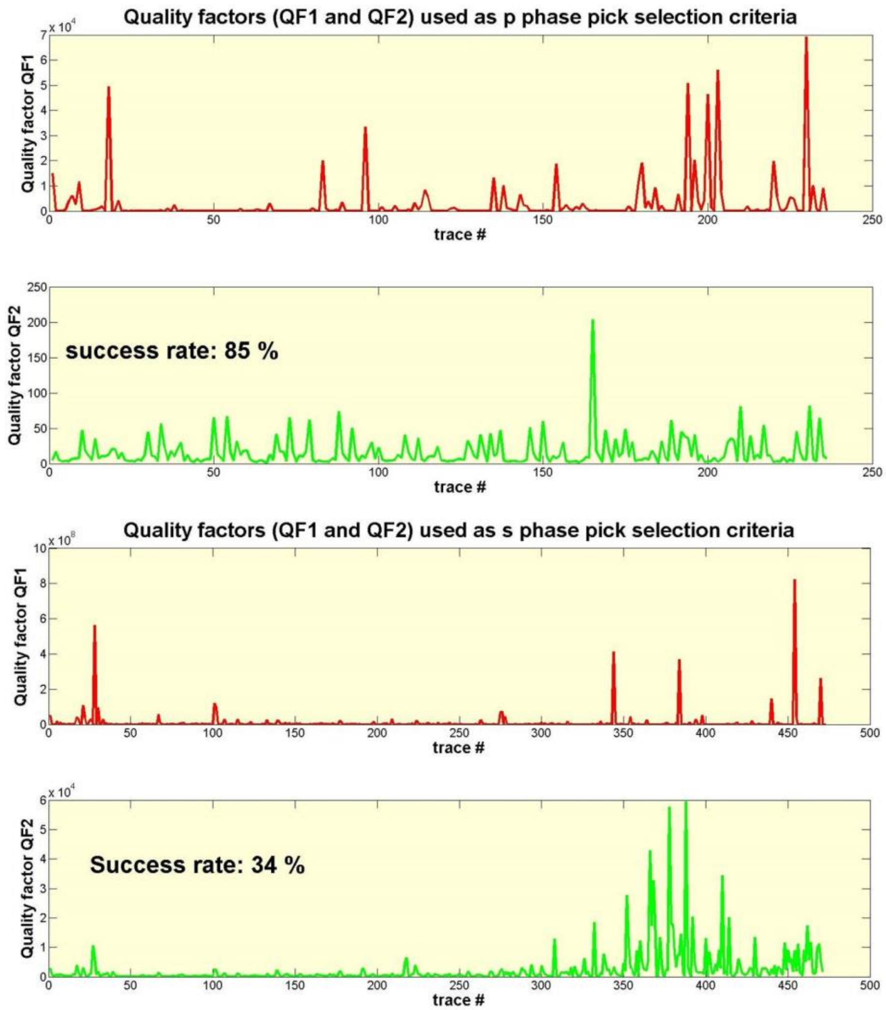

Figure 6.9: Results (successful picks) for validation set with 12 events (~720 traces). The top two graphs are for p phase autopicker (variation of quality factors with trace #) while the bottom 2 are for s phase autopicker workflow. The quality factors are combined (using cut-offs) to select usable picks

As observed a very high percentage of successful p phase picks were made but the percentage of successful s phase picks was comparatively low. This was expected as the detection of distinct s phase arrivals may or may not be possible contingent upon various factors including noise levels, phase energy, propagation effects, survey geometry, geologic factors, etc. to name a few. However, when compared with contemporary s phase autopicking algorithms under study, the results were found to be satisfactory with respect to percentage of successful picks being made as well as perceived accuracy levels. Figure 6.10: shows a comparative display of the results from two contemporary autopickers as well as the results from the designed integrated ANN autopicker. The sample cases indicated the validity of the p phase picks being made and also validate the high degree of accuracy obtained in the case of p phase arrivals.

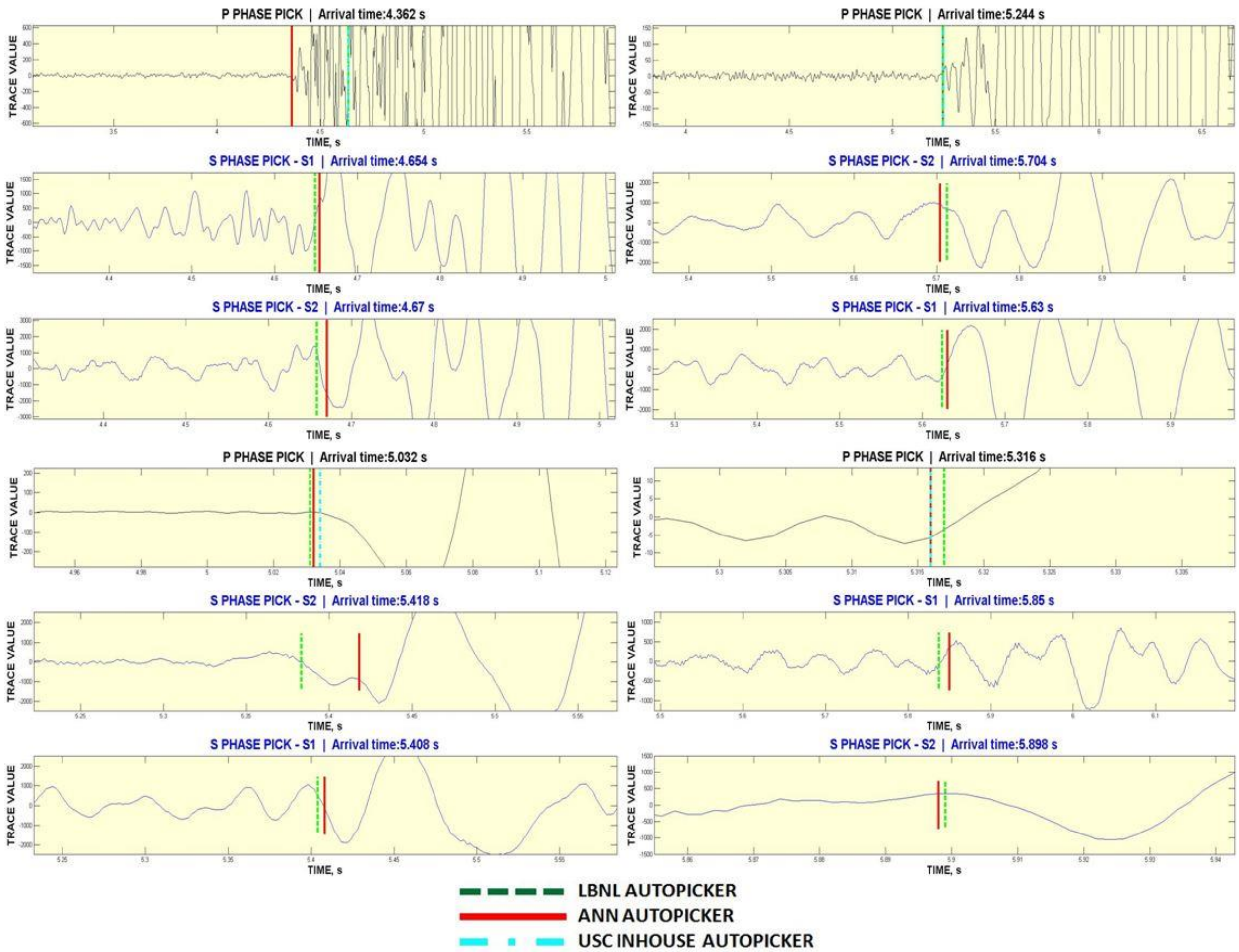

Figure 6.10: Comparison of USC autopickers (ANN as well as contemporary p phase picker) with autopicker in use with LBNL

A statistical study was conducted with the aim of looking at how close the picks being made were when compared with the contemporary autopicker. The comparison was based on an attribute which gives the maximum possible value (1) for the pick being at the same location and a minimum value (0) for picks being outside a specified window with the score decreasing exponentially. For p phase picks, a window size of 5 was chosen (which corresponds to ± 0.004 dseconds) while for s phase picks a window size of 61 (± 0.06 seconds) was decided on considering the inaccuracies associated with s phase energy arrivals as discussed before. Considering only those cases where both the contemporary (LBNL) autopicker as well as the ANN autopicker made successful picks (as per defined criteria), Figure gives an outline of the match obtained. It is believed that with the proposed use of more advanced hybrid ANN autopicker designs (as discussed in the conclusion section), the comparative window sizes can be reduced from 5 and 30 respectively. Moreover, it should also improve the percentage of total successful matches for both p and s phase arrivals.

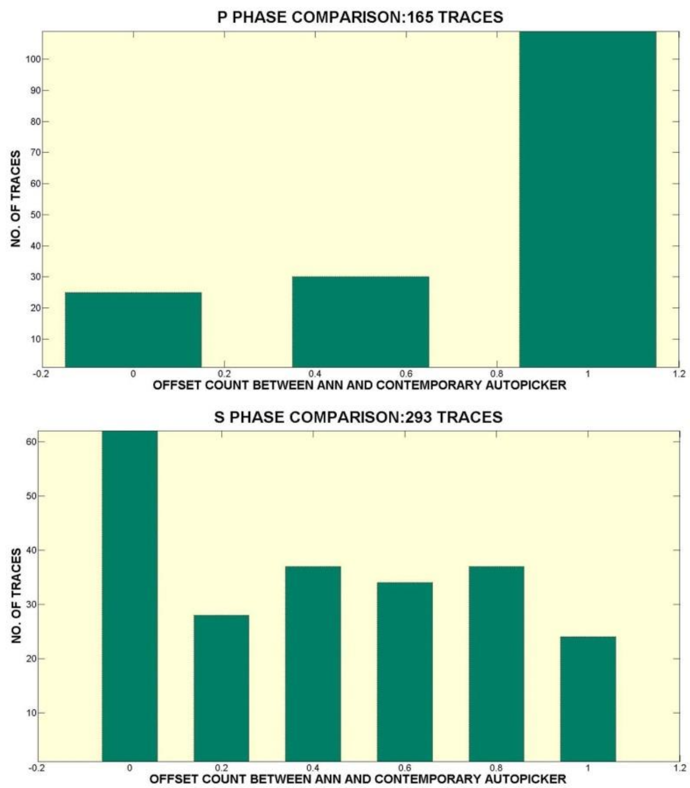

Figure 6.11: Match between ANN and contemporary (LBNL) autopicker for both p and s phase arrivals falling within specific window as per discussion. 1 implies perfect match while 0 implies no match

6-6: Validating improvement using quick inversion for location (hypoinverse)

To further validate the usefulness of the proposed approach, particularly in those scenarios where the number of available recording stations was limited, we extracted data from the minimum number of stations required for running hypoinverse (4 p and 2 s phase picks) to find out how the results varied with the contemporary autopicker and the ANN autopicking workflow. A sample set was selected from the Geysers dataset and from each of the event files, a smaller subset of stations was selected to validate the possible improvements with the new approach. The files were run through a contemporary autopicker first followed by the ANN autopicker and respective phase files were generated for use with hypoinverse (Klein, 2002). Figure 6.12: shows the hypocenters obtained for each of these individual events (a total of 8 event files were used). It is clear that with limited station coverage, the differences in the results observed were appreciable.

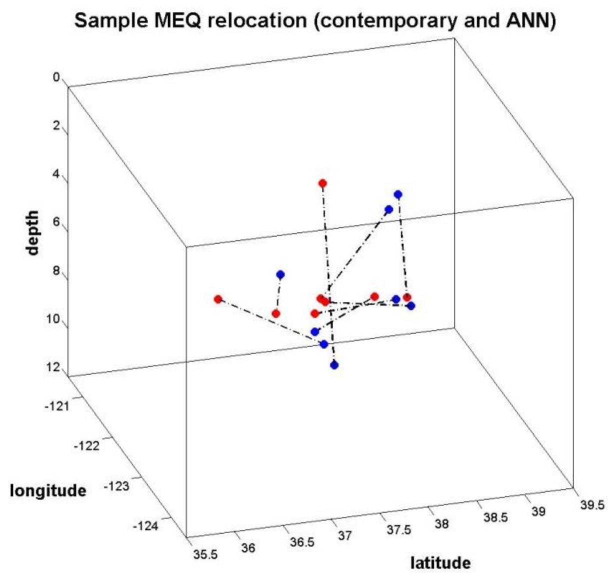

Figure 6.12: Hypocenters generated with phase cards from contemporary USC autopickers (red) and ANN autopicker (blue) indicating relocation due to changes in the detected phase arrival times with selected autopickers

Increasing the number of stations should constrain the evaluation and a better location should be possible. Comparisons with locations obtained with the LBNL autopicker (from the catalogue) should provide further validation of the said improvement and is planned for future analysis.

6-7: Future Work

Future work would involve further improvement in phase detections using a neuro-fuzzy (hybrid ANN-FL) based approach to decide on the nodal inputs to the ANN based on fuzzy inference rules. Adaptive Neuro-Fuzzy inference systems (Jang and Gully, 1995) can be used for complex pattern recognition problems as demonstrated by Nikravesh (2001). We hope to build a fuzzy inference system with optimized memberships and therefore obtain best possible results with a given set of inputs.

Apart from the new approach, we are also working on implementing the workflow in an integrated framework (Matlab environment) to have a software package which implements all of the discussed steps and generates phase files for further processing.

7- Technology Transfer and Other Accomplishments

One of the key elements of the current project is the technology transfer and public dissemination of the results. To accomplish this we have focused on three areas. They include external publications, monthly seminars and promotion of our USC Center for Geothermal Studies (CGS).

7-1: USC-Indonesia geothermal education capacity building project

As geothermal development expands worldwide, the demand for geothermal engineers and earth scientists has never been greater. Thanks to a grant from USAID, USC has joined forces with the Institute of Technology in Bandung (ITB) to expand educational opportunities in geothermal technologies in Indonesia. The US - Indonesia Education Capacity Building (USIECB) Program also provides opportunities for USC and ITB to collaborate in the development and enhancement of geothermal education programs through partnerships in Indonesia, one of the most geothermal resource-rich areas of the world. The active involvement of the industry advisory board ensures geothermal industry participation in education initiatives and coordination between academia and industry. Thanks to the success of the 2012-2013 USIECB program, USAID extended the support through 2Q 2015. Some key elements are:

- ITB-USC Geothermal Seminar and Workshops
- Teaching material for a course "Environmental Impact Assessment”
- Develop a course on “Introduction to Geothermal Systems”
- Initiation of Geothermal Research Center
- Measurements and testing course for polytechnic schools

7-2: Distinguished Lecture Program (DLP)

We strive to have a steep increase in both the quality and the volume of R&D work and in geothermal energy. We want to fully leverage our ongoing technical work in connection with the current DOE funded program (the subject of this report). We have established the new Distinguished Lecture Program (DLP). The funding for this initiative has originally been provided by a grant awarded from Research Innovation Funding from USC. Subsequent funding was provided by Ormat Technology, and more recently, by USAID, through the USC-ITB geothermal education capacity building project.

DLP has been effective in bringing experts who are either carrying out technical and applied work in geothermal energy related disciplines or their scientific work has the potential for geothermal applications. Making the program available through webinar has further expanded the reach of the project. The following is the list of our 2011, 2014 and 2015 DLP seminars:

- Seismicity at The Geysers, Katie Boyle, Lawrence Berkeley National Laboratory, February 21, 2011

- Bombs, Bears and Hot Water: Geothermal Prospecting at Mt. Spurr, Alaska, Brigette Martini, Senior Geologist, Ormat Technologies, Inc., March 23, 2011.
- Induced Seismicity: Issues and Paths Forward, Ernest Majer, Lawrence Berkeley National Laboratory, May 17, 2011.
- Advances in integrated EM for geothermal exploration, Kurt M. Strack, KMS Technologies, June 30, 2011.
- California Energy Commission’s Geothermal Program: Development of Geothermal Energy in California, Pablo S. Gutierrez, Geothermal Program, California Energy Commission, July 25, 2011.
- Geothermal Development in Indonesia, Jim Slutz, Director, Star Energy–North America, August 23, 2011.
- Advanced Seismic Imaging for Geothermal Development, John N. Louie, Professor, University of Nevada, October 06, 2011.
- Tomographic Investigation in Indonesian Geothermal fields, Rachmat Sule, Professor, Institute of Technology at Bandung Indonesia, December 2014.
- Developing an Integrated Exploration Assessment for Geothermal Systems, Joe Iovenitti, Consulting Geoscientist/Advisor to the USC Center for Geothermal Studies, January 15, 2015.
- Induced Seismicity in the Geysers Geothermal Field, California: Prati-32 Injection Test, Lawrence Hutchings, Researcher, Lawrence Berkeley National Laboratory, February 10, 2015.
- Geophysical Applications to Geothermal Resource Assessment and Their Uncertainty, William Cumming, Cumming Geoscience, March 12, 2015.
- Using the Geochemistry of Hydrothermal Fluids to Understand and Manage Geothermal Resources Exploration, Assessment, Development and Operations, Jill Haizlip, GEOLOGICA Geothermal Group, Inc., April 9, 2015

7-3: USC Center for Geothermal Studies (CGS)

The USC Center for Geothermal Studies (CGS) was established in the fourth quarter of 2010 to promote excellence in research and development with practical focus and multi-disciplinary education for geothermal energy. The Center spans different technical disciplines to deal with the operational challenges associated with geothermal energy from exploration and production to its usage and transmission in a safe and cost effective manner. The Center's aim includes developing new research programs and initiatives as well as courses and workshops and help transferring new technologies to the industry. We will facilitate multi-disciplinary research in collaboration with other institutes and departments at USC where we can identify potential applications to geothermal energy. Our website http://cgs.usc.edu provides further details about CGS and the ongoing activities.

8- External Publications

During the period of this work, we have participated in several technical conferences, including the Geothermal Resources Council (GRC), Society of Exploration Geophysicists (SEG), and American Geophysical Union (AGU) meetings as well as the DOE-sponsored peer review (Appendix 8-1) meeting and a Geothermal Energy Association (GEA) meeting. We have also submitted two papers for publication in Computer and Geosciences journal and Bulletin of the Seismological Society of America. Our publications list includes:

- **Fred Aminzadeh, Debotyam Maity, and Tayeb A. Tafti, 2013, An integrated methodology for sub-surface fracture characterization using microseismic data: A case study at the NW Geysers, Computer and Geosciences 54, 39-49.**

Abstract

Geothermal and unconventional hydrocarbon reservoirs are often characterized by low permeability and porosity. So, they are difficult to produce and require stimulation techniques, such as thermal shear deactivation and hydraulic fracturing. Fractures provide porosity for fluid storage and permeability for fluid movement and play an important role in production from this kind of reservoirs. Hence, characterization of fractures has become a vitally important consideration in every aspect of exploration, development and production so as to provide additional energy resources for the world. During the injection or production of fluid, induced seismicity (micro-seismic events) can be caused by reactivated shears created fractures or the natural fractures in shear zones and faults. Monitoring these events can help visualize fracture growth during injection stimulation. Although the locations of microseismic events can be a useful characterization tool and have been used by many authors, we go beyond these locations to characterize fractures more reliably.
Tomographic inversion, fuzzy clustering, and shear wave splitting are three methods that can be

applied to microseismic data to obtain reliable characteristics about fractured areas. In this article, we show how each method can help us in the characterization process. In addition, we demonstrate how they can be integrated with each other or with other data for a more holistic approach. The knowledge gained might be used to optimize drilling targets or stimulation jobs to reduce costs and maximize production

- **Tayeb A. Tafti, Muhammad Sahimi, Fred Aminzadeh, and Charles G. Sammis, 2012, Using Microseismicity to Map the Fractal Structure of the Fracture Network at The Geysers Geothermal Field in California, Bull. Seism. Soc. Am., submitted for publication.**

- **Tayeb A. Tafti and Fred Aminzadeh, 2011, Application of high-resolution passive seismic tomographic inversion and estimating reservoir properties, AGU Fall Meeting, San Francisco, CA**
- **Tayeb A. Tafti and Fred Aminzadeh, 2011, Fracture characterization at the geysers geothermal field using time lapse velocity modeling, fractal analysis and microseismic monitoring, Geothermal Resources Council Transactions, Vol. 35, pp. 547-551.**
- **Fred Aminzadeh, Debotyam Maity, Tayeb A. Tafti, and Friso Brouwer, 2011, Artificial neural network based autopicker for micro-earthquake data, In: SEG Annual Meeting. pp. 1623-1626.Link:** http://library.seg.org/doi/pdf/10.1190/1.3627514.

Aim: To develop a p and s phase autopicker with improved resistance to noise and increased applicability across different data sources.
Method: An artificial neural network (ANN) based approach is used with different attributes defined and selected for use as node inputs and results verified with contemporary autopickers.
Use: Useful in situations where MEQ data is collected including unconventional reservoir developments such as hydraulic fracturing schemes, geothermal settings, etc.
Observations: Good match with contemporary autopickers and improved applicability with higher applicability in situations where contemporary autopickers fail.

Our Geysers papers as well as seismology advances derived from or associated with The Geysers work or which The Geysers led to are listed below and are available at http://gen.usc.edu/publication/**:**

- **Characterizing Fractures in Geysers Geothermal Field by Micro-seismic Data Using Soft Computing, Fractals, and Shear Wave Anisotropy**

Characterizing Fractures in Geysers Geothermal Field by Micro-seismic Data, Using Soft Computing, Fractals, and Shear Wave Anisotropy

Fred Aminzadeh[1,2], Tayeb Ayatollahy Tafti[1]
[1]Department of Petroleum Engineering, [2]Energy Institute
University of Southern California, Los Angeles, CA 90089-1211, USA

Introduction

Developing improved methods to better characterize fractures in Enhanced Geothermal System (EGS), new methodologies to characterize geothermal reservoir northwest part of the Geysers, and gain better knowledge of their porosity, permeability, fracture size, fracture spacing and reservoir discontinuities (faults and shear zones) is the main objective of our research team. This will be accomplished by creating a 3-D seismic velocity model of the field using the microseismic data. Exploiting the anisotropic and fractal nature of the rocks gives better understanding the fracturing system. In addition soft computing is used for processing and analyzing the passive data.

Predicting characteristics of fractures and their orientation prior to drilling new wells, also determining location of fractures, spacing and orientation during drilling, as well as characterizing open fractures after simulation help identify the location of fluid flow pathway within the EGS reservoir.. These systems are created by injecting water, and stimulating fracture development in hot wet rocks, and hot dry rocks. The fractures thus created enhance the permeability of the hot rock formations, thus enabling better circulation of water for the purpose of producing the geothermal resource. Better understanding the mechanisms for fracture stimulation can be used to obtain more information for a better exploitation of geothermal resources of the Geysers field (Sonoma County, California) and other similar fields.

Micro-seismic data analysis both for compressional waves and shear wave using soft computing, anisotropic inversion and fractals can be used to develop and test new data collection analysis techniques. This enables us to analyze and interpret micro-seismic data and create velocity fields using tomography. Neuro-fuzzy approach can be used to create a hybrid MEQ event picking.

Process Charts

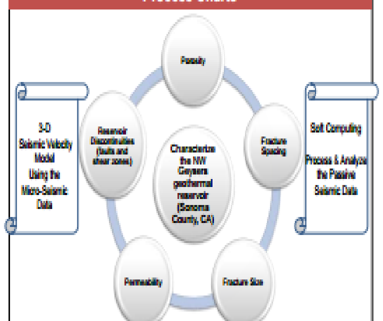

Scheduled Tasks

- Use of the augmented receiver network in the NW Geysers.
- Develop a 3-D seismic velocity model beneath the largely-undeveloped 10 sq. mile area of NW Geysers where Calpine is proposing further development.
- Use the 3D velocity field, constructed based on them, to create a fracture map and monitor low-level micro-seismicity occurring in response to deep, low-rate water injection, in order to precisely locate and characterize fracturing occurring in response to injection into the deep high temperature reservoir.

Geologic Cross-Sections of the Geysers

The seismicity data is overlaid with an approximate temperature distribution. The more pronounced distribution of seismicity below and around the injection wells is noticeable.

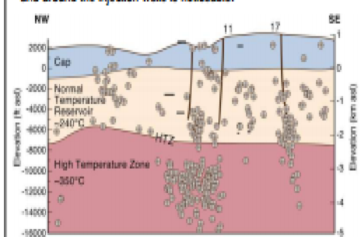

Figure 1 - NW-SE cross-section through The Geysers geothermal field showing 2002 MEQ hypocenters, injection wells, power plants, and top of the high temperature zone (HTZ) (Stark, 2003).

Using Microseismicity to Map the Fractal Structure of the Fracture Network

Field observations (Stark, 2003) and geomechanical modeling (Rutqvist and Oldenburg, 2007) have concluded that injection-induced seismicity at the Geysers geothermal field is the result of shear failure on critically stressed fractures caused by the reduction of normal stress associated with thermal contraction. It follows that a spatial analysis of the locations, sizes, and source mechanism of induced events may reveal the structure of the fracture network in the Geysers reservoir. The basic assumptions are that the hypocenters are located on the fractures, that larger events occur on larger fractures, and that the source mechanism constrains the orientations of the activated fractures.

Collaborating with the geomechanical group at Berkeley to use their models to simulate the expected response of a fractal network to the thermal stresses generated by injection.

Location of EGS Candidate Well

Only surface and near-surface faults in the reservoir cap rock are reasonably well characterized by lithology. The more subtle faults and fractures (in the massive graywacke reservoir rock) that will require application of soft computing based techniques, exploiting their anisotropic and fractal behavior that help their identification and mapping. (Figure 2)

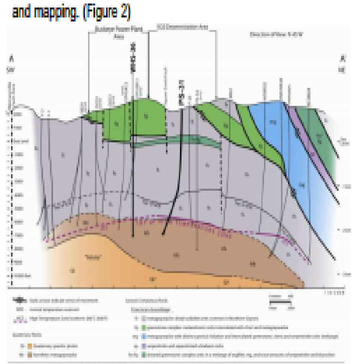

Figure 2 - Geologic cross-section of The Geysers and location of EGS candidate well Prati State 31 (PS-31). – From Calpine-LBL proposal (FOA DE-PS36-08GO98008).

Anisotropic Velocity Tomography

The location of MEQs events may delineate the locations of new subsurface fractures and fracture zones. The location of these MEQs depends upon an accurately known distribution of subsurface seismic velocities (both P and S). These velocity fields must include accurate distributions of seismic anisotropy. For this purpose the following steps should be performed:

1. Form initial isotropic P-velocity field, MEQs locations are determined.
2. The error-ellipsoids for each location are calculated.
3. Refinements to the velocity field are driven by these error-ellipsoids.
4. Refined error-ellipsoids for each location are calculated.
5. A lower symmetry of anisotropy is selected (eg,Tilted orthorhombic)
6. Refinements to the anisotropic velocity field (ie distributions of anisotropic parameters) are driven by the error-ellipsoids.
7. Refined error-ellipsoids for each location are calculated.
8. Steps 5-8 are repeated until no significant further precision in the locations is achieved.

If data quality permits, the distribution of S-wave anisotropic parameters can be estimated, following a similar program but also taking advantage of the special phenomena of shear-wave splitting.

Use of Soft Computing to analyze passive seismic data

Soft computing (including neural networks, fuzzy logic and genetic algorithms) has been used extensively in geosciences and energy related applications. Yet, very few such applications could be found for exploration and exploitation of geothermal resources. seismology and soft computing is less commonly used in geothermal and mineral exploration and development, but has great potential for growth; pioneering work has proven valuable in mapping mineral deposits. The challenge is to adapt the vast body of work on soft computing applications to seismic data from the petroleum industry, adapting it to non-layered and steeply dipping targets in metamorphic and crystalline rocks found in most geothermal fields. Imaging and microearthquake monitoring holds great potential for geothermal energy exploration and production.

Careful analysis of the MEQ and microseismic data in the Geyser field and using the power of neuro-fuzzy approach in the processing of the MEQ data and in developing a mathematical framework for the velocity fields may result to develop a more practical velocity field. Using the neuro-fuzzy approach as described in Aminzadeh and Brouwer (2006) helps with the automation process and its improvement of picking MEQ seismic events. Handpicked events in selected seed points will be used as the training set for the neuro-fuzzy auto-picker. The results are compared against the current auto-picker being used by LBL as well as the picks by human. We expect our hybrid approach become superior in both ability to pick the subtle events and the efficiency of the process.

Fuzzy Compressional and Shear Wave Velocity Relationship

Given the usually poor quality of microseismic data, simultaneous analysis of S and P wave data to deduce information on shear wave splitting from fractured reservoirs is usually difficult. Aside from the compressional velocity fields, looking into the shear wave velocities and the fuzzy relationship between those velocities for different rock types may be necessary.

Figure 3 shows the fuzzy nature of the velocities for different rock categories. And also demonstrates the impact of fuzziness in P-wave and S-wave velocities in the separation of different rock types according to their respective S and P wave impedances. Developing a "fuzzy velocity" field, extrapolate and validate the velocity field from microseismic data measurements by using a large number of well data from the existing wells, in conjunction with the analysis of MEQ data . Reservoir characterization with fuzzy velocities can be examined.

Utilizing various neural - network - based approaches can be applied to better understand the fracturing system, as applied to

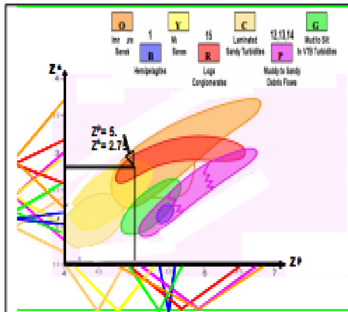

Zp=5, Zs=2.75

$\mu_{sand,immature} = 0.13$, $\mu_{sand,mature}=0.5$, $\mu_{conglomerate}=0.37$

Figure 3 - Impact of fuzziness in P-wave and S-wave velocities in the separation of different rock types

conventional seismic data, adapting them to those from geothermal fields. Specifically, examining the use of different seismic attributes such as similarity, eccentricity, and curvature for fracture modeling and interpretation may be helpful. One such example is where a hybrid neural network and fuzzy logic approach is used to create a more reliable reservoir map. This approach can be extended to examine and analyze the microseismic data acquired in the course of this project and develop an accurate fracture map for the area.

Acknowledgements

This project is a joint effort by USC, Calpine Energy and Lawrence Berkeley National Laboratories. We acknowledge important contributions from Mark Walters and his team at Calpine, as well as Ernie Majer, and Leon Thomsen of LBNL. We also acknowledge contributions from our USC colleagues: Iraj Ershaghi, Don Paul, Muhammad Sahimi and Charles Sammis.

References

- Aminzadeh, F. and Brouwer, F. Integrating neural networks and fuzzy logic for improved reservoir property prediction and prospect ranking. Extended Abstracts of Society of Exploration Geophysicist Annual Meeting in New Orleans, 2006.
- Rutqvist, J. and Oldenburg, C., Analysis of cause and mechanism for injection-induced seismicity at the geysers geothermal field, California, Annual Meeting of the Geothermal Resources Council, 31, 441-445, 2007.
- Stark, M., Seismic evidence for a long-lived enhanced geothermal system (EGS) in the northern geysers reservoir, Annual Meeting of International Collaboration for Geothermal Energy in the Americas - Geothermal Resources Council, 27, 727-731, 2003.

- **Characterizing Fractures in Geysers Geothermal Field using Soft Computing**

Abstract
Developing improved methods to better characterize fractures in Enhanced Geothermal System (EGS), new methodologies to characterize geothermal reservoir northwest part of The Geysers, and gain better knowledge of their porosity, permeability, fracture size, fracture spacing and reservoir discontinuities (faults and shear zones) is the main objective of this article. In addition, soft computing is used for processing and analyzing the microseismic events.

Some of these fracture systems are created by injecting water, and stimulating fracture development in hot wet rocks, and hot dry rocks. The fractures thus created enhance the permeability of the hot rock formations, enabling better circulation of water for the purpose of producing the geothermal resource. Better understanding of the mechanisms for fracture stimulation leads to a better exploitation of geothermal resources. Our initial test bed for the newly developed methods will be The Geysers field located in Sonoma County, California to be followed by application to other fields with similar sub-surface characteristics.

Careful analysis of the MEQ data in The Geysers field by unleashing the power of neuro-fuzzy approach for the processing of the MEQ data can provide us with a mathematical framework to develop a more practical velocity field. Further, we demonstrate that utilizing various neural-network-based approaches also leads to a better understanding of the fracturing system. This will be accomplished by adapting some of the attributes of the conventional seismic data used in the oil and gas exploration and production to similar activities in geothermal fields. Some of such seismic attributes we would like to examine include similarity (coherency), eccentricity, and curvature to carry out fracture modeling analysis and interpretation.

Micro-earthquake (MEQ) data analysis both for compressional waves and shear waves, with the aid of soft computing and fractal techniques, demonstrate the versatility and flexibility of the methods. This enables us to analyze and interpret subtle micro-seismic data effectively. We also show the use of Neuro-fuzzy approach for a hybrid MEQ event picking.

Finally, hybrid neural network and fuzzy logic approach is used to create a more reliable reservoir map. This approach extended to examine and analyze the microseismic data acquired in this article and develop an accurate fracture map for the area. Handpicked events in selected seed points are used as the training set for the neuro-fuzzy auto-picker. Our hybrid approach becomes superior in both ability to pick the subtle events and the efficiency of the process.

- **Analysis of Microseismicity using Fuzzy Logic and Fractals for Fracture Network Characterization**

Analysis of microseismicity using fuzzy logic and fractals for fracture network characterization

Fred Aminzadeh[1,2] Tayeb A. Tafti[1,2] Debotyam Maity[1,2], Katie Boyle[4], Charles Sammis[2,3], Muhammad Sahimi[1,2]

[1]Department of Petroleum and Chemical Engineering, [2]Center for Geothermal Studies, [3]Earth Sciences Department
University of Southern California, Los Angeles, CA 90089, USA
[4]Lawrence Berkeley National Laboratory
Berkeley, California, 94720, USA

Abstract

Microseismic (MEQ) event occurrence may be correlated with the fracture network at a geothermal field. If certain mechanisms are operative, cluster of the MEQ events should represent a connected fracture network. Drilling new EGS wells (both injection and production wells) in these locations may facilitate the creation of an EGS reservoir.

Here, we use fuzzy clustering to locate the fracture networks in the Geysers field. We show how the cluster centers move in time, representing fracture propagation or fluid movement within the fracture network. We also conduct fractal analysis to develop an accurate fracture map for the reservoir. Combining the fuzzy clustering results with the fractal analysis allows us to better understand the mechanisms for fracture stimulation and better characterize the evolution of the fracture network.

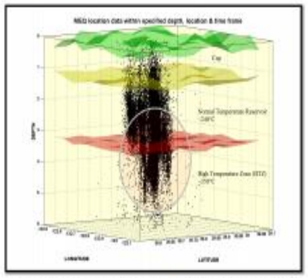

Figure 1 - 3D Distribution of microseismic events at The Geysers for the years 2006 to 2009

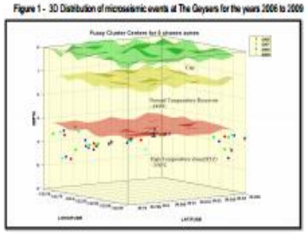

Figure 2 - Fuzzy cluster centers for all the years at the HTZ zone.

Fuzzy Clustering

Soft computing (fuzzy logic, neural networks, genetic algorithms) has been used extensively in geosciences and energy-related applications, yet few have been for exploration and exploitation of geothermal resources. Fuzzy clustering of the microseismic events in both discrete time windows and locations leads into accurate fracture map for the area. Careful review of the time windows of each specific location also demonstrates the fracture network propagation direction.

We consider four mechanisms to explain the occurrences of these MEQ events in a geothermal field. Those are the pore-pressure increase, the temperature change, the volume change due to fluid withdrawal/injection and the chemical alteration of fracture. Then, the area where the large number of MEQ events occur have a good correlation with of the fracture network in the geothermal field.

A viable geothermal reservoir, requires a large aerial distribution of fracture network. Clusters of the MEQs could represents a connected fracture network (Figure 1). Cluster centers show significant movement at the HTZ (Figure 2). Direction of arrows indicate the direction of movement of MEQ clusters over time. We believe this may represent the fracture network propagation direction (Figure 3). Large movements may be related to a faulting mechanism. Consequently, as it is shown in Figure 10, we have created a recommended drilling program for the injection and production wells, corresponding to the arrows with acceptable size and direction.

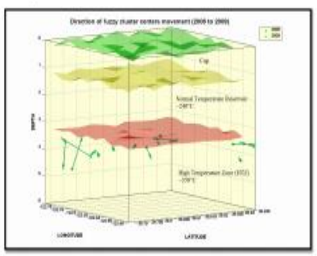

Figure 3 - Fuzzy cluster center movement from 2006 to 2009

Fractal Analysis

Name of Cluster	b-Value	Fractal Dimension	Number of events
Whole Study area	1.32	2.59	11407
(-.2-1.1)M		2.59	8433
(1.1-4.3)M		2.49	4012

Name of Cluster	b-Value	Fractal Dimension	Number of events
Region 1		2.23	698
Region 1 (-.2-1.1)M		2.22	517
Region 1 (1.1-4.3)M		2.18	199

Name of Cluster	b-Value	Fractal Dimension	Number of events
Region 2	1.36	2.65	8787
Region 2 (-.2-1.1)M		2.64	6541
Region 2 (1.1-4.3)M		2.53	3030

Name of Cluster	b-Value	Fractal Dimension	Number of events
Region 2-1	1.35	2.6	1556
Region 2 -1(-.2-1.1)M		2.53	1229
Region 2 -1(1.1-4.3) M		2.49	493

Name of Cluster	b-Value	Fractal Dimension	Number of events
Region 2-2	1.54	2.58	2404
Region 2 -2(-.2-1.1) M		2.49	1799
Region 2 -2(1.1-4.3) M		2.41	844

Name of Cluster	b-Value	Fractal Dimension	Number of events
Region 2-3	1.32	2.52	3326
Region 2 -3(-.2-1.1) M		2.51	2391
Region 2 -3(1.1-4.3) M		2.41	1220

Name of Cluster	b-Value	Fractal Dimension	Number of events
Region 2-4	1.15	2.27	1323
Region 2 -4(-.2-1.1) M		2.3	1006
Region 2 -4(1.1-4.3) M		2.1	419

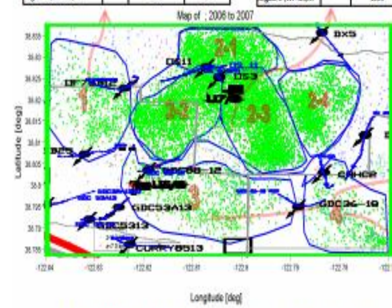

Figure 4 – Seismicity map for 2006 events in the study area at The Geysers geothermal field. (2map)

Name of Cluster	b-Value	Fractal Dimension	Number of events
Region 3	1.32	2.55	860
Region 3 (-.2-1.1)		2.41	529
Region 3 (1.1-4.3)		2.44	404

Name of Cluster	b-Value	Fractal Dimension	Number of events
Region 4	1.16	1.73	477
Region 4 (-.2-1.1)		1.77	298
Region 4 (1.1-4.3)		1.87	219

Green Rectangular

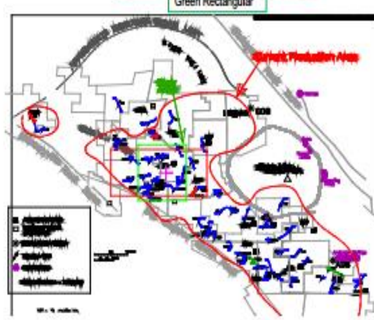

Figure 5 – The Geysers map and locations of the study areas. The map is modified from original one which is provided by Joseph Beall from Calpine

Seismicity has fractal structures in space and magnitude distributions, as articulated by the fractal dimension *D*, and the *b* value. The fractal dimensions are calculated using the correlation integral. And b-value is the slope of the frequency-magnitude relationship, and predicted by the maximum curvature method.

The results illustrate that the relation $D=2b$ between the *b* value and the fractal dimension *D* of fracture planes, is valid in the seismicity distribution at The Geysers geothermal field. Fractal dimension of 2.5 and b-value of about 1.25 on most regions of seismicity distribution also is another indicator of the induced seismicity at The Geysers as opposed to a tectonic event where fractal with fractal dimension of 2.

This result is further proof for our hypothesis that cluster of the MEQs represents a connected fracture network at The Geysers.

Conclusions

Fuzzy logic can be helpful in analyzing the MEQ data, especially when dealing with the weak events. As an example, fuzzy clustering technique was used to find the most likely and significant location of the fracture networks. The cluster centers may represent the locations of drilling new EGS well. These centers probably are the centers of the connected fracture network which is ideal for creating a geothermal reservoir.

The fractal dimension and b-value analysis also illustrate the behavior of the MEQ events at The Geysers. Comparing the fractal dimension and b-value of tectonic events with these events further prove that cluster of MEQevents could represent the connected fracture network.

The relationship between b-value and fractal dimension is also verified in this article with real data from NCEDC.

We are hopeful that our new findings can be tested by actual drilling. Once confirmed, hopefully such new applications of soft computing will find their use in the exploration and exploitation of geothermal resources in the future.

Acknowledgements

We acknowledge important contributions from Ernie Majer of LBNL. We also acknowledge contributions from Mark Walters and Joseph Beall at Calpine.

References

Aminzadeh, F. and Brouwer, F. Integrating neural networks and fuzzy logic for improved reservoir property prediction and prospect ranking. Extended Abstracts of Society of Exploration Geophysicist Annual Meeting in New Orleans, 2006.
Rutqvist, J. and Oldenburg, C., Analysis of cause and mechanism for injection-induced seismicity at the geysers geothermal field, California, Annual Meeting of the Geothermal Resources Council, 31, 441-445, 2007.
Beall, J. J., Wright, M. C., Pingol, A. S., & Atkinson, P. (2010). Effect of High Rate Injection on Seismicity in The Geysers. *Geothermal Resources Council Transactions*, *34*, 1203-1208.

- **Integrated Workflow for Characterizing Fracture Network in Unconventional Reservoirs using Microseismic Data**

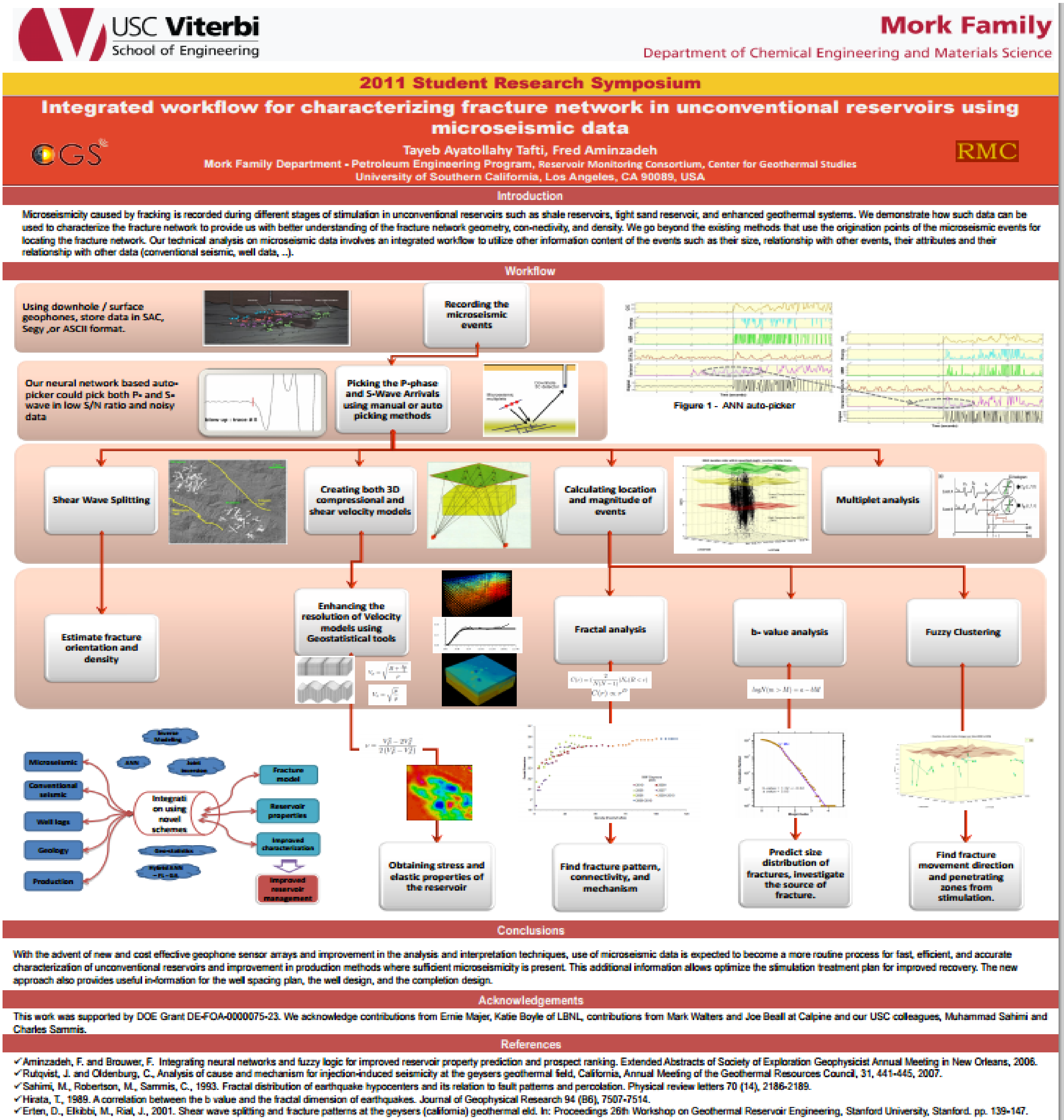

- **Artificial Neural Network based Autopicker for Microearthquake Data**

  Aim: To develop a p and s phase autopicker with improved resistance to noise and increased applicability across different data sources.
  Method: An artificial neural network (ANN) based approach is used with different attributes defined and selected for use as node inputs and results verified with contemporary autopickers.
  Use: Useful in situations where MEQ data is collected including unconventional reservoir developments such as hydraulic fracturing schemes, geothermal settings, etc.
  Observations: Good match with contemporary autopickers and improved applicability with higher applicability in situations where contemporary autopickers fail.

- **Reservoir Characterization of an Unconventional Reservoir by Integrating Microseismic, Seismic, and Well Log Data**

SPE 154339

Reservoir Characterization of an Unconventional Reservoir by Integrating Microseismic, Seismic, and Well Log Data

D. Maity, and F. Aminzadeh, SPE, University of Southern California

This paper was prepared for presentation at the SPE Western Regional Meeting held in Bakersfield, California, USA, 19–23 March 2012.

Abstract

Varied data types including geophysical data as well as well logs have been used frequently in the past to characterize reservoirs. However, the use of microseismic data as a potential source of useful information and its integration with conventional seismic data for reservoir characterization is an area of opportunity where properties predicted from the microseismic data can be used as a vital source of information which can then be tied with the overall characterization scheme in a seamless manner.

In this paper we discuss the characterization scheme followed for an unconventional reservoir associated with a promising geothermal prospect. The field involves microseismic data acquisition being done continually as part of the field monitoring operations and extensive well control due to the presence of large number of injection and production wells and finally a 3D conventional seismic survey done to try and better define the reservoir. We have applied an integrated approach with these data sources in order to better characterize the reservoir in question using novel data analysis schemes where necessary to get optimum results.

The approach shared in this paper can be applied to any type of reservoir setting with microseismic, seismic and well log data being available. What we present is a workflow to integrate these data types to generate useful property predictions including important rock property estimates with the aim of obtaining useable reservoir property maps to aid in reservoir development. This approach shows how a modest data acquisition program can still lead to useful characterization of reservoirs particularly with the inclusion of microseismic data in the workflow. We have used novel methods as part of our workflow including multi-attribute analysis, geostatistical techniques and soft computing techniques such as ANN[1] based property prediction and mapping which are discussed in brief.

Keywords: reservoir, characterization, microseismic, seismic, well logs, ANN, fracture

- **Framework for Time Lapse Fracture Characterization using Seismic, Microseismic & Well Log data**

  Abstract
  Extensive work has been done in the recent years involving use of conventional and passive seismic data for fracture characterization. This is particularly the case with unconventional reservoirs such as shale gas, shale oil and geothermal fields. The purpose of our study is to combine the benefits of conventional seismic data that provides relatively higher resolution reservoir characteristics with the relatively low resolution property estimates available from inversion of micro-earthquake data. Given the lower cost of the latter, we propose a cost effective dynamic reservoir characterization approach using a self- sustaining evaluation framework. The resulting time lapse fracture characterization technique is most suitable for those developments which involve the use of low cost passive seismic data acquisition arrays for reservoir monitoring. Our proposed method should allow for optimal use of microseismic data generated as part of passive seismic arrays common in unconventional field developments and thereby provide time lapse reservoir property predictions without having to carry out relatively expensive 4D seismic surveys.

- **Fracture Network Interpretation Through High Resolution Velocity Models: Application to the Geysers Geothermal Field**

  Abstract
  Steam at many geothermal fields including The Geysers is produced from a network of fractures in crystalline rocks. Some of these fracture networks have been created by injecting cool water into the hot rock while others are natural tectonic fractures associated with the nearby San Andreas Fault plate boundary. Due to very low permeability of the formation matrix in The Geysers reservoir, production depends on the presence of these natural or induced fractures. Hence, locating and characterizing fracture networks is of vital importance. During injection of water, newly created fractures induce microseismic events. A small number of triggered seismicity could also be created from fault failures. Although pinpointing the locations of microseismic events is a useful characterization tool, we go beyond the simple locations identification to characterize fractures more reliably.

  We apply tomographic inversion to the microseismic data to obtain high resolution compressional (P) and shear (S) wave seismic velocity volumes of the area of interest. We show how these velocity models can help us in characterization process. In addition, we demonstrate how P and S velocity volumes can be integrated with each other or with other data sets to derive additional reservoir property volumes. Such additional information can then be used to optimize injection schedule, improve the production rates or locating the potential zones for enhanced geothermal systems.

- **Use of Microseismicity for Determining the Structure of the Fracture Network of Large-Scale Porous Media**
- **Integrated Reservoir Characterization for Unconventional Reservoirs using Seismic, Microseismic and Well Log Data**
- **Integrated Fracture Characterization And Associated Error Evaluation Using Geophysical Data For Unconventional Reservoirs**

Integrated Fracture Characterization and Associated Error Evaluation Using Geophysical Data for Unconventional Reservoirs*

Debotyam Maity[1], Qiaosi Chen[1], and Fred Aminzadeh[1]

Search and Discovery Article #41142 (2013)**
Posted June 30, 2013

*Adapted from extended abstract prepared in conjunction with oral presentation given at Pacific Section AAPG, SEG and SEPM Joint Technical Conference, Monterey, CA, April 19-25, 2013

[1]University of Southern California, Los Angeles, CA (maity@usc.edu)

Abstract

This study discusses a new workflow for fracture characterization using microseismic and seismic data along with independent reservoir information (such as well log data). The framework is ideally suited for unconventional environments such as Monterey Shale where modern technologies such as the use of hydraulic fracturing and passive seismic monitoring allow application of the proposed workflow.

In this article, we demonstrate how reservoir property estimates can be made from such studies by using an artificial neural network (ANN) based property modeling approach to independently combine the different properties estimated from passive seismic data (such as phase velocities and associated rock properties) as well as property maps obtained from conventional seismic data using attribute analysis. New fracture identifier properties have been defined and the models have been used to characterize fracture zones, reservoir connectivity and reservoir compartmentalization for a representative unconventional reservoir. Production/injection trends have been used to validate the said observations. In order to circumvent the issue of data with multiple scales (low resolution passive and high resolution active data), Sequential Gaussian Simulation (SGS) has been used to improve the final property estimates and independently, error analysis has been carried out to better quantify the final results and enhance definition of the uncertainties in the analysis and interpretations made.

The proposed method allows for improved understanding of shale and other unconventional reservoirs through fracture mapping (Figure 1) and provides a workflow for improved volumetrics of the reservoir through the use of reservoir simulators and history matching. It also provides a valuable framework for pseudo 4D characterization where a single 3D seismic survey can be used as the basis to characterize the reservoir in time lapse fashion using new information collected in time through passive seismic data as well as new well logs being obtained.

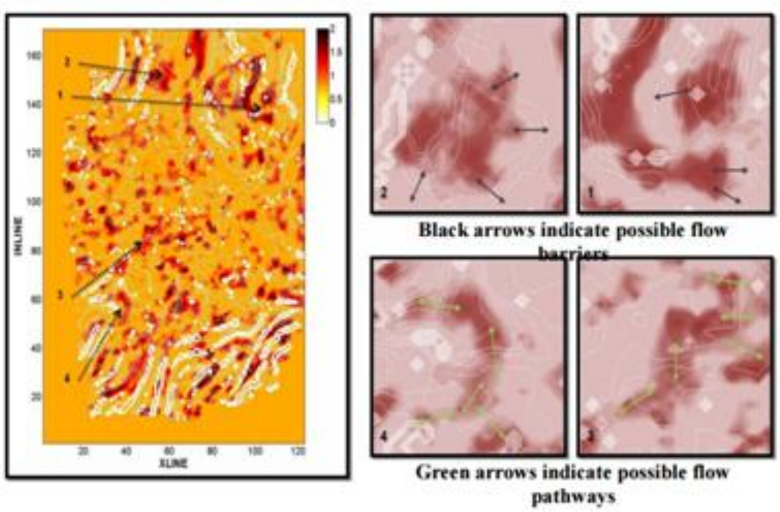

Figure 1. Fracture Zone Identifier (FZI) attribute and edge discontinuity maps (1000 m from reference) with reservoir connectivity analysis.

- **Fracture Characterization in Unconventional Reservoirs Using Active and Passive Seismic Data With Uncertainty Analysis Through Geostatistical Simulation**

SPE 166307

Fracture Characterization in Unconventional Reservoirs using Active and Passive Seismic Data with Uncertainty Analysis through Geostatistical Simulation

D. Maity, and F. Aminzadeh, SPE, University of Southern California

This paper was prepared for presentation at the SPE Annual Technical Conference and Exhibition held in New Orleans, Louisiana, USA, 30 September–2 October 2013.

Abstract
This study discusses a new workflow for fracture characterization and modeling using geophysical (microseismic and 3D surface seismic) data along with independent reservoir information (such as well logs). The framework is ideally suited for unconventional environments such as shale and tight reservoirs where modern technologies such as the use of hydraulic fracturing and passive seismic monitoring allow application of the proposed workflow.

The workflow involves generating geomechanical property estimates (including stress and weakness estimates) as derived from passive seismic data analysis and relevant seismic attributes derived from 3D seismic data combined using ANN based reservoir property modeling framework. The training information for the networks is generated based on a-priori information through image logs. Resolution of passive seismic derived velocity models is improved by using sequential Gaussian co-simulation by combining low resolution velocity maps high resolution seismic impedance data for phase velocity estimation. Uncertainty estimates are quantified by adequate number of realizations and associated probability density functions for fracture properties within study volume.

In this paper, different properties estimated through ANN modeling have been shared. New fracture identifier (FZI) properties have been defined and the models have been used to characterize fracture zones and major discontinuities for a representative unconventional reservoir (geothermal setting) used in our study. We also share uncertainty estimates for the identified fracture zones for improved characterization. Finally fracture property estimates for the study area (derived using FZI and other properties) have been generated for future reservoir simulation studies.

The proposed method allows for improved understanding of shale and other unconventional reservoirs through fracture mapping and provides a workflow for improved volumetrics of the reservoir by making use of identified properties for fracture modeling. This work validates the potential for using relatively low resolution passive seismic data for improved reservoir characterization using Geostatistical tools. It also provides a valuable framework for pseudo 4D characterization where a single 3D seismic survey can be used as the basis to characterize the reservoir in a time lapse fashion using new information collected in time through passive seismic arrays as well as new well logs being obtained within the area of interest.

Introduction
Use of geophysical tools for reservoir characterization and monitoring is fairly well understood and has been used extensively in recent years. Passive seismic monitoring has found applications in development of unconventional reservoirs such as geothermal systems involving injection and production of hot water or steam from the reservoir, tight gas and oil systems which require hydraulic fracturing and finally monitoring of injection wells (waste water, CO_2, etc.) among others. In the field of conventional seismic, techniques such as multi-attribute analysis and integrated analysis techniques are being used extensively for reservoir characterization. While conventional seismic data is rarely available for small unconventional reservoir developments, the use of microseismic data is limited to better understanding of the fracturing process including diagnosis and volumetrics but is seldom used

as a tool for reservoir property prediction. In our study, we have used seismic as well as microseismic data along with well logs to better predict the reservoir properties and understand the fractures within the study volume. This workflow involves simultaneous use of MEQ and Seismic data as well as mapped log derived properties as outlined in **Figure 1**. An ANN algorithm is used for fracture zone identification and characterization providing indication of zones with presence of open fractures. While this paper does not deal with actual modeling of fracture properties, it provides some of the necessary information for required fracture properties which in turn can be used as inputs for modeling workflows. Our aim is to demonstrate the potential for this workflow for small unconventional developments to improve understanding of the reservoir behavior with time and to optimize overall productivity from the reservoir over its development cycle.

The area of study is a shallow geothermal system within a complex sedimentary basin and an active geologic setting (Gulf of California Rift Zone). The study area has reasonably good well control with multiple production/ injection wells and associated well logs. A passive seismic array is used to continuously monitor the operations of the field. The acquisition array for the data used in this study includes 5 recording sensors placed in shallow boreholes, each recording 3 component continuous data. A single 3D field-wide seismic survey was conducted and the processed data was used in our attribute analysis workflow. Well logs were independently interpreted and evaluated properties (such as V_{sh} and ϕ) were mapped for the entire study volume using an ANN based attribute mapping scheme. Finally, crustal models were obtained from SCEC for local velocity field estimates as the available seismic data was made available without any velocity information.

Microseismic data analysis

A simple energy ratio based autopicker is used for preliminary detection of events. The triggered data is run through an advanced ANN based autopicking workflow (Aminzadeh et al. 2011) and the final picks obtained are used to detect phase arrivals for use with inversion algorithms for both location and velocity. Due to the nature of the data as well as limitations with the monitoring array design, only ~6% of the detected events are used in further analysis. **Figure 2** shows the final selected event epicenters along with the study area of interest plotted together indicating the potential noise and bias issues. The primary selection of detected events to be used in inversion is based on pick quality estimates. HypoDD (Waldhauser 2001) is used to obtain hypocentral locations using the event arrival times based on generated phase data as well as the baseline crustal models. Further pruning of events is done based on failure of inversion algorithm to properly resolve events based on iterative HypoDD runs. The final "selected" events are then used to generate improved velocity models by using SimulPS inversion algorithm (Thurber 1993). SimulPS uses phase information along with preliminary velocity estimates and progressively iterates over all of the phase data available to provide final hypocentral and velocity estimates. The final velocity models obtained are used as a baseline estimate for the area of interest. **Figure 3** shows sample V_P and V_S maps estimated at reference depth (0.5 km) confined within the study area alone.

3D seismic & well log analysis

Seismic attribute analysis is carried out to first identify major discontinuity features and other artifacts. These include Laplacian edge enhancement filter, curvature and similarity features, dip, variance and other attributes. Laplacian (edge enhancement methods based on dip steered 2nd order spatial derivatives (Jahne 1993)) and Amplitude variance as an edge preserving method (Bakker et al. 1999) are used for baseline discontinuity mapping for our study. **Figure 4** shows some of the mapped properties at the reference depth (0.5 km). Rock properties (such as ϕ, ρ) are estimated using ANN rock property prediction workflow using sample training and validation data from processed well logs and training attributes selected based on observed correlation between log properties and attributes. Relative acoustic impedance (Lancaster 2000) is used as a proxy for structural features in the subsurface and is used to improve the resolution of both the V_P and V_S models using COSGSIM algorithm.

Due to lack of available velocity models from seismic data processing and lack of depth migrated seismic volumes, a rudimentary time to depth conversion workflow is followed where well logs are used to obtain seismic to well ties. Due to the absence of sonic logs in most wells, pseudo sonic logs are generated wherever necessary using resistivity log data. Wells with available sonic logs are used to obtain a generalized relationship between travel time and resistivity and the relation is used within other wells to obtain pseudo sonic logs (Rudman et al. 1976). These are combined with density log data to generate impedance logs. Impedance logs in turn provide the reflection coefficients which are then convolved with a selected seismic wavelet (extracted from the actual seismic data) to obtain synthetic seismic trace. The synthetic traces are compared with the actual seismic traces observed from within a volume around the well track (mean computed over a cylindrical volume with 8 nearest traces) and major reflectors are matched to get acceptable ties (process is repeated for all available wells).

The modified seismic volume and logs obtained are used to predict reservoir wide log properties such as porosity and density maps using an ANN based approach. Seismic attributes (Chopra and Marfurt 2007) are calculated from the actual seismic data and these attributes are used as inputs in a supervised ANN modeling framework which tries to match for the desired property as the output. These properties are useful inputs in the fracture characterization workflow and they also help in evaluating geomechanical properties using phase velocities. Impedance is then used to predict rock properties (ϕ, ρ, etc.) using data along well tracks for supervised ANN training and prediction. Relative acoustic impedance is independently computed using colored inversion workflow where a single inversion operator is derived that optimally inverts the data and honors available well data in a global sense. Since this requires sonic travel time data, only two control wells (with available sonic logs) are used in the inversion scheme. Pseudo logs from properties estimated using ANN based modeling are compared with actual logs to validate the property estimates before their use in characterization workflows if required.

Data integration and analysis

Next, we use SGEMS to populate the entire study volume by making use of COSGSIM algorithm involving seismic derived relative acoustic impedance as the secondary hard data. The choice of algorithm is based on its ability to reduce local uncertainty and improve resolution with adequate weight given to known structural features of the reservoir. Since the inputs need to conform to Gaussian distribution, normal score transformation is used to transform the input random function to a standard Gaussian distribution (Goovaerts 1997). Simulation uncertainty is computed based on normalized standard deviations observed at each evaluation point. The final selection of V_P and V_S model for further analysis and calculations is based on least square error evaluation using the original (sparse) velocity fields. **Figure 5** shows V_P and V_S realizations and final selected model at two randomly selected locations (Inline/ Crossline co-ordinates) for reference.

V_P and V_S can be related to elastic rock properties including bulk modulus, shear modulus and Poisson's ratio and these properties can be used to characterize zones of interest using available frameworks to relate the geophysical and geomechanical properties with reservoir attributes such as fractures (Toksoz and Johnston 1981). We know that compressional and shear velocities can be used to derive Lame's parameters using density data (Eq. 1 and Eq. 2). The Lame's parameters are in turn used to estimate the inertial properties of the rock using standard equations of elastic moduli (Eq. 3, Eq. 4 and Eq. 5).

$$\mu = \rho {V_S}^2 \quad \text{.......... (1)}$$

$$\lambda = {V_P}^2 \rho - 2\mu \quad \text{.......... (2)}$$

$$K = \lambda + 2\mu/3 \quad \text{.......... (3)}$$

$$E = 9K\lambda/(3K + \mu) \quad \text{.......... (4)}$$

$$\nu = \lambda/2(\lambda + \mu) \quad \text{.......... (5)}$$

We can further calculate estimates of extensional and hydrostatic stresses directly using V_P and V_S estimates obtained earlier (Toksoz and Johnston 1981) as shown in Eq. 6 and Eq. 7.

$${\sigma_E}^2 = V_S^2(3V_P^2 - 4V_S^2)/(V_P^2 - V_S^2) \quad \text{.......... (6)}$$

$${\sigma_H}^2 = {V_P}^2 - (1.33){V_S}^2 \quad \text{.......... (7)}$$

Considering Hudson's fracture model using effective medium theory (Hudson 1990) and HTI anisotropy, weakness estimates (Hsu and Schoenberg 1993) can be measured based on selected fracture density "e" value. In this study, a sparse fracture density map based on image logs was used to estimate values over entire study volume under consideration. However, fracture density from other independent sources such as shear wave analysis or from prestack seismic data can also be used if available. Normal and tangential weaknesses can therefore be estimated as shared in Eq. 8 and Eq. 9.

$$\Delta_N = 4e/\{3(V_S/V_P)^2 \times [1 - (V_S/V_P)^2]\} \quad \text{.......... (8)}$$

$$\Delta_T = 16e/\{3 \times [3 - 2(V_S/V_P)^2]\} \quad \text{.......... (9)}$$

Extensional stress is known to have a direct bearing on fracture opening (Toksoz and Johnston 1981) while tangential weakness provides an estimate of fracture density (Downton and Roure 2010). While indicative in nature, more robust relationships can be developed and used for fracture properties based on core analysis. As an example, Rutqvist showed that fracture aperture can be calculated from effective normal stress (Rutqvist and Tsang 2003) which we have modified to define the normalized fracture aperture expandability (Eq. 10).

$$F_E = (b - b_r)/b_{max} = e^{\alpha\sigma_E} \qquad (10)$$

Where b_r, b_{max} and α parameters are obtained from laboratory and field measurements using empirical relations involving rock classification index. There are a number of observations which can be made using many of the estimated property maps, particularly by combining with properties estimated from seismic attributes. Apart from stress and weakness estimates, we also know that closing of small fractures due to increasing pressure with depth or cementation effects should cause an observed increase in seismic velocity. However, increased fracturing, chemical alteration and extreme temperature gradients, etc. can cause a reduction in seismic velocities. Fluid saturation tends to reduce V_S and enhance V_P/V_S ratio as well as Poisson's ratio. For highly fractured zones we can generally expect low V_P and V_S values as well as reduced compressional to shear velocity ratios. These and other effects such as effect of fractures on porosities, acoustic impedance, bulk densities, etc., can be used within an integrated characterization framework to identify fractured zones within the study area. **Figure 6** and **Figure 7** show sample maps for these derived properties at the reference depth of 0.5 km.

Fractured zone identification and characterization

The reservoir property estimates obtained from microseismic data analysis as well as those obtained from 3D seismic data using ANN – well log property prediction workflow can be combined based on the expected behavior of said properties within fracture zones. These include relatively high estimated porosities, lower densities and low impedance values. In addition, due to velocity attenuation effects, low V_P/V_S ratio anomalies and low V_P anomalies could be fracture induced. Similarly, low extensional stress anomalies can possibly indicate zones with open fractures (Hutchings et al. 2001 and Martakis et al. 2006). Each of these individual properties by themselves may not be indicative of fracturing with high degree of certainty due to similar observations under different reservoir conditions. As an example, while low V_P anomalies could be fracture induced, it could also be indicative of gas bearing formations. Therefore, a holistic look is necessary to map the fractured intervals based on the property perturbations in the study area. This is accomplished by combining the individual property maps into newly devised FZI attributes. While there could be many ways of designing such an attribute (based on which properties are defined as ANN nodal inputs), we use a simple relationship as defined in Eq. 11 for this study.

$$FZI = f(\phi_n, \rho_n, f_n, Z_n, V_{Sn}, V_{Pn}, \sigma_{En}, \Delta_{Tn}) \qquad (11)$$

The FZI modeling for this study is performed using a simple multiplayer RBF algorithm where the activation functions used in the network are radial basis functions. **Figure 8** shows sample training data used for network training before application of the trained models on the entire study volume. Based on the available fracture logs, some locations are used for the training process while the others help in validation of the designed ANN model. Fracture opening can be mapped in a similar fashion as demonstrated with Eq. 12.

$$FZI_A = f(\phi_n, f_n, Z_n, F_E) \qquad (12)$$

Fracture permeability can be estimated empirically based on Darcy flow using fracture density estimate (fractures per unit length) and fracture aperture estimate. However, since fracture density is unknown in absolute terms, we use mapped FZI probability to estimate fracture density by preselecting "minimum" and "maximum" fracture density values based on analysis of available image logs and generating scaled fracture density values for the entire study volume. Since we only have normalized fracture aperture estimates (FZI_A), fracture density map is also normalized. The following equation (Eq. 13) is used for fracture permeability estimation:

$$k_{Fi} = e_n FZI_A{}^3/12 \qquad (13)$$

Where the normalized fracture density estimate is computed using the predefined densities as mentioned earlier. **Figure 9** shows sample FZI and k_{Fin} maps at reference depth of 0.5 km. All of the defined properties can be used in an integrated approach to characterize fracture dominated zones and better understand reservoir communication and well performance. However, before mapping the properties and making interpretations, zones showing very high uncertainties are trimmed out of these maps based on simulation and inversion uncertainties. The process of defining the cumulative uncertainty estimate is based on the model inputs being used for FZI property calculations. The velocity estimate uncertainties are evaluated using the estimated inversion error (e_i) as well as the simulation error (u_{VPs} and u_{VSs}) evaluated based on normalized model standard deviation as shared in Eq. 14a and Eq. 14b for V_P and V_S respectively.

$$u_{VP} = e_i u_{VPs} \quad (14a)$$

$$u_{VS} = e_i u_{VSs} \quad (14b)$$

Based on the evaluated velocity model errors, we can compute property estimate errors based on the rock physics models originally used in their evaluation. Despite significant errors in seismic derived properties, they are assumed to have insignificant estimation errors in order to simplify uncertainty evaluation. The following relations (Eq. 15, Eq. 16 and Eq. 17) provide the estimated errors for extensional stress and tangential weakness values:

$$u_{\sigma E} = u_{VS}^2(3u_{VP}^2 - 4u_{VS}^2)/(u_{VP}^2 - u_{VS}^2) \quad (15)$$

$$u_{\Delta T} = u_{VP}^2/u_{VS}^2 \quad (16)$$

$$u_{FZI} = w_{VP}u_{VP} + w_{VS}u_{VS} + w_{\sigma E}u_{\sigma E} + w_{\Delta T}u_{\Delta T} \quad (17)$$

Figure 10 shows the normalized inversion and simulation uncertainty maps as well as normalized uncertainty for the modeled FZI property for the same reference depth of 0.5 km. These uncertainty values are used to quality any qualitative or quantitative interpretations that may be made based on the final fracture attributes. **Figure 11** shows potential flow behavior near well locations at depths of 0.5 km and 1.0 km based on observed discontinuities and FZI attribute behavior. This method can be used to identify the zones of interest, either horizons within existing wellbores or new areas of interest within the study volume. Moreover, the identified fracture properties, though only indicative in nature, can provide estimates for inputs to fracture modeling and flow simulation workflows as deemed necessary.

Summary

Our work successfully demonstrates the possibility of using microseismic data to evaluate geomechanical properties which can provide a framework for fracture zone identification and characterization when combined with other information. This method can be applied under most unconventional reservoir settings (which incorporate passive seismic monitoring and have had atleast one baseline seismic survey) and allows use of microseismic data for characterization purposes (and not just injection monitoring). While we have developed a framework for fracture zone identification, the method can easily be used for other characterization workflows including for lithology, fluid type, fracture orientations, etc. Moreover, additional information such as injection/ production data and geologic models can also be integrated within the workflow to add additional constraints into the modelling process. Finally, this method also provides a framework for time lapse fracture characterization within the field by making use of temporally segmented catalogs of microseismic data.

Acknowledgements

This work was supported by Ormat Inc. and we acknowledge Ezra Zemach, Skip Matlick and Patrick Walsh from Ormat for providing us with the datasets to work with and for providing valuable guidance as and when requested. We used dGB's OpendTect software in this study and thank them for providing requisite student licenses to USC. We have used Matlab extensively including implementation of ANN modeling and would like to acknowledge Mathworks for providing required licenses.

Nomenclature

ANN = Artificial Neural Network
COSGSIM = Sequential Gaussian Co-Simulation
E = Young's modulus, m/Lt^2, kg/ms^2
F_E = normalized fracture expandability parameter
FZI = Fracture Zone Identifier
FZI_A = Fracture Zone Identifier - Aperture
HTI = Horizontal Transverse Isotropy
K = bulk modulus, m/Lt^2, kg/ms^2
LVQ = Linear Vector Quantizer
MEQ = Micro Earthquake
RBF = Radial Basis Function
SCEC = Southern California Earthquake Center
SGEMS = Stanford Geostatistical Modeling Software
V_P = compressional velocity, L/t, m/s
V_{Pn} = normalized compressional velocity
V_S = shear velocity, L/t, m/s

V_{Sn} = normalized shear velocity
V_{sh} = volumetric fraction of shale
Z_n = normalized impedance
b = aperture, L, μm
b_r = residual aperture, L, μm
b_{max} = maximum aperture, L, μm
e = fracture density, n/L^3, m^{-3}
e_i = inversion error
e_n = normalized fracture density
f_n = normalized frequency
k_{Fi} = fracture permeability
u_{FZI} = uncertainty in FZI estimate
u_{VP} = overall uncertainty for V_P
u_{VPs} = simulation uncertainty for V_P
u_{VS} = overall uncertainty for V_S
u_{VSs} = simulation uncertainty for V_S
$u_{\Delta T}$ = uncertainty in tangential weakness estimate
$u_{\sigma E}$ = uncertainty in extensional stress estimate
w_{VP} = trained ANN nodal weight for V_P node
w_{VS} = trained ANN nodal weight for V_S node
$w_{\sigma E}$ = trained ANN nodal weight for σ_E node
α = aperture calculation parameter (constant)
λ = Lame's parameter
μ = Lame's parameter
ν = Poisson's Ratio
ϕ_n = normalized porosity
ρ = density, m/L^3, kg/m^3
ρ_n = normalized density
σ_E = extensional stress, m/Lt^2, kg/ms^2
σ_{En} = normalized extensional stress
σ_H = hydrostatic stress, m/Lt^2, kg/ms^2
Δ_N = normal weakness
Δ_T = tangential weakness
Δ_{Tn} = normalized tangential weakness

References

1. Aminzadeh, F., Maity, D., Tafti, T. and Brower, F. 2011. Artificial Neural Network based Autopicker for Micro Earthquake Data. Expanded Abstracts, SEG Annual International Meeting, San Anotnio, TX, USA, 1623-1626.
2. Bakker, P., Vanvliet, L.J. and Verbeek, P.W. 1999. Edge Preserving Orientation Adaptive Filtering. Proc., IEEE Int. Conf. Computer Vision, Pattern Recognition, Fort Collins, CO, USA, Vol. 1, 535-540.
3. Beer, F.P., Johnston, E.R., Dewolf, J. et al. 2009. *Mechanics of materials*. Singapore: McGraw Hill. ISBN: 0073380288.
4. Chopra, S. and Marfurt., K.J. 2007. Seismic Attributes for Prospect Identification and Reservoir Characterization. SEG. ISBN: 1560801417.
5. Downton, J. and Roure, B. 2010. Azimuthal simultaneous elastic inversion for fracture detection. Expanded Abstracts, SEG Annual International Meeting, Denver CO, USA, 263-267.
6. Faust, L.Y. 1953. A Velocity Function Including Lithologic Variation. *Geophysics* **18** (2): 271-288. http://dx.doi.org/10.1190/1.1437869.
7. Goovaerts, P. 1997. Geostatistics for Natural Resources Evaluation. Oxford University Press. ISBN: 0195115384.
8. Hsu, C.J. and Schoenberg, M. 1993. Elastic wave through a simulated fractured medium. *Geophysics* **58** (7): 964-977. http://dx.doi.org/10.1190/1.1443487.
9. Hudson, J.A. 1990. Overall elastic properties of isotropic materials with arbitrary distribution of circular cracks. *Geophys J Int* **102** (2): 465-469. http://dx.doi.org/10.1111/j.1365-246X.1990.tb04478.x.
10. Hutchings, L., Wagoner, J. and Berge, P. 2001. Rock Physics Interpretation of P Wave, Q and Velocity Structure, Geology, Fluids and Fractures at the South East Portion of the Geysers Geothermal Reservoir. Transactions, GRC Annual Meeting, San Diego, CA, USA, 1-23.
11. Jahne, B. 1993. Digital Image Processing, Concepts, Algorithms and Scientific Applications. Berlin: Springer. ISBN: 3540592989.
12. Lancaster, S. and Whitcombe, D. 2000. Fast track coloured inversion. Expanded Abstracts, SEG Annual International Meeting, Calgary, Canada, 1298-1301.
13. Maity, D. and Aminzadeh, F. 2012. Framework for time lapse fracture characterization using seismic, microseismic & well log data. Expanded Abstracts, SEG Annual International Meeting, Las Vegas, NV, USA. 1-6.
14. Martakis, N., Kapotas, S. and Tselentis, G. 2006. Integrated Passive Seismic Acquisition and Methodology: Case Studies.

Geophys Prospect 54 (6): 829-847. http://dx.doi.org/10.1111/j.1365-2478.2006.00584.x.

15. Mavko, G., Mukherji, T. and Dvorkin, J. 2003. The Rock Physics Handbook. Cambridge University Press. ISBN: 9780511738876.
16. Rudman, A.J., Whaley, J.F., Blakely, R.F. et al. 1976. Transformation of resistivity to pseudo velocity logs. *AAPG Bull* 59: 1151-1165.
17. Rutqvist, J. and Tsang, C. 2003. Analysis of thermal–hydrologic–mechanical behavior near an emplacement drift at Yucca Mountain. *J Contam Hydrol* 62-63: 637-652. http://dx.doi.org/10.1016/S0169-7722(02)00184-5.
18. Thurber, C.H. 1993. Local Earthquake Tomography: Velocities and Vp/Vs – Theory. In *Seismic Tomography: Theory and practice*, ed. H.M. Iyer and K. Hirahara, 563-583: Chapman and Hall.
19. Toksoz, M.N. and Johnston, D.H. 1981. Seismic Wave Attenuation. SEG. ISBN: 0931830168.
20. Waldhauser, F. and Ellsworth, W.L. 2001. A double-difference earthquake location algorithm: Method and application to the northern Hayward fault. *Bull Seismol Soc Am* 90 (6), 1353-1368. . http://dx.doi.org/10.1785/0120000006.

Figures

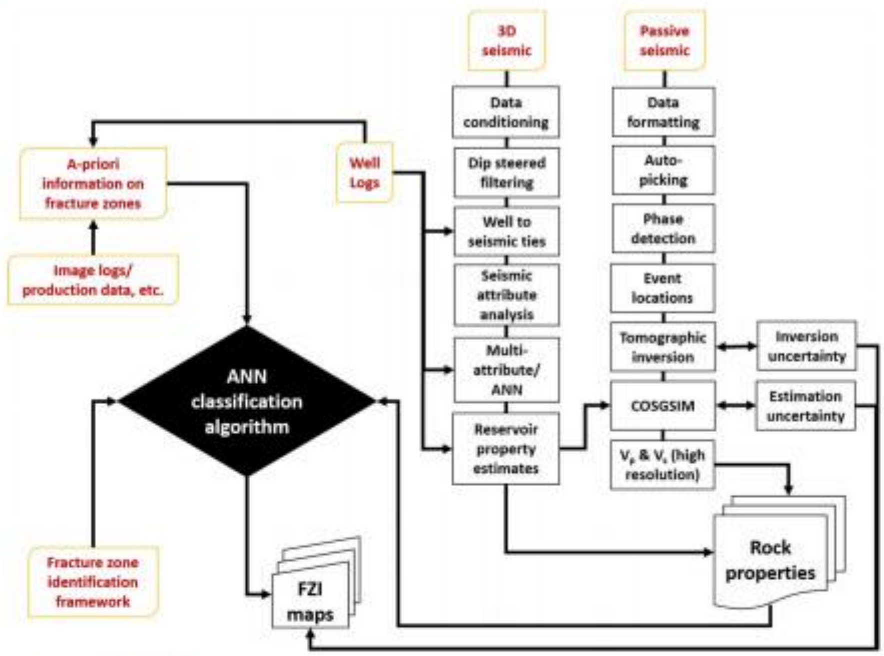

Figure 1: Fracture attribute (FZI) characterization workflow using 3D surface seismic, passive seismic and well log data

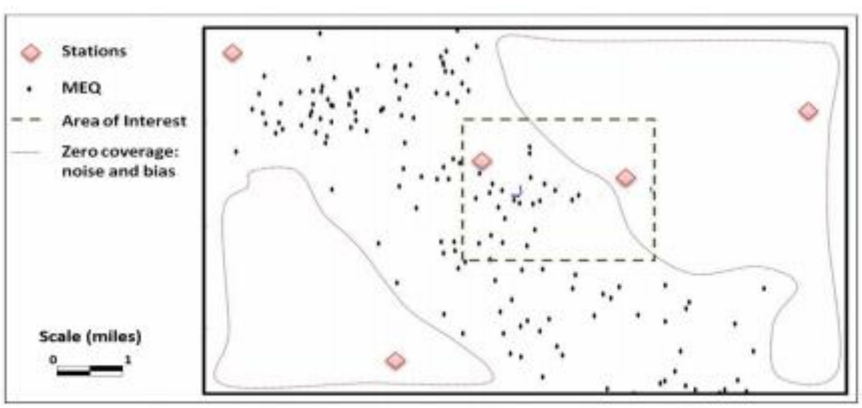

Figure 2: Spatial expanse of SimulPS 'finite node grid' with stations, events and study volume plotted for reference

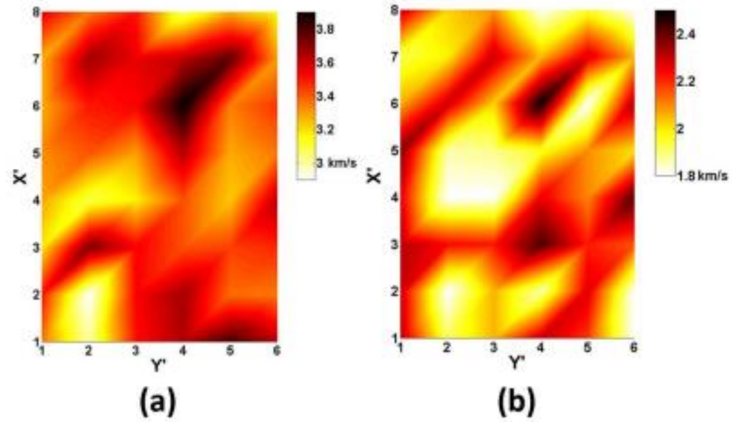

Figure 3: (a) V_P and (b) V_S maps from inversion (data range extracted from original velocity maps so as to conform to study volume dimensions)

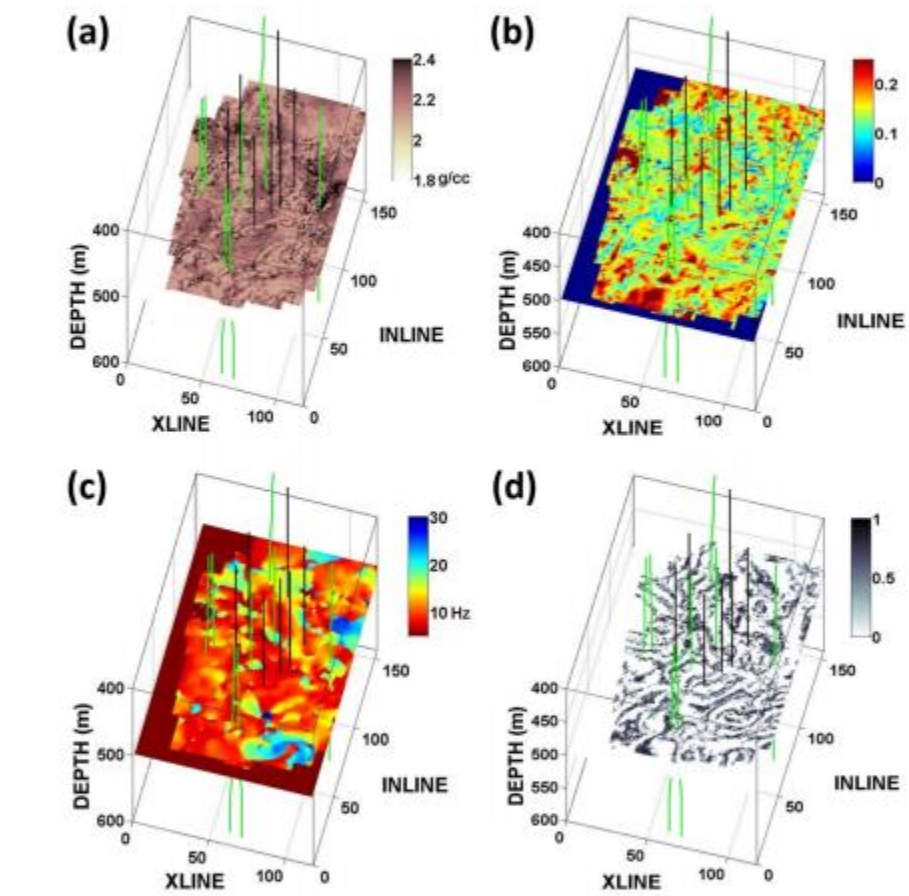

Figure 4 (a) Density, (b) Porosity, (c) Instantaneous frequency and (d) Discontinuity (ANN) map as observed at 0.5 km depth interval with injection (green) and production (black) well tracks

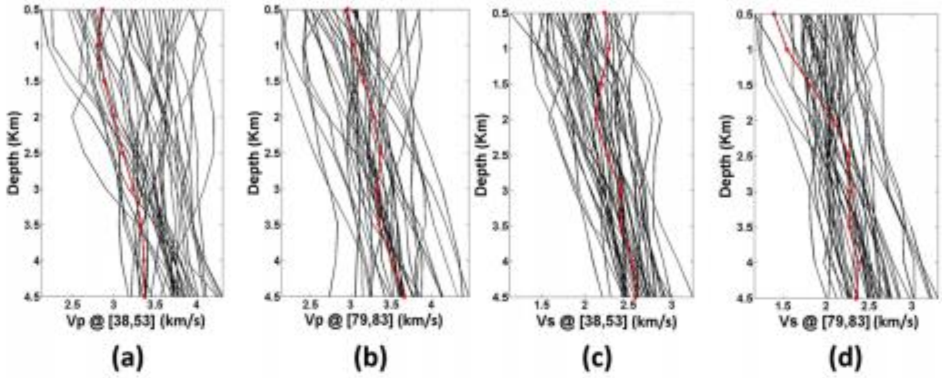

Figure 5: Subplots (a) and (b) show sample V_P realizations at two indexed locations and the final selected model (red) while subplots (c) and (d) show sample V_S realizations at the same selected locations including the final model (red)

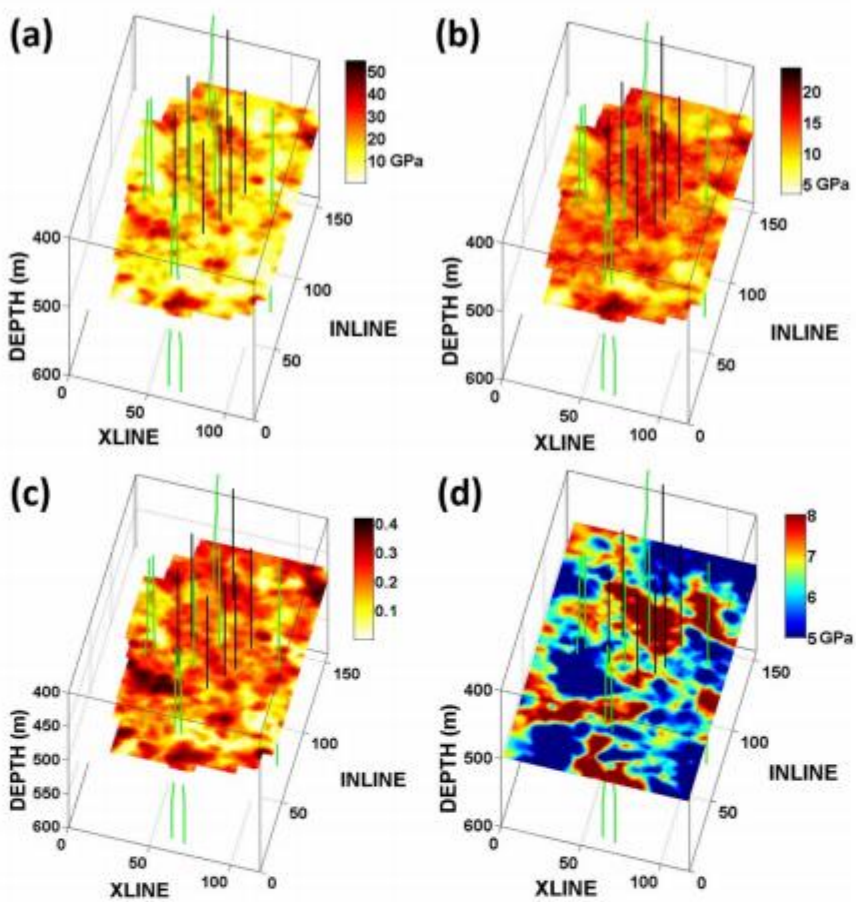

Figure 6: (a) Young's Modulus, (b) Bulk Modulus, (c) Poisson's Ratio and (d) Extensional stress mapped at reference depth of 0.5 km with injection (green) and production (black) well track inserts

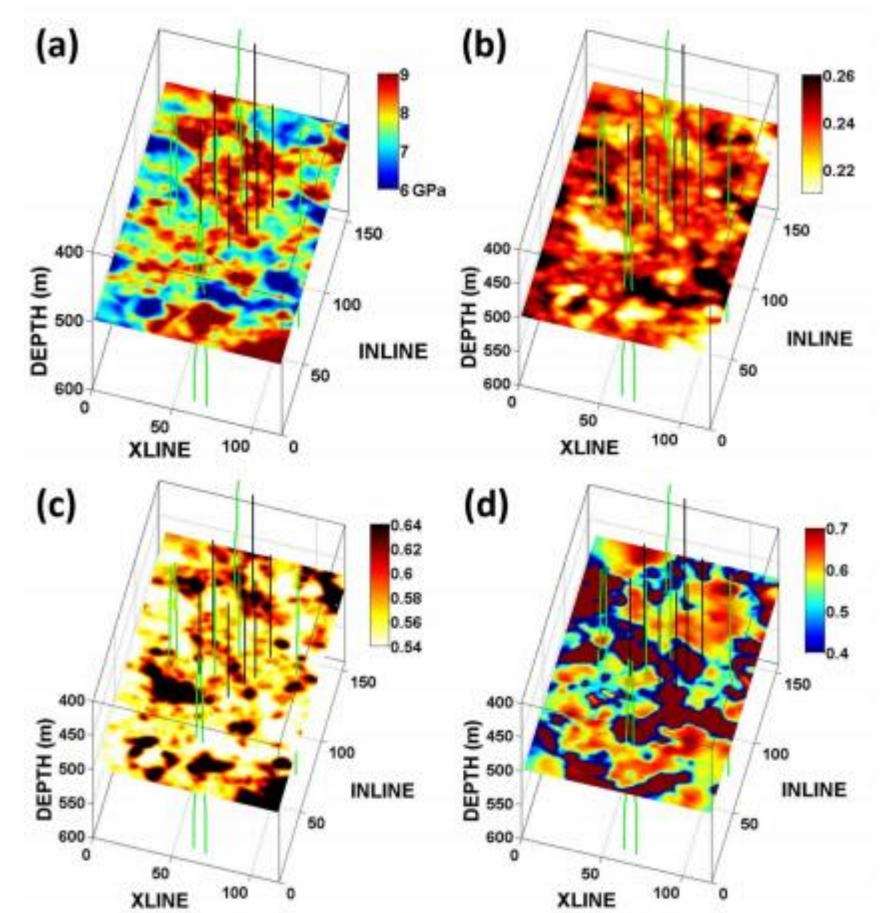

Figure 7 (a) Hydrostatic stress, (b) Tangential weakness, (c) Normal weakness and (d) Fracture aperture expandability mapped at reference depth of 0.5 km with injection (green) and production (black) well inserts

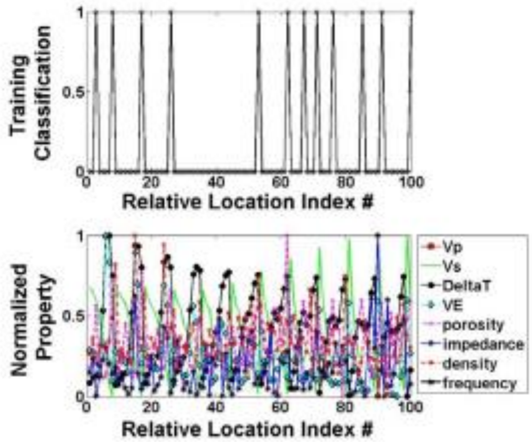

Figure 8: Sample training data and input properties used for derived FZI property mapping. The selected properties are normalized and used as inputs through ANN nodes

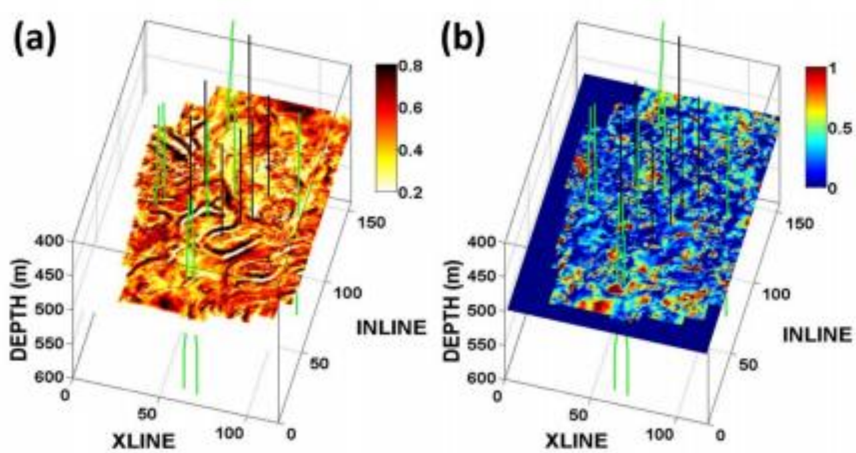

Figure 9: (a) FZI and (b) normalized k_H maps at reference depth of 0.5 km

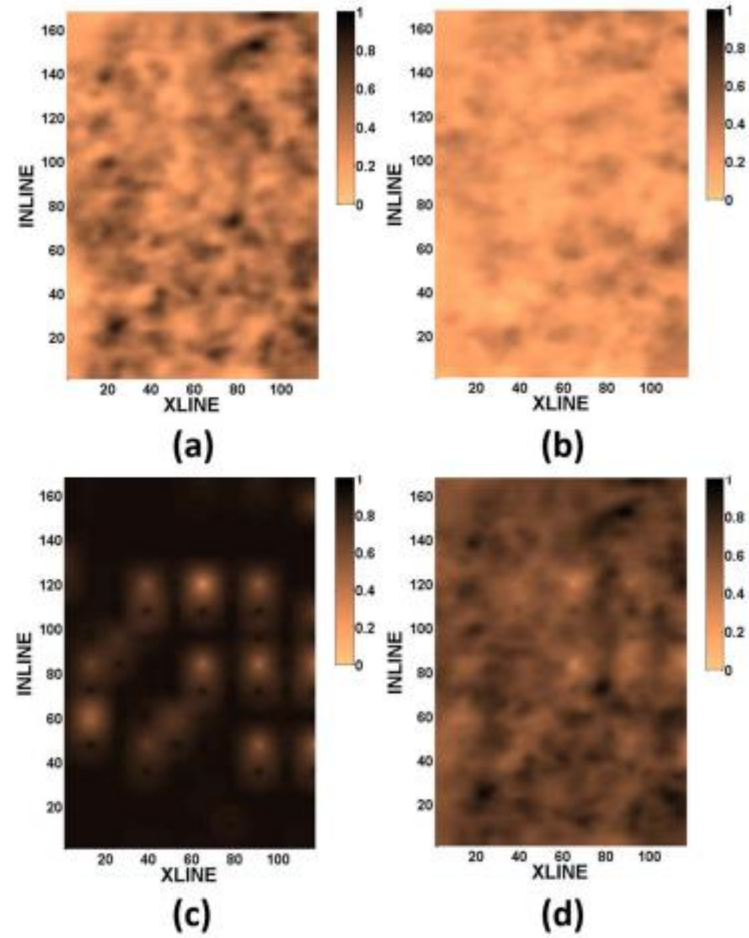

Figure 10: (a) V_P simulation uncertainty map, (b) V_S simulation uncertainty map, (c) inversion uncertainty map and (d) FZI uncertainty map at reference depth of 0.5 km

16 SPE 166307

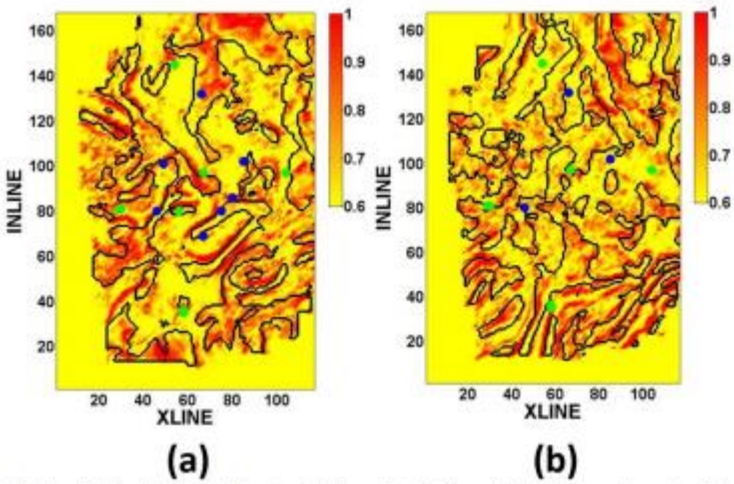

Figure 11: FZI with discontinuity derived from 3D seismic data used to identify and validate flow regimes close to known injectors (green inserts) and producers (blue inserts). Subplot (a) shows mapping at 0.5 km while (b) shows mapping at 1.0 km. Some wells align with major edge boundaries and/ or fall within high FZI zones.

- **Dynamic Characterization of Fracture Network Using Seismic, Microseismic & Well Log Data**
- **A New Approach Towards Optimized Passive Seismic Survey Design With Simultaneous Borehole And Surface Measurements**
- **A Geomechanical Approach for Microseismic Fracture Mapping**

9- Appendices

In this section we provide a brief overview of all the appendices to the report. The Appendix numbering is based on the respective section number in the body of the main report where the Appendix is first referred to. It includes both the original research proposal, more technical details on the accomplishments and subsequent publications, description of some of the software developed and links to the PhD dissertations.

Appendix 1-1- The Original Proposal Summary- Characterizing Fractures in Geysers Geothermal Field by Micro-seismic Data, Using Soft Computing, Fractals, and Shear Wave Anisotropy

Appendix 4-4- LBNL Work- Anisotropy Tomography for Micro-earthquake Location and Subsurface Physical Characterization

Appendix 6-1- Abstract for Maity (2013) Dissertation- Integrated Reservoir Characterization for Unconventional Reservoirs Using Seismic, Microseismic and Well Log Data.

Appendix 6-2- Abstract of Tafti (2013) Dissertation- Integrated Workflow for Characterizing and Modeling Fracture Network in Unconventional Reservoirs Using Microseismic Data.

Appendix 8-1- Peer Review Comments and Principal Investigator Responses

Appendix 8-2- External Publications

10- Acknowledgements

We acknowledge the contributions of the original team members of the project and other contributors (noted with *). They include:

USC Team:

Faculty:

Prof. Fred Aminzadeh (PI), Prof. Charles Sammis and Prof. Mohammad Sahimi,
Dr. David Okaya*

Past Students:

Tayeb A. Tafti (Currently with California Resources Corporation)

Debotyam Maity (Currently with Gas Technology Institute)

Aditya Tiwari (Currently with National Energy Technology Laboratory)

Budget Analyst:

Aimee Bernard (former), Jason Ordonez (current)

Advisor to USC Center for Geothermal Studies:

Joe Iovenitti

Lawrence Berkeley National Laboratory:

Dr. Ernie Majer, Dr. Leon Thomsen, Katie Boyle*, Lawrence John Hutchings*

Calpine:

Mark Walters; Craig Hartline

11- References

Aki, K. (1981). A probabilistic synthesis of precursory phenomena, in earthquake prediction: an international review. In D. W. Simpson & P. G. Richards (Eds.), *AGU, Maurice Ewing ser.* (Vol. 4, pp. 566-574). Washington D.C.

Allen, R. V. (1978). Automatic earthquake recognition and timing from single traces, *Bull. Seism. Soc. Am.* **68** 1521-1532.

Aminzadeh, F., S. Katz, and K Aki (1994). Adaptive Neural Nets for Generation of Artificial Earthquake Precursors, *IEEE Trans. Geosci. Rem. Sens.* **32** 6.

Aminzadeh, F., Tafti, T. A., & Maity, D. (2010). Characterizing Fractures in The Geysers Geothermal Field Using Soft Computing. *Geothermal Resource Council Transaction*, *34*, 1193-1198.

Baer, M., and U. Kradolfer (1987). An automatic phase picker for local and teleseismic events. *Bull. Seism. Soc. Am.* **77** 1437-1445.

Berge, P., Hutchings, L., & Wagoner, J. (2001). Rock Physics Interpretation of P-Wave Q and Velocity Structure, Geology, Fluids and Fractures at the Southeast Portion of The Geysers Geothermal Reservoir. *Geothermal Res. Council, Transactions*, *14*, 1-21.

Berge, P., Hutchings, L., Wagoner, J., & Kasameyer, P. (2001). *Rock Physics Interpretation of P-Wave Q and Velocity Structure, Geology, Fluids and Fractures at the Southeast Portion*

Boitnott, G. N. (2003). *Core analysis for the development and constraint of physical models of geothermal reservoirs*. Davis, CA; The Geothermal Resources Council; 1998.

Boyle, K., Jarpe, S., Hutchings, L., Saltiel, S., & Peterson, J. (2011). Preliminary investigation of an aseismic “doughnut hole” region in the northwest geysers, California. *Thirty-Sixth Workshop on Geothermal Reservoir Engineering* (Vol. 1995).

Coppens, F. (1985). First arrival picking on common-offset trace collections for automatic estimation of static corrections, *Geophys. Prospec.* **33** 1212-1231.

Elkibbi, M., & Rial, J. A. (2005). The Geysers geothermal field: results from shear-wave splitting analysis in a fractured reservoir. *Geophysical Journal International*, *162*, 1024-1035.

Eneva, M. (1996). Effect of limited data sets in evaluating the scaling properties of spatially distributed data: an example from mining-induced seismic activity. *Geophysical Journal International*, *124*(3), 773-786.

Jang, J. S. R., and N. Gulley (1995). Fuzzy logic toolbox, *MathWorks*, Natick, MA.

F. W. Klein (2002). User's Guide to HYPOINVERSE-2000, a Fortran Program to Solve for Earthquake Locations and Magnitudes.

McCormack, M. D. (1990). Seismic trace editing and first picking using neural networks, *Extended Abstracts 59th SEG Annual Conference* 716 - 718, Dallas, TX.

Nikravesh, M., and F. Aminzadeh (2001). Mining and fusion of petroleum data with fuzzy logic and neural network agents, *J. Petrol. Sci. Eng.* **29** 221-238.

Robertson, Michelle C., Sammis, Charles G., Sahimi, Muhammad, & Martin, A. J. (1995). Fractal analysis of three-dimensional spatial distributions of earthquakes with a percolation interpretation. *Journal of Geophysical Research*, *100*(B1), 609.

Sabbione, J. I., and D. Velis (2010). Automatic first breaks picking: New strategies and algorithms, *Geophysics* **75** 67-76.

Sahimi, M., Robertson, M.C., & Sammis, C.G. (1993). Fractal distribution of earthquake hypocenters and its relation to fault patterns and percolation. *Physical review letters*, *70*(14), 2186–2189. APS. Smith, L. A. (1988). Intrinsic limits on dimension calculations. *Physics Letters A*, *133*(6), 283–288. Elsevier.

Saragiotis, C. D., L. J. Hadjileontiadis, and S. M. Panas (2002). PAI-S/K: A robust automatic seismic P phase arrival identification scheme, *IEEE Trans. Geosci. Rem. Sens.* **40** 1395-1404.

Tokosoz, M. N., & Johnson, D. H. (1981). *Seismic wave attenuation*. *Journal of Geophysical Research* (Geophysics., Vol. 78). Society of Exploration Geophysicists.

Veezhinathan, J., D. Wagner, and J. Ehler (1992). First break picking using a neural network, *Expert Systems in Exploration*, SEG Publication.

Zhao, Y., and K. Takano (1999). An artificial neural network approach for broadband seismic phase picking, *Bull. Seism. Soc. Am.* **89** 670-680.

Appendix 1-1: The Original Proposal Summary

Characterizing Fractures in Geysers Geothermal Field by Micro-seismic Data, Using Soft Computing, Fractals, and Shear Wave Anisotropy

Topic Area 23: Fracture Characterization Technology

This is a joint technology application collaborative project between the University of Southern California (USC), Geysers Power Company, "Calpine", and Lawrence Berkeley National Laboratory (LBNL), to develop improved methods for better characterization of fractures in an enhanced geothermal system (EGS). The ultimate objective of the project is to develop new methodologies to characterize the northwestern part of the Geysers geothermal reservoir (Sonoma County, California), gaining better knowledge of their porosity, permeability, fracture size, fracture spacing, reservoir discontinuities (leaky barriers) and impermeable boundaries. This will be accomplished by creating a 3-D seismic velocity model of the field using the micro-seismic data, collected under another DOE-funded project. We will exploit the anisotropic and fractal nature of the rocks in order to better understand the fracturing system. We will use soft computing to process and analyze the passive seismic data.

The proposed program will focus on predicting characteristics of fractures and their orientation prior to drilling new wells. It will also focus on determining the location of the fractures, spacing and orientation during drilling, as well as characterizing open fractures after stimulation to help identify the location of fluid flow pathway within the EGS reservoir. These systems are created by passively injecting cold water, and stimulating the permeation of the injected water through existing fractures into hot wet and hot dry rocks by thermo-elastic cooling shrinkage. The stimulated, existing fractures thus enhance the permeability of the hot rock formations, hence enabling better circulation of water for the purpose of producing the geothermal resource. The main focus of the project will be on developing better understanding of the mechanisms for the stimulation of existing fractures, and to use the information for better exploitation of the high temperature geothermal resources located in the northwest portion of the Geysers field and similar fields.

Several complementary processing approaches will be used to develop and test new techniques for data collection and analysis. They include micro-seismic data analysis both for compressional and shear waves using soft computing, anisotropic inversion and fractal concepts. This will enable us to analyze and interpret micro-seismic data and create velocity fields using tomography. Neuro-fuzzy approach will be used to create a hybrid MEQ event picking. This project will combine the technical expertise of USC team with the operational expertise and experience of Calpine as well as the long history of pioneering work of LBNL on geophysical technology applications in geothermal fields.

This effort will complement and enhance the ongoing EGS experiment in the northwest Geysers, under DOE funded LBNL-Calpine project from FOA Number DE-PS36-08G098008. We will utilize the data gathered in the Geyser to better understand and characterize the fracture system that provides fluid storage, transmissivity and an efficient boiling at the Geysers. This work is expected to complement the ongoing Calpine-LBNL EGS project. Furthermore, we believe that many of the techniques developed and tested under this project will be applicable to many other geothermal fields in California and elsewhere in the country.

Applicant: University of Southern California,

PI: Fred Aminzadeh, (Research Professor, USC Petroleum Engineering Program and Global Energy Advisor to USC Energy Institute)
Other USC team members: Charles Sammis, Muhammad Sahimi, Tayeb Ayatollahy Tafti (Graduate student), Post Doc (TBD)

External sub-contractors

Calpine, Mark Walters, PI, Keshav Goyal, Alfonso Pingol, Julio Garcia

Laurence Berkeley National Laboratory (LBNL) Ernie Majer, PI, Leon Thomsen,

1- Statement of Project Objectives:

The main objective of the project is to develop reservoir information, such as porosity, permeability, fracture size, fracture spacing, reservoir discontinuities (leaky barriers) and impermeable boundaries in the northwest part of the Geysers by creating a 3-D seismic velocity model of the field. Using the velocity field, we will precisely locate the very small micro-seismic events. With that information, we will identify and map the fractures in the field to determine the impact of water injection in the fracture system, and use the information to better exploit the geothermal reservoir in the northwest part of the field. The primary focus of this project are

I- Developing better understanding of the mechanisms for the stimulation of existing fractures,

II-Using the information for better exploitation of the high temperature geothermal resources located in the northwest portion of the Geysers field and similar fields.

To accomplish the goals of the project we will use several complementary processing approaches. We will develop and test new techniques for microseismic data evaluation and analysis. As described in the Project Management Plan (PMP) we will conduct following technical work:

- **i.** We will conduct a general evaluation of the MEQ data collected as well as the augmented data to be collected (see details in section 5-1)
- **ii.** We will use anisotropic inversion to create shear wave and compressional wave velocity fields using tomography (see details in section 5-2)

iii. We will use fractal concepts for accurate characterization of the fracture map. tomography (see details in section 5-3)

iv. We will use neuro-fuzzy approach (see details in section 5-2) to

a. Create a hybrid MEQ event picking,

b. Process, analyze and interpret microseismic data with higher level of accuracy and provide more suitable input data to (i) and (ii),

c. Gain improvements in fracture reservoir characterization.

Tasks and Deliverables: In what follows we will provide more specifics tasks and deliverables to reach our goals and objectives.

2-1 Tasks:

2-1-1- Use of the augmented receiver network at the DOE-funded Calpine EGS Demonstration Project in the northwest Geysers.

I. The augmented arrays would complement the existing LBNL surface station array already in place in the area of the experiment. The combined data set will have better coverage with improved signal/noise for the present purpose than either of the data sets alone.

II. Additional monitoring, processing and analysis of the high-precision seismic data from the existing LBNL arrays (per the tasks described below)

2-1-2- Develop a 3-D seismic velocity model beneath the largely-undeveloped 10 sq. mile area of northwestern part of the Geysers where Calpine is proposing further development.

I. The seismic data of the field, needed for the 3-D analysis, are available at Calpine and LBNL. Whether to model only the northwest part, or the entire Geysers field, is to be decided by USC.

II. Recent publications on fracturing in the Geysers are collected in the Geysers Monogram, GRC Transactions and Stanford Workshop Proceedings, and are available to the team.

III. Data related to the Geysers production and injection, and well geology, are available at DOGGR (California Department of Oil, Gas and Geothermal Resources).

2-1-3- Use the 3D velocity field, constructed based on them, to create a fracture map and monitor low-level microseismicity occurring in response to deep, low-rate water injection, in order to precisely locate and characterize fracturing occurring in response to injection into the deep high temperature reservoir.

2-2 Deliverables:

I. **Create a reservoir image,** and monitor 4D changes created by the injection of cold water into hot, already fractured rock.

II. **Create a map comprised of the spatial distribution of the fractures** in the Geysers geothermal reservoir. From the 3-D seismic velocity model and the high precision monitoring network, the project will attempt to satisfy the operational needs of Calpine by accomplishing the following, in order of priority:

a. Define fracture size and fracture spacing.
b. Identify reservoir discontinuities (leaky barriers) using the 3-D velocity model and historic micro-seismic events of northwest Geysers.
c. Identify impermeable boundaries, if they exist (and their extent), using the 3-D seismic velocity model of northwest Geysers.
d. Characterize the permeable section of the HTZ, as determined by MEQ activity in the EGS demonstration area.
e. Determine the reservoir bottom, as defined by the micro-seismic distribution in the EGS demonstration area

III Develop a neuro-fuzzy based hybrid process for picking MEQ seismic events. This will involve using selected handpicked seed points as the training set for a semi-automatic event picker, combining the benefits of hand-picked approach and automated pickers.

IV Develop empirical and semi-empirical engineering equations for better defining fracture permeability and porosity for the reservoir's model.

3- Complementary nature of this proposal with FOA DE-PS36-08G09808:

The proposed USC project would complement the LBNL surface-located MEQ monitoring array already in-place in the northwest Geysers under the Calpine-LBL-08 project (**FOA DE-PS36-08G09808)**. The planned augmented arrays involving four MEQ stations to be added to the existing surface array this summer will allow the required sensitivity to detect the MEQs of about magnitude 1. The direct involvement of LBNL in this proposed project will ensure proper use of their data by the USC team and increases the leveraging opportunities of the existing and proposed work.

In what follows we describe the current CalpineLBNL-08 work where it relates to the current proposal, followed by the statement of the work by LBNL in connection with this current project (USC-Calpine-LBNL-09).

3-1 CalpineLBNL-08 Project Overview Figure 1, from Stark (2003), gives a rough subsurface structural image from a cross section in the study area. The seismicity data are overlaid with an approximate temperature distribution. Locations of a number of injection wells are also shown. The more pronounced distribution of the seismicity below and around the injection wells is noticeable.

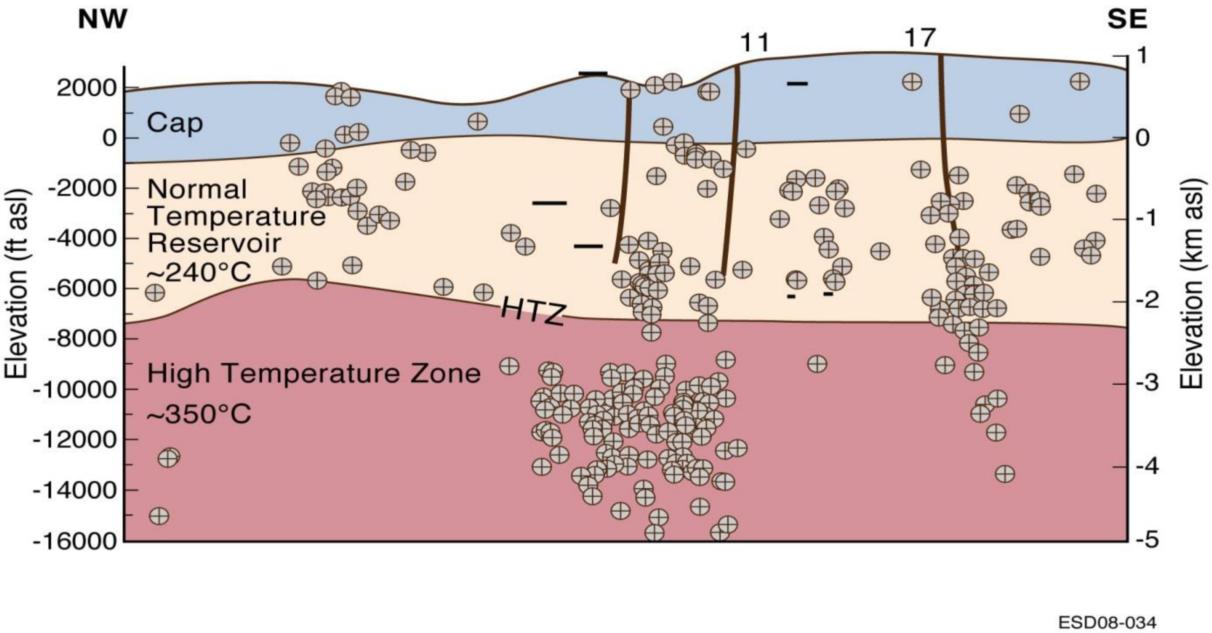

Figure 1 *Northwest-southeast cross-section through the Geysers geothermal field, showing 2002 MEQ hypocenters, injection wells, power plants, and top of the HTZ (Stark, 2003).*

The aspect of this proposal most closely related to Calpine-LBNL project is in connection with their 3-D tomography and high-precision location of the MEQs effort. As we describe in various parts of this proposal, we expect to provide complementary technologies to help enhance the 3-D seismic wave tomography that, in turn, will provide three-dimensional mapping of the P- and S-wave velocities as well as P-wave and S-wave attenuation parameters. Specifically, our fractal approach, anisotropic velocity investigation, and soft computing methodology, combined with the tools developed at LBNL, will be utilized to develop an accurate geological model and the corresponding rock properties. This effort will further enhance Calpine-LBNL deliverables in utilizing a simultaneous solution for MEQ location, seismic velocity structure and energy dissipation of the P- and S-waves to perform tomographic inversion. High-precision MEQ locations in combination with the augmented stations will help us map more accurately the progress of the stimulation during the injection, and to identify and map the fractures.

The assumption is that most MEQs occur along faults or fractures, and can be induced by fluid flow. As shown in Figure 2, the major faulting and general geologic features of the area have already been characterized reasonably well. It is the more subtle faults and fractures that will require application of our soft computing-based techniques, exploiting their anisotropic and fractal behavior that will help their identification and mapping. In collaboration with Calpine and LBNL, we will use the information from numerous data logs and field data for the specific wells (e.g., PS31, P30, P32, and P37), as well as other nearby wells to fine tune the 3D geologic model of the EGS area (Figure 2). Below, we provide a brief statement of the new work by LBNL and Calpine in conjunction of this proposed project.

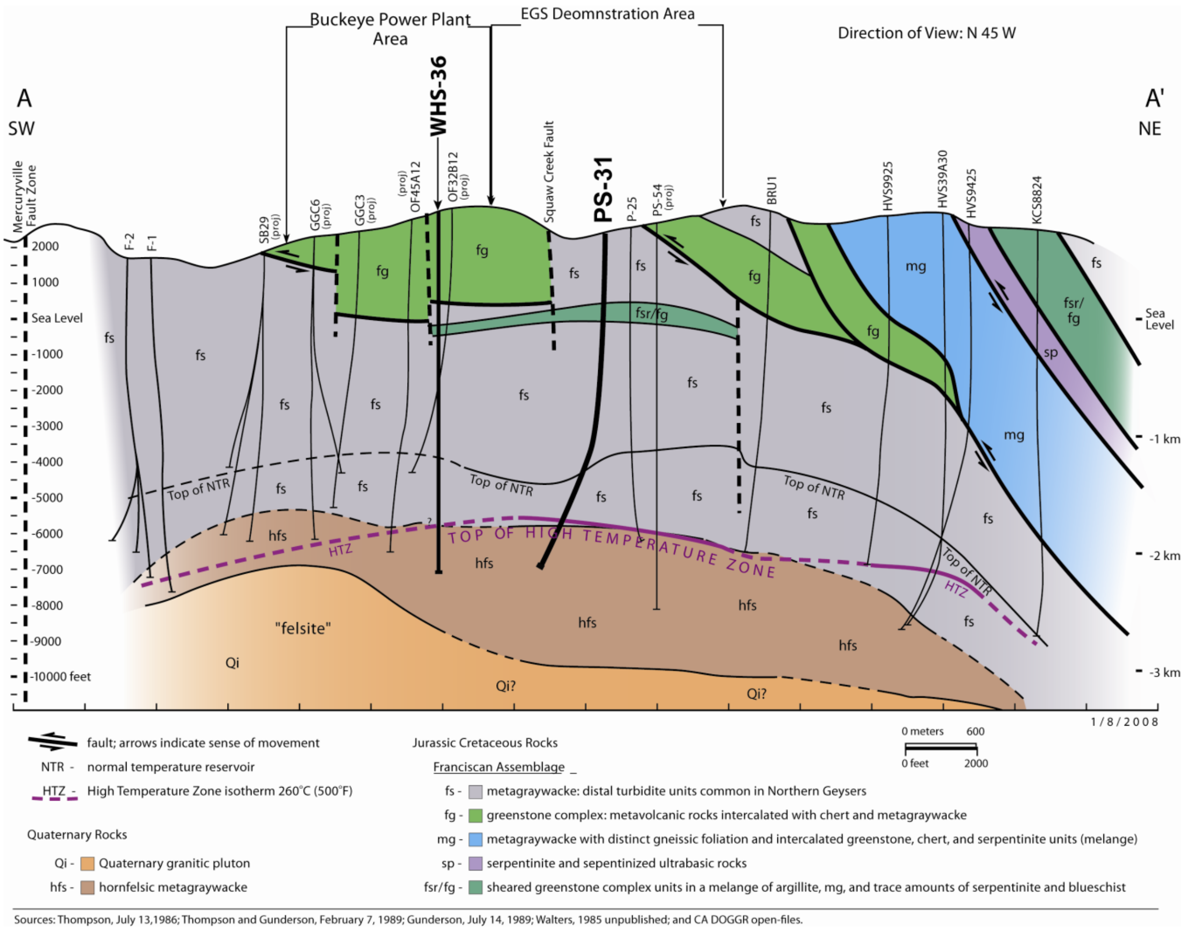

Figure 2 *Geologic cross-section of the Geysers and location of EGS candidate well Prati State 31 ("PS-31). – From Calpine-LBNL proposal (FOA DE-PS36-08G09808).*

3-2 LBNL Statement of the Work

Over the last 10 years, LBNL has installed and operated a 23 element high resolution microseismic array over the entire Geysers geothermal field. Due to induced seismicity issues, the operators and community have agreed that LBNL serve as an independent entity and be the sole operator of the array. The data from the array are now being archived by the USGS - Northern California Data Center (NC DC) for general use by the scientific community.

Recently two new operators will be expanding the power generation from the Geysers field, Alta Rock Energy and Bottle Rock Geothermal Inc. Both of these operations will involve injection and potential seismicity changes. Alta Rock Inc. will be expanding capacity in the SW Geysers and Bottlerock Geothermal Inc. will be expanding in the NE Geysers area. Although Alta Rock will be installing a focused array, it will be necessary to add additional stations to the current 23 stations LBNL to properly monitor the fieldwide seismicity. The expanded array will be 29 stations in total, once it is completed in mid-2009.

In addition to the Bottle Rock and Alta Rock Energy injection projects, Calpine is planning to open closed wells in the northwest Geysers area that have been drilled into the HTZ (over 500

°F temperature) and convert them into injection wells. If exploited properly, the northwest Geysers could offer a significant energy source. This area is just north of the current array and expansion of the seismic array will be done to follow the paths and effects of the injected fluids.

LBNL will be undertaking a five year program to not only continue the operation of and expansion of the array, but also analyzing the data for the effect of the injected water. Although seismicity is being used to manage the reservoir, there are still many unanswered questions about the relation between seismicity and reservoir behavior in geothermal systems. There are two prime objectives of this work:

1. To continue operation of current high resolution seismic array and expand the array to the above-mentioned areas. The data will be archived and made available to the public through the NCDC as well as the LBNL website; and
2. To use MEQ monitoring to understand and intelligently manage the effects of fluid injections and stimulations to aid in the optimization of Enhanced Geothermal Systems (EGS).

Calpine and NCPA will provide at least 20% cost share through providing well and reservoir access, facilities support (instrumentation space, internet support, etc.), field support for the stations, land access, unpublished and "hand-picked" data from past MEQ analysis/ reservoir data and focused experiments on injection and related seismicity effects. The expansion of the Geysers offers an excellent opportunity to study in detail such issues as fracture creation, stress redistribution and many other issues related to high temperature reservoirs that will be common to enhanced geothermal systems in general. In addition, this effort will provide continuity in high resolution seismic monitoring such that the data can be provided to the scientific community and the Seismic Monitoring Advisory Committee (SMAC) on a regular basis.

4- Background on Passive Seismic Data for Exploration of and Production from Geothermal Fields

The seismic refraction technique has been used for exploration and production from geothermal fields, mainly as a reconnaissance tool for mapping velocity distributions. The focus has been primarily in the top few kilometers of the crust, from which faults, fracture zones, intrusions, rock types and other structural features are inferred. Several studies have demonstrated the usefulness of the technique in geothermal areas. Among them are Hill (1976), Majer and McEvilly (1978), Gertson and Smith (1979), and Hill et al. (1981).

Investigation of MEQs (magnitude range: 1–3) in tectonically active and volcanic areas has shown that major hydrothermal convection systems are often characterized by a high level of MEQ activity (Ward et al., 1969; Lange and Westphal, 1969; Ward and Bjornsson, 1971; Hamilton and Muffler, 1972; Combs and Rotstein, 1976; Ward et al., 1979; and others). MEQ surveys have the potential to contribute to identification of locations of drilling wells. Several other MEQ studies have been reported in the geothermal areas, e.g., Bjornsson and Einarsson (1974) in the Reykjanes Peninsula in Iceland, Combs and Hadley (1977) in East Mesa, California, Combs and Rotstein (1976) in Coso, and Hunt and Lattan (1982) in Wairakei in New Zealand.

The seismic noise surveys are carried out using a closely spaced group of seismic stations recording for at least 48 hours (Iyer and Hitchcock, 1976). Their analysis techniques included computation of the average noise level in several frequency bands, using carefully selected noise samples, and plotting their spatial variations. Very often power spectra, cross spectra, azimuth and velocity waves are also calculated. Iyer and Hitchcock (1976) summarized the results obtained at four geothermal fields in the United States: the Geysers, Imperial Valley and Long Valley in California, and Yellowstone National Park in Wyoming. They concluded that all four seismic areas have high noise levels in the 1–5Hz frequency band. But the cultural noise present at the Geysers and the East Mesa Valley makes it difficult to interpret the geothermal noise.

Iyer et al. (1979) reported large tele-seismic delays, exceeding 1 s (from Mount Hanna, near the Clear Lake volcanic field and from the Geysers in California), for P-waves traveling through critical zones at these sites. They postulated that a molten magma chamber under the surface volcanic rocks of Mount Hanna, and a highly fractured steam reservoir at the Geysers are responsible for the observed delays. Other sources of the P-wave delays include large-scale alteration, compositional differences, lateral temperature variations, and locally fractured rock (Iyer and Stewart, 1977). Therefore, it is necessary to analyze the results of tele-seismic surveys, together with the information obtained using other geological and geophysical techniques, before inferring a geothermal cause for the variations in P-wave travel times.

Young and Ward (1980) developed techniques to estimate the attenuation of tele-seismic P-waves, and discovered a zone of large attenuation coinciding with a zone of large delays, at the Geysers in California.

Anomalous P-wave travel time delays and attenuations in the high-frequency range have been reported for a number of geothermal fields (Iyer, 1978). Combs et al. (1976b) used an array of nine short-periods, high-gain three-component seismographs at the East Mesa geothermal field in California to investigate the travel time and attenuation anomalies. Records of several well-located MEQs from the Brawley swarm of 1975, with epicentral distances varying from 20 to 50 km, were examined. They discovered significant P-wave travel time delays for ray paths passing through the zone of high heat flow. Spectral analyses of the observed seismic waves from the swarm showed that the relative attenuation of body wave amplitudes increased in the frequency range of 10Hz and higher, along the ray paths through the East Mesa geothermal field.

In a study of the Geysers geothermal area, Gupta et al. (1982) derived regional P- and S-wave velocities using analysis of MEQ data. Absorption coefficients determined from the MEQ data can indicate the presence of fluid-filled, steam-filled, or silica-filled fractures (Wright et al., 1985). Determination of the Poisson's ratio from MEQ surveys helps distinguishing between water and vapor-dominated reservoirs. At the Geysers geothermal field, the Poisson's ratio ranges from 0.13 to 0.16 within the production zone, compared to much higher values, exceeding 0.25, outside the production zone (Majer and McEvilly, 1979; Gupta et al., 1982). The lowering of Poisson's ratio has been partly explained due to a decreased seismic P-wave velocity.

Velocity and attenuation, as well as Vp/Vs variations with depth, in the Geyser geothermal field have been studied extensively. For example, Romeo et al. (1995) showed that velocity and attenuation variation from MEQ data correlate with the known geology and hydrology of the field. Highly consolidated units have high velocity anomalies, whereas poorly-consolidated units exhibit low velocity anomalies in northwestern part of the Geysers. In addition, the steam reservoir, with partial liquid- saturated rock, is inferred from low Vp/Vs and high attenuation to lie between depths of 1 and 3 km, while high values of Vp/Vs delineate liquid-saturated regions of the geothermal field. Large numbers of MEQs take place beneath injection wells, and high resolution MEQ locations should locate the flow paths from these injection wells. This correlation is predictable, implying that intelligent injection procedures should help Calpine to control the increase in seismicity, and permeability (Major and Peterson, 2007).

It was also shown that heat extraction changes the P-wave or S-wave quality factors in hot dry rock geothermal reservoirs. Decline in these factors are attributed to micro-fracturing which is caused by heat extraction. Fehler et al. (1984) showed that the sudden loss of shear-wave energy is correlated with the sudden loss of high frequencies in the seismic signals from pressurized zones. This was based on an experiment at the Geysers field at a depth of 2635 m, wherein the pressurized signals probably indicated the top of a zone of large fractures that are normally closed, but have the potential to open under pressure, with a corresponding increase of reservoir permeability. In addition, self-propped fractures are characterized by a second loss of high frequencies, correlated with a sudden loss of signal amplitude in the unpressurized spectral power log.

Furthermore, as shown by Sato et al. (1991), the production and injection zones boundary, the density, and the orientation of the aligned fractures can be estimated by the shear-wave polarization analysis, and by the relative delay of acoustic emission events.

A fractal-based technique was used by Li et al. (2003) to characterize the capillary pressure curve of the Geyser rock. In this approach the capillary pressure is related to the saturation through a power law, in which the power or exponent is the fractal dimension of the pore space. This was necessitated by the fact that the Brooks-Corey model (conceived for Berea sandstone) is not applicable for the Geysers rock. When well activity is fairly constant over the periods of time, there is a positive correlation between the seismic activity and the fractal dimension. Conversely, there is a negative correlation between seismicity and fractal dimension when there is a rapid change in the water injection rate. This was demonstrated by Henderson et al. (1999).

Stark (2003) presented a model to explain an unusual spatial distribution of seismicity observed in the northwestern part of the Geysers. His model is based on the hypothesis that reservoir hot rock and injected cold water trigger MEQs by their contact. The model indicated that great amounts of the injected water descend into depths within the HTZ. The correlation with Gambill's (1991) results suggests that much of the water is boiled and produced in accordance of the EGS concept of Nielson et al. (2001).

Tester et al. (2007) attempted to identify the technology needs for stimulating the EGS reservoirs and converting geothermal heat to electricity in surface power and energy recovery systems. Economic modeling was used to develop long-term projections for the EGS for supplying electricity and thermal energy. Sensitivities to capital costs for drilling, stimulation and power plant construction, and financial factors, the learning curve estimates, and the uncertainties and risks were all considered.

Rutqvist et al. (2007) concluded that the most probable mechanism of induced seismicity at the Geysers is shear slip along existing fractures. They also indicated that thermal-elastic cooling shrinkage is the main cause of stress changes near injection and production wells due to injection-induced seismicity. Both thermal-elastic cooling shrinkage and increased fluid pressure reduce the effective stress of deep injection-induced seismicity at greater depth below the injection and production wells. In the shallow parts of the system and in the cap rock, stress redistribution from injection-induced cooling shrinkage within underlying reservoir, leading to injection-induced seismicity.

5- Additional Technical Details

Here, we provide additional technical details for different components of the proposed work.

5-1- Data Evaluation- As it we described in sections 3-1 and 3-2, a large body of MEQ data has been and will be collected in the project area. This data collection is done under a separate DOE funded project (Calpine-LBNL-08). We will conduct a thorough examination of the MEQ data collected as well as the augmented data to be collected. We will evaluate the data set and develop a plan on how best to use these data sets for different data analysis approaches discussed below.

5-2 Anisotropic Velocity Tomography

A principal outcome of the proposed field program will be the recording of many MEQs, caused by injection and production activities by the field operator, Calpine. The locations of these events will delineate the locations of new subsurface fractures, which will necessitate the development of new fracture permeability estimates and correlations. It is important to understand the distribution of the permeability, in order to maximize efficiency of future injection and production activities.

The location (in 3-D space) of the MEQs depends upon an accurately known distribution of the subsurface seismic velocities (both P and S). In this context, the velocity fields must include accurate distributions of seismic anisotropy. In its general form, seismic anisotropy is too complex to be useful in this context, so approximations will have to be made:

- Assumptions concerning the (local) symmetry of the subsurface formations, e.g.:
  - Isotropic (almost certainly too simplistic)
  - Vertical polar anisotropic (“VTI”; probably too simplistic)
  - Tilted polar anisotropic (“TTI”; probably too simplistic)
  - Vertical orthorhombic (possibly sufficient)
  - Tilted orthorhombic (probably sufficient)
- For each of the symmetries, the assumption of weak anisotropy is essential, in order to simplify the equations, so that they can be applied in practice. In this approximation, certain *combinations* of the elastic moduli control most of the anisotropic sensitivity and, thus, the equations are re-cast in terms of such *combinations*, in order to analyze the data. Such *combinations* are called *anisotropic parameters* (e.g., Thomsen, 2002), and their distributions (in 3D space) will be derived.

The program will then proceed by successive approximations (in collaboration with LBNL):

a. Starting from an initial isotropic <u>P-velocity</u> field, The MEQ locations are determined.

b. The error-ellipsoids for each location are calculated.
c. Refinements to the velocity field are driven by the error-ellipsoids.
d. Refined error-ellipsoids for each location are calculated.
e. A lower symmetry of the anisotropy is selected from the list above.
f. Refinements to the anisotropic velocity field (i.e., distributions of anisotropic parameters) are driven by the error-ellipsoids.
g. Refined error-ellipsoids for each location are calculated.
h. Steps 5-8 are repeated until no significant further precision in the locations is achieved.

(The extent of the refinement of locations will depend upon the quality of the data, including the distribution of the receivers, and of MEQs, which cannot be known a priori. Other parts of this proposal describe the considerations that lead to the design of the field program.)

If the data quality permits, the distribution of the S-wave anisotropic parameters will be estimated, following a similar program, but also taking advantage of the special phenomenon of *shear-wave splitting*. (In anisotropic formations, *two* shear modes may propagate in each direction, each with a velocity that depends upon its polarization, which depends upon the symmetry of the formation.) In simple situations, this can yield valuable information about subsurface anisotropy, but in complex situations, such information may be difficult to reliably extract from the data.

The outcome of the program will be:

- more accurate determination of MEQs (which, by themselves, constitute an important indication of subsurface fracturing), and,
- an estimate of subsurface anisotropic parameters (which also constitute an important indication of subsurface fracturing)

5-3 Using microseismicity to map the fractal structure of the fracture network

Field observations (Stark, 2003) and geomechanical modeling (Rutqvist and Oldenburg, 2007) have concluded that injection-induced seismicity at the Geysers geothermal field is the result of shear failure on critically stressed fractures caused by the reduction of normal stress associated with thermal contraction. It follows that a spatial analysis of the locations, sizes, and source mechanism of induced events may reveal the structure of the fracture network in the Geysers reservoir. The basic assumptions are that the hypocenters are located on the fractures, that larger events occur on larger fractures, and that the source mechanism constrains the orientations of the activated fractures.

Sammis, Sahimi, and their students used a box-counting technique to analyze the hypocenter distributions and quantify the fractal structure of regional fault networks in Southern California (Sahimi et al., 1993a, 1993b; Robertson et al., 1995). Figure 3 shows the fractal analysis of the hypocenters' locations for the MEQ sequences in Table 1 (which summarized the point densities and fractal dimensions). The most surprising result of their analysis was that the fractal dimensions of the three-dimensional structure were equal to, or slightly, less than 2, whereas the expected result is a fractal dimension between 2 and 3. They interpreted this result as evidence that active seismicity was only occurring on the "percolation backbone" of the structure, the multiply-connected part of the structure necessary to accommodate the tectonic strain (the dead-end parts, which are singly-connected, cannot support the tectonic strain). It is known that the fractal dimension of the backbone of a 3D structure is less than, or at most equal to, 2. This implies that only a small part of the overall structure contributes to distributing and re-distributing the tectonic strain. Such insight is not only crucial to accurate characterization of the fracture map, but will also be very useful to other aspects of the work. For example, flow of water and vapor in a rock in which the fracture distribution is fractal is not similar to one in which the fracture distribution is non-fractal. This, in turn, influences identification of the locations of the target drilling wells.

We propose to collaborate with the geomechanical group at LBNL to use their models to simulate the expected response of a fractal network to the thermal stresses generated by injection. The proposed use of magnitudes and focal mechanisms to further constrain the fractal structure has, to our knowledge, never been attempted, but is a natural extension of our earlier work. It is also expected that the structure of the fault network (possibly fractal) revealed by this study will be synergistic with the proposed anisotropy analysis, and may provide an important constraint for the proposed analyses using fuzzy logic, generic algorithms, and neural networks.

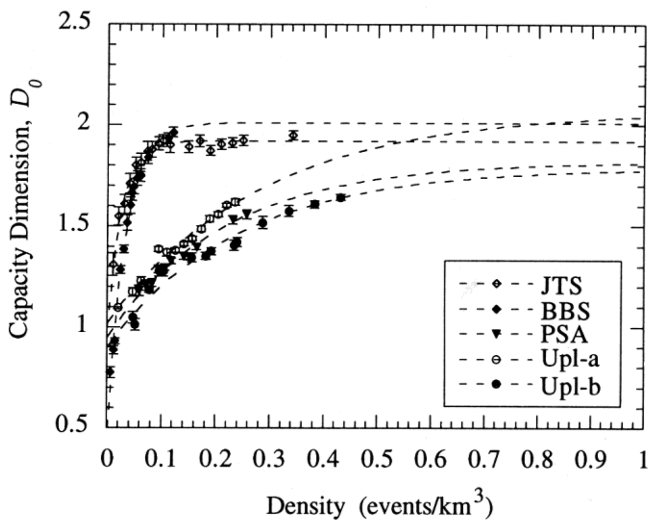

Data Set	Max ρ, events/km^3	Asymptotic Value of D_0
Joshua Tree Sequence (JTS)	0.34	1.92 ± 0.02
Big Bear Sequence (BBS)	0.12	2.01
Parkfield Sequence (PSA)	0.25	1.82
Upland Sequence (UPL-a)	0.24	2.07
Upland Sequence (UPL-b)	0.43	1.79

Figure 3. Fractal analysis of the hypocenters' distributions as a function of hypocenter density for the MEQ sequences indicated (Robertson et al., 1995).

5-4 Use of Soft Computing to Analyze Passive Seismic Data

Soft computing (including neural networks, fuzzy logic, and genetic algorithms) has been used extensively in geosciences and energy-related applications. Some of such applications have been highlighted by Nikravesh et al. (2007) and Aminzadeh and de Groot (2007). Yet, practically no such applications have been for exploration and exploitation of geothermal resources. An exception is the work by Akin (2008) who demonstrated how neural networks could be used to create volumetric pressure and enthalpy response in a geothermal field in Turkey. Ghomshei et al. (2001) used fuzzy logic to design an optimum heat pump in a geothermal field.

As explained by Dragoset et al. (2009), the oil industry has enthusiastically adopted 3D seismic reflection imaging more than 20 years ago to image structural and reservoir complexity, and more recently has developed 4D, or timelapse repeat surveys, to monitor reservoir mechanical and fluid changes during resource extraction. More recently, this is increasingly accompanied by monitoring of production-induced MEQ activity. Nevertheless, seismology and soft computing are less commonly used in geothermal and mineral exploration and development. The challenge is to adapt the vast body of the work on soft computing applications to seismic data from the petroleum industry, to the problems in geothermal fields. Seismic imaging has also been used to track mining-induced stress changes in the rocks that lead to “mine bumps,” induced seismic events, and cavern collapses, and plays a key role in mining safety measures. Similar coupled imaging and MEQ monitoring holds great potential for geothermal energy exploration and production.

Our focus in this part of the project will be on careful analysis of the MEQ and microseismic data in the Geyser field. We will use the power of neuro-fuzzy approach in the processing of the MEQ data and in developing a mathematical framework for the velocity fields to develop a more practical velocity field. We will use the neuro-fuzzy approach as described in Aminzadeh and Brouwer (2006) to help with the automation process and its improvement in picking MEQ seismic events. Handpicked events in selected seed points will be used as the training set for the neuro-fuzzy auto-picker. The results will be compared against the current auto-picker being used by LBNL as well as the hand-picked selections. We expect our hybrid approach will be superior in both ability to pick the subtle events and the efficiency of the process.

Fuzzy Compressional- and Shear Wave Velocity Relationship

Given the usually poor quality of micro-seismic data, simultaneous analysis of shear wave and P-wave data to deduce information on shear wave splitting from fractured reservoirs is usually difficult. Aside from the compressional velocity fields, we will look into the fuzzy relationships between the shear wave velocities for different rock types.

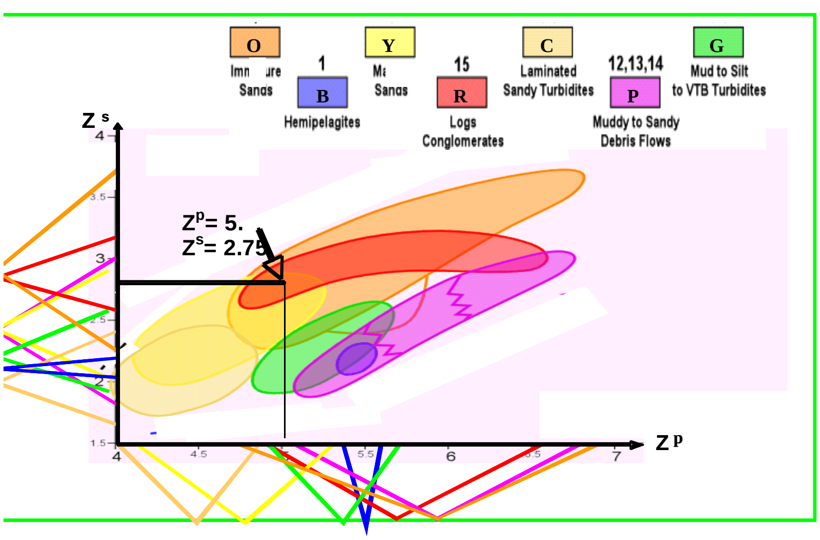

Zp=5, Zs=2.75

$_{\text{sand,immature}} = 0.13$, $\mu_{\text{sand,mature}}=0.5$, $\mu_{\text{conglomerate}}=0.37$

Figure 4- Impact of fuzziness in P-wave and S-wave velocities in the separation of different rock types

Figure 4 shows the fuzzy nature of the velocities for different rock categories. Using a large number of well data sets from the existing wells, in conjunction with the analysis of the MEQ data, we will develop a "fuzzy velocity" field and attempt to extrapolate and validate the velocity field from micro-seismic data measurements. Reservoir characterization with fuzzy velocities will be examined. Figure 4 demonstrates the impact of fuzziness on the P-wave and S-wave velocities in the separation of different rock types according to their respective S- and P-wave impedances. We will use the models described in the earlier sections and their elastic model counter parts for further investigation. Some of the concepts, highlighted by Aminzadeh and Wilkinson (2004), will be revisited and examined here.

To better understand the fracturing system, we will utilize various neural-network-based approaches, as applied to conventional seismic data, adapting them to those from geothermal fields. Specifically, we will examine the use of different seismic attributes such as similarity, eccentricity, and curvature for fracture modeling and interpretation. Some of the work reported in Aminzadeh and Brouwer (2006) will be applied here. Figure 5 is one such example where a hybrid neural network and fuzzy logic approach is used to create a more reliable hydrocarbon map.

This approach will be extended to examine and analyze the microseismic data acquired in the course of this project, and to develop an accurate fracture map for the area.

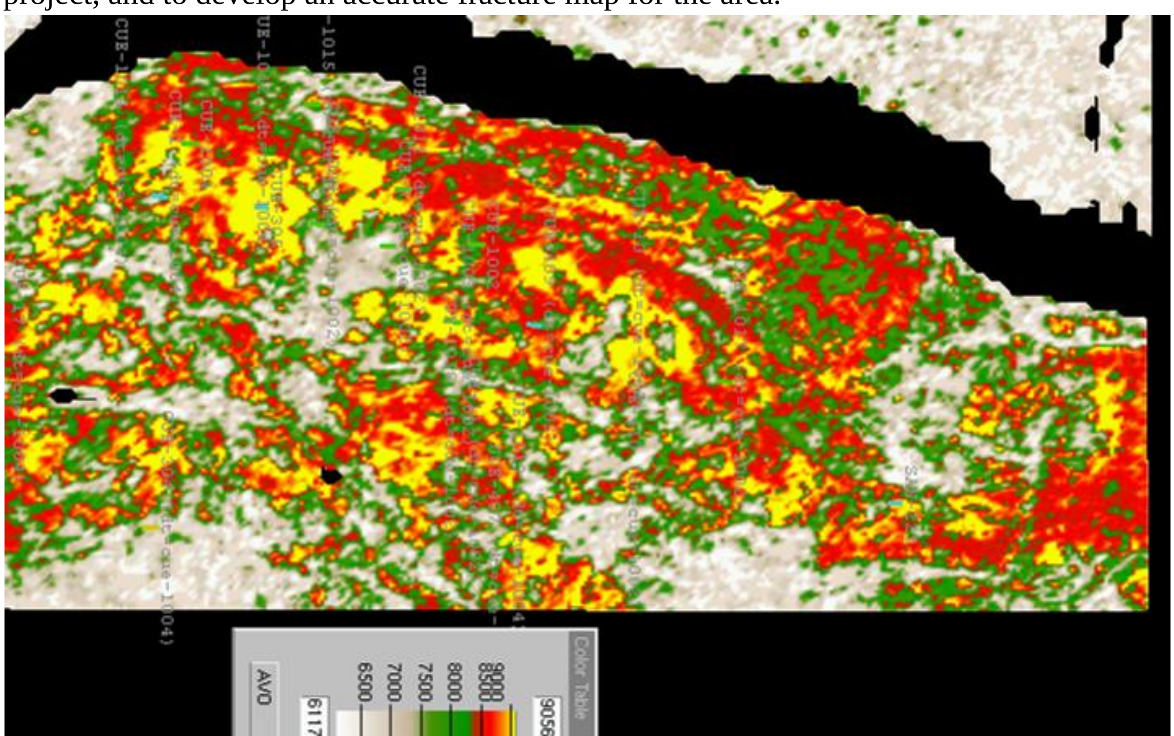

Figure 5- A neuro- fuzzy based hydrocarbon probability map.

6- References:

1. Akin, S., Optimizing of re-injection in low temperature geothermal reservoirs using neural networks and kriging proxies, Proceedings of thirty third workshop on geothermal reservoir engineering, Stanford University, January 28-30, 2008.
2. Aminzadeh, F. and Brouwer, F., Integrating neural networks and fuzzy logic for improved reservoir property prediction and prospect ranking, Extended Abstracts of Society of Exploration Geophysicist Annual Meeting in New Orleans, 2006.
3. Aminzadeh, F. and Wilkinson, D., Soft computing for qualitative and quantitative seismic object and reservoir property prediction, part 2, fuzzy logic applications, 22, 69-78,2004.
4. Aminzadeh, F., and de Groot, P., Neural networks and soft computing techniques, with applications in the oil industry, EAGE Publishing, 2006.
5. Dragoset, B., Aminzadeh, F., de Groot, P., and Louie, J., Exploration seismology and resources: energy and mining, IRIS image gallery, www.iris.edu/hq/gallery/photo/4503, 2009.
6. Degraff, J. M. and Aydin, A., Evolution of polygonal fracture patterns in lava flows, Science, 239, 471 – 476, 1988.
7. Degraff, J. M. and Aydin, A., Surface morphology of columnar joints and its significance to mechanics and direction of joint growth, GSA Bulletin, 99, 605-617, 1987.
8. Dorbath, L., Cuenot, N., Genter, A., and Frogneux, M., Seismic response of the fractured and faulted granite of Soultz-sous-Forˆets (France) to 5 km deep massive water injections, Geophysics, 2009.

9. Fehler, M. and Pearson, C., Cross-hole seismic surveys: Applications for studying subsurface fracture systems at a hot dry rock geothermal site, Geophysics, 49, 37-45, 1984.
10. Ghomshei, M. M. , Meech, D. W., Fraser, D. W., Daskin, R. A., Geothermal heat pump options: Fuzzy arithmetic for a bright decision, proceedings of the third international conference on Intelligent Processing and Manufacturing Materials (IPMM) , 2001.
11. Henderson, J.R., Barton, J., and Foulger, G.R., Fractal clustering of induced seismicity in the geysers geothermal area, California, Geophysical Journal International, 139, 317-24, 1999.
12. Johnson, L.R., and Sammis, C. G., Effects of rock damage on seismic waves generated by explosions, PAGEOPH, 158, 1869-1908, 2001.
13. Li, K. and Horne, R.N., Fractal characterization of the geysers rock, Annual meeting of international collaboration for geothermal energy in the Americas - geothermal resources council, 27, 707-710, 2003.
14. Majer, E. L. and McEvilly, T. V., Seismological investigations at the geysers geothermal field, Geophysics, 44, 246-69, 1979.
15. Majer, E. L. and Peterson, J. E., The impact of injection on seismicity at the geysers, California geothermal field, Int. J. Rock Mech. Min. Sci., 44, 1079-1090, 2007.
16. Nikravesh, M., Aminzadeh, F., Zadeh, L. A., Soft computing and intelligent data analysis, Developments in petroleum science series, Elsevier, 51, 724, 2003.
17. Robertson, M.C., Sammis, C. G., Sahimi, M., and Martin, A., The 3-D spatial distribution of earthquakes in southern California with a percolation theory interpretation, J. Geophys. Res., 100, 609-620, 1995.
18. Romero Jr., E., McEvilly, T. V., Majer, E. L. and Vasco, D., Characterization of the geothermal system beneath the northwest geysers steam field, California, from seismicity and velocity patterns, Geothermics, 24, 471-487, 1995.
19. Rutqvist, J. and Oldenburg, C., Analysis of cause and mechanism for injection-induced seismicity at the geysers geothermal field, California, Annual Meeting of the Geothermal Resources Council, 31, 441-445, 2007.
20. Ryan, M. P., and Sammis, C. G., Cyclic fracture mechanism in cooling basalt, Geol. Soc. America Bull., 89, 1295-1308, 1978.
21. Sahimi, M., Applications of Percolation Theory, Taylor and Francis, 1994.
22. Sahimi, M., Flow and Transport in Porous Media and Fractured Rock, VCH, 1995.
23. Sahimi, M., Robertson, M.C., and Sammis, C.G., fractal distribution of earthquake hypocenters and its relation to fault patterns and percolation, Phys. Rev. Lett., 70, 2186-2198, 1993a.
24. Sahimi, M., Robertson, M.C., and Sammis, C.G., Relation between the earthquake statistic and fault patterns, and fractals, and percolation, Physica A, 191, 57-68, 1993b.
25. Sato, M., Matsumoto, N., and Niitsuma, H., Evaluation of geothermal reservoir cracks by shear-wave splitting of acoustic emission, Geothermics, 20, 197-206, 1991.
26. Stark, M., Seismic evidence for a long-lived enhanced geothermal system (EGS) in the northern geysers reservoir, Annual meeting of international collaboration for geothermal energy in the Americas - geothermal resources council, 27, 727-731, 2003.
27. Tester, J.W. et al., Impact of enhanced geothermal systems on US energy, Philosophical Transactions A, 2007.ontents

Appendix 1-2: Project Management Plan (PMP)

Project Title Characterizing Fractures in Geysers Geothermal Field by Micro-seismic Data, Using Soft Computing, Fractals, and Shear Wave Anisotropy

This is a joint technology application collaborative project between the University of Southern California (USC), Geysers Power Company, "Calpine", and Lawrence Berkeley National Laboratory (LBNL), to develop improved methods for better characterization of fractures in an enhanced geothermal system (EGS). In this document, we will highlight the tasks from Statement of Project Objectives (SOPO)), proposed go/no-go decision points, a time schedule for the accomplishment of the activities/tasks the spending plan associated with the activities/tasks, the plan for project management and oversight, especially in light of the multi-organization and multi-disciplinary nature of the project. We will provide a plan for expected dates for the release of outcomes as well as the technology transfer plans.

1- SOPO- The proposed program will focus on predicting characteristics of fractures and their orientation prior to drilling new wells. It will also focus on determining the location of the fractures, spacing and orientation as well as characterizing open fractures after stimulation to help identify the location of fluid flow pathway within the EGS reservoir.

- a. **The main focus** of the project will be on
    - **i.** Developing better understanding of the mechanisms for the stimulation of existing fractures,
    - **ii.** Using the information for better exploitation of the high temperature geothermal resources located in the northwest portion of the Geysers field and similar fields.
- b. **How we will accomplish the goals**? Several complementary processing approaches will be used to develop and test new techniques for microseismic data collection and analysis.
    - **i.** We will conduct a general evaluation of the collected MEQ and the augmented data (see details in project narratives, section 5-1)
    - **ii.** We will use anisotropic inversion to create shear wave and compressional wave velocity fields using tomography (see details in project narratives, section 5-2)
    - **iii.** We will use fractal concepts for accurate characterization of the fracture map. tomography (see details in project narratives, section 5-3)
    - **iv.** We will use neuro-fuzzy approach (see details in Section 5-4) to
        - a. Create a hybrid MEQs event picking,
        - b. Process, analyze and interpret microseismic data with higher level of accuracy and provide more suitable input data to (i) and (ii),
        - c. Gain improvements in fracture reservoir characterization.

2- Project Management and oversight, In light of the multi-organization and multi-disciplinary nature of the project, a matrix project management will be used to help exchange of information, data, and technology development efforts.

- a. **General Project Management and Geophysics Discipline Coordination -** Fred Aminzadeh (FA) will be responsible for general project management and coordination. FA will also be responsible for the all aspects of **geophysics discipline** coordination.
- b. **Geology and Reservoir Disciplines Coordination will be done by** Charles Sammis and Muhammad Sahimi

c. **Seismic Data Acquisition and Management.** All the data used in this study and issue related data handling and distribution among the team members will be done by Ernie Major

d. **Well Data Collection, Simulation and other Injection and Production Well Coordination will be done** by Mark Walters

e. **Project Task Coordinators**

   i. Anisotropy: Leon Thomsen

   ii.Fractals: Sammis/Sahimi

   iii. Neuro-Fuzzy- Fred Aminzadeh

For two reasons we expect to have extensive communication and interactions among the team members:

f. The proposed project (USC-LBL-Calpine 09) is a multi-organization and multi-disciplinary project. Both discipline related and task related activities among team members from all here organizations to work closely with each other.

g. The proposed project (USC-LBL-Calpine 09) will complement and enhance the ongoing EGS experiment in the northwest Geysers, under DOE funded LBNL-Calpine project from FOA Number DE-PS36-08G098008, (Calpine-LBL-08) there will be extensive communication and exchange of information between the team members of the two projects.

For a smooth and effective flow of information, data and research results we will have a monthly conference call. We also plan to conduct quarterly face to face review meetings, rotating the meeting locations between USC (Southern California) and Calpine/LBL (Northern California). The key conclusions of these quarterly meetings will be part of the reporting mechanism to the DOE, to be discussed below.

Intellectual Property Ownership- The intellectual properties created through this project will be owned by the organization where they are developed. To allow free exchanges when confidential information need to be shared, if deemed necessary, a confidentiality agreement will be executed before divulging sensitive information.

3- Proposed go/no-go decision points.

The proposed project has a total time period of 24 months. We expect to use the first year to complete review of all the data available. This includes older data, the data collected by (LBL) through (Calpine-LBL-08) as well as the augmented data to be collected through the end of 2009. Upon complete evaluation of the data (through first half of 2010) and preliminary work on the data (through end of 2010), we will make a determination on whether the data quality is sufficiently good to complete the three major technical tasks (items 1-I, 1-ii and 1-iii). At the end of 4Q 2010 we will determine whether one or more of the technical task should be discontinued or we should re-allocate the funds. We will send DOE a written assessment by the end of 2010 and advise whether aspect of the project needs any modification.

4- Time schedule for the accomplishment of the activities/tasks and the spending plan associated with the activities/tasks,

Given the fact that the requested funding is for research and development work and the expenditure is roughly proportional to time spent by the investigators, no separate expenditure plan is deemed necessary. That is, no funds are requested for data acquisition (we will use the data from other DOE sponsored project, CalpinelLBL-09) or no funds are requested for major capital expenditure or equipment. As such, the following timeline can be considered as the project spending plan:

Project Timeline

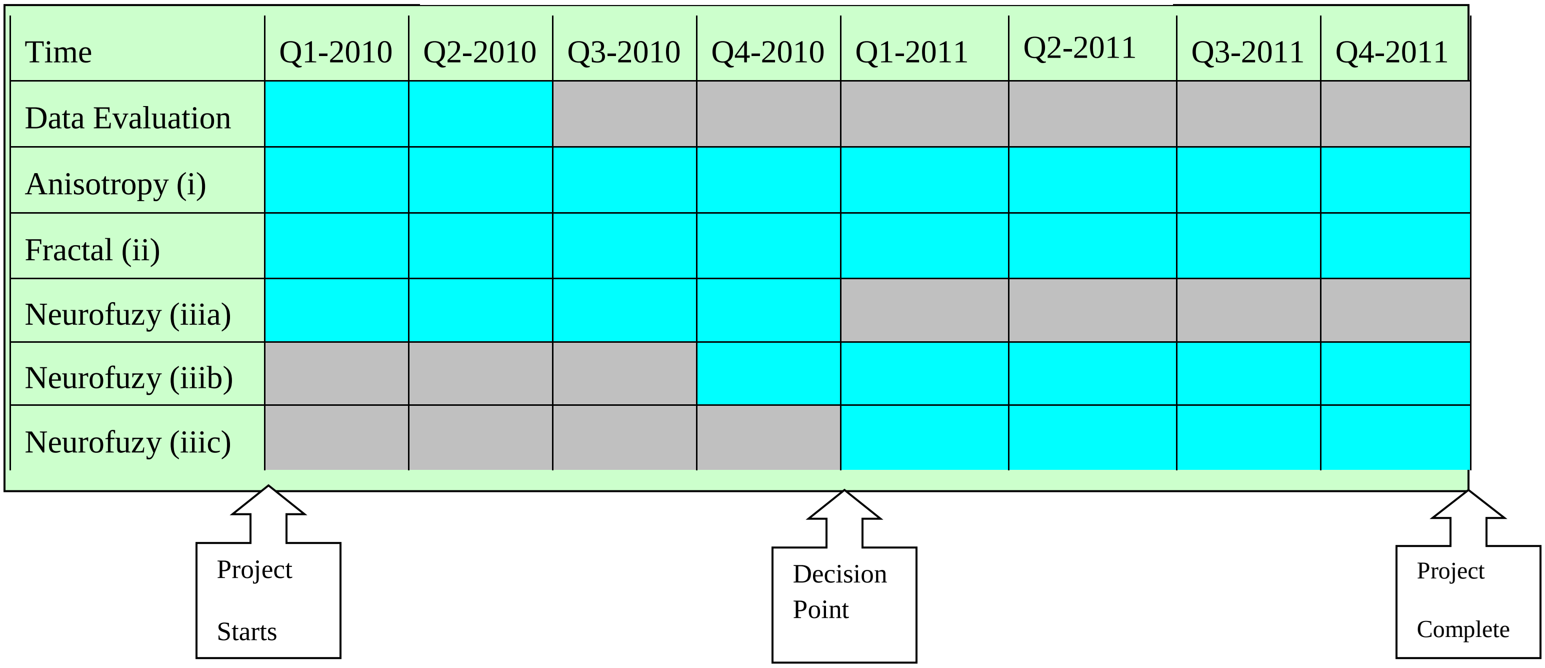

5- Expected dates for the release of outcomes and Technology transfer plans.

As discussed under Project management plan, we expect to release a quarterly report upon the conclusion of each quarterly review meeting. The review meeting for each of the first three quarters will take place within two weeks before or after the end of each quarter (RQ1, RQ2 and RQ3). These reports will be released within a month after each quarter. A more substantial (annual) report will be prepared within a month after the end of the fourth quarter (RQ4). The first annual report will also include the conclusions of the decision point regarding any possible modifications different tasks. The second annual report will be considered as the final report of the project.

Technology transfer and student participation in the project will be an important aspect of the project. To fulfill this goal, we plan to make frequent presentations in the appropriate technical meetings and conventions. Furthermore, we will present the preliminary results to various local companies and professional societies. Finally, we expect to conduct at least one workshop towards the end of the Q2-2011 to introduce our findings to the technical geothermal producer communities and solicit their feedback. We will utilize the feedback from this workshop to finalize project and establish a procedure for further dissemination of our findings within the technical and geothermal producer communities.

Appendix 4-4: Anisotropy Tomography for Micro-earthquake Location and Subsurface Physical Characterization

Lawrence Hutchings and Leon Thomsen
Lawrence Berkeley National Laboratory

Introduction

The purpose of this paper is to apply the theory of anisotropic wave propagation to tomographic inversion of micro-earthquake arrival times, in the context of a complex subsurface and complex surface topography. The result of this analysis is the development of three-dimensional models of anisotropic structure, P and S-wave anisotropic velocity models, and identification and characterization of subsurface fractures. We work with the assumption that locally (within each elemental volume, voxel), the anisotropy is uniform polar anisotropy, and of course we recommend our approach only for situations where this assumption is plausible. We do not specify the local orientation of the pole of symmetry, rather we solve for it, finding two Euler angles as well as five elastic parameters in each voxel.

Anisotropy can be due to thin-layer bedding, mineral or pore alignments, or fractures and faults. In our model, these are the planes of symmetry we identify with polar anisotropy. We use the terms “fractures” and “faults” to mean planar discontinuities in the rock mass, affecting wave propagation and possibly fluid flow, without implication regarding physical causes. In addition to the tomographic inversion for anisotropy, we identify faults from the location of micro-earthquakes and their focal mechanism solutions. The orientation of fractures and faults, can also be obtained from standard shear-wave splitting interpretations (Lou and Rial, 1997). This, and focal-mechanism solutions are applied in our inversion program as constraints when available. Generally, however, we rely on the plane of symmetry solved for in the tomographic invasion as indicating the orientation and location of anisotropic geology. Further interpretation is required to characterize the permeability.

Travel time tomography from micro-earthquake recordings is more difficult than the corresponding problem from controlled-source surveys, since it includes the complication of locating the earthquakes. This is a difficult task, as we need to know the velocity of the subsurface in order to locate the earthquakes accurately, which is what we are solving for. It also adds four unknowns (3 spatial source coordinates, plus origin time) for every earthquake; adding to the 7 unknowns previously mentioned for each voxel. Further, earthquakes generally are at depths of 1 – 5 km in geothermal or hydrofracking environments, so that obtaining physical parameters at depths can be difficult.

This is also a circularity problem when using focal mechanism solutions to identify the orientation of fractures. The focal mechanism solutions depend upon interpreting the radiation pattern from earthquakes and in anisotropic media the radiation pattern is affected by the anisotropic wave propagation (Chapman and Pratt, 1992). Similarly, anisotropic wave propagation adds the complications of obtaining moment tensor solutions (Chapman and Leaned, 2012).

We modified the computer program stimulus (Thurber, 1983; Eberhard-Phillips, 1992) to include inversion for anisotropic parameters, double difference earthquake locations (Wald Hauser and Ellsworth, 2000), and added common ray path inversion (discussed below). The program applies standard linearized least squares inversion to minimize the residual between observed arrival times and those calculated from tracing rays though the volume. We use this application to get absolute earthquake locations and initial geologic velocity structure. We added double difference calculations to the program as herein described. The double-difference earthquake locations takes advantage of the travel time difference between closely located events to get accurate relative locations. This is applied in the location loop of the program. In the tomography loop for anisotropic parameters, we common ray path by identify overlapping ray paths to common stations and localize the inversion to the portions of the path between two events. In this application the two events do not need to be closely lactated (common source location), rather have overlapping ray paths to a common station (common ray path approach). The new program is called Simulate (anisotropic and double-difference).

We apply our inversion to data from The Geysers geothermal field in Sonoma County, California. The lithology of The Geysers geothermal reservoir is dominated by low-grade metamorphism fractured greywackes that commonly lack schistosity, warranting the general assumption that it is composed of stress-aligned fracturing in an otherwise isotropic medium. Recent projects and permeability studies suggest that open fractures and open veins in the meta-greywackes are principally vertical, or steeply dipping, and are related to the regional strike-slip environment of The Geysers (Nielson & Nash 1997; Hulen & Nielson 1996). The hypothesis of pervasive subvertical to vertical open fractures agrees with the theory that stress-aligned cracks in the crust tend to extend parallel to the maximum compressive stress and perpendicular to the direction of minimum compressional stress, which are both typically horizontal (Crampin & Booth 1989, Elkibbi, 2005).

In sedimentary, igneous, and metamorphic geological environments with rocks predominantly fractured by a single crack system, percentages of shear-wave velocity anisotropy ("SWA") are expected to range between SWA = 1-5% (Crampin 1993). In terms of crack density ε, this is approximately equivalent to ε = 0.01-005 (Crampin 1993), provided that the Poisson's ratio of the uncracked medium is about 0.25 (Vp/Vs = 1.732). In geothermal environments, however, high heat flow may cause shear-wave velocity anisotropy to be higher than normal and to potentially reach values as high as 10 per cent, equivalent to a crack density of $\varepsilon = 0.1$ (Crampin & Booth 1989, Elkibbi, 2005). Hydrofracking operations may produce similar anisotropy, depending on intensity of the fracking treatment, the distance from the borehole, and the permeability of the shale, pre-frac.

Theory

Solutions to Wave Equation in Anisotropic Media

The standard wave equation in seismology can be expressed by (sec. 2.1, eq. 2.13 and 2.18; Aki and Richards (2009) (hereafter "A&R"), Thomsen (2002) eq. 1.22 for homogeneous media):

$$\rho \frac{\partial^2 u_i}{\partial t^2} = f_i + C_{ijmn} \frac{\partial^2 u_m}{\partial x_n \partial x_j} \tag{1}$$

where, f_i is the source term and C_{ijmn} is the standard fourth rank elastic stiffness tensor for a medium (which relates stress to strain), u_i is displacement and ρ is the density of the medium. This equation assumes local homogeneity (on the scale of the wavelength); we use it here even though this assumption is probably not strictly valid in our context. The solution to equation (1) when f_i is an impulsive point source is the elasto-dynamic Green's function. With substitution, and following Betti's theorem (A & R, sec 2.4), we arrive at the solution for displacement from a point source (A&R, chapter 3, eq. 3.18):

$$u(x,t)_i = A_{x'}\left\{C_{kjmn}[s(x',t')_k]v(x')_j\right\} * \frac{\partial G_{im}}{\partial x_n} \tag{2}$$

where *x'* and *t'* are the space-time locations of the source, while *x* and *t* are those of the receiver, *G* is the Green's function, * is the convolution operator, and [ ] designates differential movement across the dislocation surface. Here we are assuming a point source, so the integral in A&R is replaced by the elemental area of the point source, at position x', $A_{x'}$. The terms in { } make up the moment density tensor, which determines the strength and geometry of the source per unit area, where: s_k is the amplitude of slip along the fault in the *k* direction as a function of time, v_j is the unit normal to the slip surface at position *x'*. This along with the unit area is often identified as the moment tensor *M*:

$$M(x',t')_{mn} = A_{x'}\left\{C_{kjmn}[s(x',t')_k]v(x')_j\right\} \tag{3}$$

In this equation, C_{kjmn} are the elastic constants at the source, assumed to be locally homogeneous. The elastic constants for wave propagation are part of the Green's function, and are the parameters we will be solving for in the inversion.

The solution of (2) in a homogeneous whole space, excluding intermediate- and near-field terms, near the source (A & R, sec. 4.3) is:

$$u(x,t)_i = M^o_{mn} * G_{im,n} = M^o_{mn}\frac{A_{\mathrm{imn}}}{r}\left(t-\frac{r}{\alpha}\right) - M^o_{mn}\frac{B_{\mathrm{imn}}}{r}\left(t-\frac{r}{\beta}\right) \tag{4}$$

where the geometrical constants A_{imn} and B_{imn} are described in A & R, sec 4.3, and *r* is radial distance from the source, and the local isotropic *P*- and *S-plane-wave* velocities are α and β.

In the general solution given by A&R, the source signature is not specified. Here we assume a step source time function (with a delta function time derivative), so the time dependence of the moment tensor is lost and M^o_{mn} in (4) is the time-integrated moment tensor, and only controls the radiation pattern and the strength of the earthquake. This is approximately true if the duration of the fault is much shorter than the periods of the arrivals that we utilize in the tomography. In this study we are not interested in the strength of the earthquakes or the radiation pattern, only the time of the first motion. The Green's function derivative, excluding intermediate- and near-field terms (which die out as r^{-2} and r^{4}, generally don't reach the receivers), is:

$$G_{im,n} = \frac{A_{imn}}{r}\left(t - \frac{r}{\alpha}\right) - \frac{B_{imn}}{r}\left(t - \frac{r}{\beta}\right) \tag{5}$$

So, near the source, the displacement propagates as two delta functions with spherical wavefronts traveling at the P- and S- wave velocities, α and β .

Rewriting equation (4) in the form of a ray series (Cerveny, 1972):

$$u(x,t)_i = \sum_n \left(u_i^n(x_i)\left(t - \frac{r}{\alpha}\right) - u_i^n(x_i)\left(t - \frac{r}{\beta}\right) \right) \tag{6}$$

where, $u_i^n(x_i)$ is the amplitude term and is a function of geometrical spreading, strength of the source and focal mechanism solution.

The P-wave solution above is equivalent to the frequency domain solution as a sum of all frequencies:

$$u(x,t)_i = \sum_{\omega} u_i^{\omega}(x_i)\, e^{i(k_i x_i - \omega t)} \tag{7}$$

with wavenumber $k(\omega)$ and frequency ω . Propagation velocity is $\alpha = \omega / k$. The wavefront propagation from a point source satisfies $t = \omega / k$. Such plane wave solutions form a complete basis set, so that any function of (x, t) can be represented by a sum of such waves. We use this formalism to deduce the equivalent solution for anisotropic wave propagation. Plugging equation 7 into equation 1, with $f_i = 0.0$ away from the source, yields:

$$u_i = \frac{C_{ijmk} n_j n_k}{\rho} \frac{k^2}{\omega^2} U_m \tag{8}$$

The term $\frac{C_{ijmk} n_j n_k}{\rho}$, where n_j is the direction cosine in the *j* direction, is referred to as the Christoffel matrix (Chapman & Pratt, 1992).

The approach of Wu and Lees (1999) follows equations 6 to obtain three families of geometrically spreading plane waves (one quasi-P wave, and two quasi-S waves), polarized according to the local eigen-directions of the medium) . The three eigen-values $v^2 = (\omega/k)^2$ of these solutions are the squares of the three corresponding anisotropic plane wave velocities. Wu and Lees note that there exists a closed P-velocity surface with respect to spherical coordinates φ and ψ that can be synthesized, via Cartesian products of unit vectors $\hat{x}$, as a basis set of expansion. $v(\hat{x})=v(\varphi,\psi)\ \ f(x)\ \ (x)\leq 1\ \ v(\varphi,\psi)\ \ f(x)$ The relation obtained when the decomposition is truncated at second order is:

$$v(\hat{x})\approx(v_o I_{ij}+C_{ij})\hat{x}_i\hat{x}_j=A_{ij}\hat{x}_i\hat{x}_j \tag{9}$$

where v_0 is the average velocity. This is based strictly on tensor calculus; the truncation to second order corresponds to the assumption of weak anisotropy. Since A_{ij} is a symmetric positive definite tensor of dimension 3, there are only six independent components. Individual values for A_{ij} can be obtained for specific anisotropy conditions. For example, for polar anisotropy with vertical symmetry axis, $A_{11}=A_{22}$, $A_{12}=0$, and $A_{13}=A_{23}$; which leaves only three independent components. The resultant fourth order travel time equation is linear in A_{ij}, thus they use linear inversion.

We follow Thomsen's (2002) solution, he solves for the eigenvalues of the matrix (equation 6) and finds three velocities, one P- and two S-waves (see his Figure 1-35):

$$V_p^2(\theta)=V_{P0}^2\left[1+\varepsilon\sin^2\theta\right]+D' \tag{10a}$$

$$V_{S1}^2(\theta)=V_{S0}^2\left[1+\varepsilon\frac{V_{P0}^2}{V_{S0}^2}\sin^2\theta\right]-\frac{V_{P0}^2}{V_{S0}^2}D' \tag{10b}$$

$$V_{S2}^2(\theta)=V_{S0}^2\left[1+\gamma\sin^2\theta\right] \tag{10c}$$

where, for polar anisotropy:

$$C_{ijkl}=C_{1111},C_{3333},C_{2323},C_{1212},C_{1133} \tag{11}$$

and ,

$$V_{P0}=\sqrt{\frac{C_{3333}}{\rho}}\qquad V_{S0}=\sqrt{\frac{C_{2323}}{\rho}} \tag{12}$$

and,

$$\varepsilon = \frac{C_{1111} - C_{3333}}{2C_{3333}} \qquad \delta = \frac{(C_{1133} - C_{2323})^2 - (C_{3333} - C_{2323})^2}{2C_{3333}(C_{3333} - C_{2323})} \qquad \gamma = \frac{C_{1212} - C_{2323}}{2C_{2323}} \quad (13a)$$

also, $\delta = \left(\frac{C_{3333} + C_{1133}}{2C_{3333}}\right)\left(\frac{C_{1133} + 2C_{2323} - C_{3333}}{C_{3333} - C_{2323}}\right)$, from Berryman (2008) (13b)

and,

$$D' = \frac{\left(1 - \frac{V_{S0}^2}{V_{P0}^2}\right)}{2}\left\{\left[1 + \frac{4(2\delta - \varepsilon)}{\left(1 - \frac{V_{S0}^2}{V_{P0}^2}\right)}\sin^2\theta\cos^2\theta + \frac{4\left(1 - \frac{V_{S0}^2}{V_{P0}^2} - \varepsilon\right)\varepsilon}{\left(1 - \frac{V_{S0}^2}{V_{P0}^2}\right)}\sin^4\theta\right]^{\frac{1}{2}} - 1\right\} \qquad (14)$$

As complicated as this appears there are only 5 unknowns as shown in equation (11), plus density ρ . θ is the angle of wave propagation relative to the pole of the anisotropic plane. So, if we solve for ε , δ , γ , V_{P0} and V_{S0} there are five unknowns. V_{P0} and V_{S0} are the P- and S-wave anisotropic velocities aligned with the pole of the plane of symmetry (θ = 0), and are not the isotropic solution for these values. ρ only appears in V_{P0} and V_{S0} , which we solve for. The five unknowns have significance in oil and gas exploration, where they are commonly applied with the assumption of a vertical pole of symmetry. At this point we have made no assumptions of whether the anisotropy is *weak* or *strong*. Berryman (2008) urges one to avoid approximations using *weak* anisotropy and we follow this argument so as to preserve the solution for *strong* anisotropy.

In the case where the anisotropic parameters ε and δ are <<1, Eqs. 8 may be linearized as

$$V_P(\theta) = V_{P0}\left[1 + \delta\sin^2\theta\cos^2\theta + \varepsilon\sin^4\theta\right] \qquad (15a)$$

$$V_{S1}(\theta\theta = V_{S0}\left[1 + \left(\frac{V_{SP}}{V_{S0}}\right)^2(\varepsilon - \delta)\sin^2\theta\cos^2\theta\right] \qquad (15b)$$

$$V_{S2}(\theta) = V_{S0}\left[1 + \gamma\sin^2\theta\right] \qquad (15c)$$

which is consistent with Wu and Lees' result, equation (7) above, and are Thomsen's equations for weak polar anisotropy. However, we continue with equations 8a, 8b, and 8c above, and follow Berryman. This arrives at the following (eqs. 18, 19 and 24; Berryman, 2008):

Geometric Parameters

Two angles are necessary to solve for the orientation of pole of the anisotropic plane relative to the geologic reference frame (usually oriented parallel to the earth's surface). We solve for the pole of symmetry, relative to the reference frame, by solving for two Euler angles Ψ and Φ. Figure 1 shows the reference frame in blue and the anisotropic orientation in red.

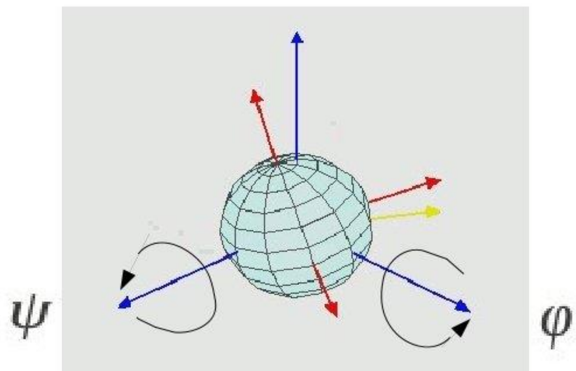

Figure 1. Orientation of the anisotropic plane (red) and the reference frame (blue).

Further, including the problem of locating the earthquakes, each earthquake adds four parameters to solve for: 3D location and origin time.

Tomography

Here we describe the steps performed by SimuDD to execute double difference anisotropic tomography, and the theory. We modified SimulPS (Thurber, 1984) to perform double difference tomography for earthquake location and anisotropic velocity structure. In SimiulDD, instead of finding events located close to one another, and eliminating a term in the travel time equation by assuming they travel the same path (Zhang, 2003), we identified events that had overlapping rays to the same station, "common rays" (Figure 4).

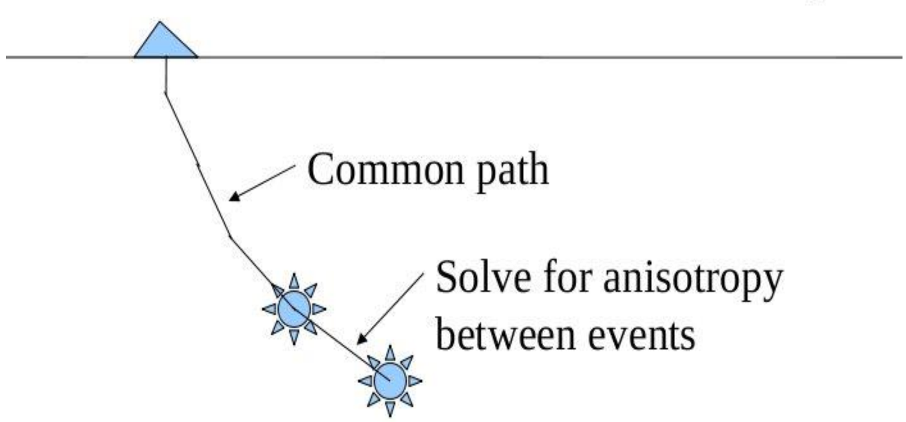

Figure 4. Overlapping ray paths to the station.

So, with the usual arrival time equation:

$$T_k^{i\_obs} = \tau^i + \int uds \tag{16}$$

where T_k^i is arrival time to station k from event i, τ^i is origin time of event i, and the remaining term is the travel time, which is dependent upon the velocity of travel and the location of the earthquake. Following the usual linearization of this highly non-linear relationship:

$$r_k^i = T_k^{i\_obs} - T_k^{i\_cal} = \sum \frac{\delta T_k^{i\_cal}}{\delta x_l} \Delta x_l + \Delta\tau^i + \int \epsilon \, \mathrm{ds} \tag{17}$$

where, Δx_l are changes in model parameters that include the velocity model and earthquake location, and $\Delta\tau^i$ is the change in origin time, and the last term is the error along the travel path due to not knowing the velocity model or the earthquake location precisely and higher order Taylor series values. This is the classic form for linearized inversion, GM = d, and the solution is well described in many any texts, i.e. Menke (2010). Following Waldhausr and Ellsworth (2000), the classic double difference equation is written as:

$$(T_k^i - T_k^j)^{\mathrm{obs}} - (T_k^i - T_k^j)^{\mathrm{cal}} = \sum \frac{\delta T_k^{i\_cal}}{\delta x_l} \Delta x_l + \Delta\tau^i - \sum \frac{\delta T_k^{j\_cal}}{\delta x_l} \Delta x_l - \Delta\tau^j - \int \epsilon \, ds \tag{18}$$

where terms are described in Waldhausr and Ellsworth (2000). In our application we make the second event along the path to a common station a temporary station , so the integral over the path in the last term is from event i to event j, where the paths don't overlap. The arrival time of station k is equal to the origin time estimate of event i plus the relative travel times of the two events events to the actual station. However, since event j is now a station, T_k^j is equal to zero, and:

$$r_m^i = \sum \frac{\delta T_k^{i\_cal}}{\delta x_l} \Delta x_l + \Delta\tau^i + \int \epsilon \, ds \tag{19}$$

where, r_k^j is zero, since there is no travel path between event j and the new station m, and the origin time and travel time are zero from event j to the station at the same location. This is the form of the solution in equation 7. Here we use relative travel time instead of absolute travel time. The temporary station is only for this event pair and is imposed only for the one iteration. After each iteration new pairs are identified and new temporary stations are established. Parameter separation, where the event location step is used to fill in the G matrix in the inversion along with the model parameters to provide the equivalent of a simultaneous inversion (Thurber, 186). In the solution described here, the arrival time of the temporary station is estimated, and updated after each iteration. If events are close enough to fulfill a quarter wavelength criteria for waveform similarity, then cross-correlation is used to refine the relative travel-times between events.

For the double difference tomography system, since the path anomaly biases between event pairs are taken

Then:

$$d_k^{ij} \equiv r_k^i - r_k^j = \sum \frac{\delta T_k^i}{\delta x_l^i} \Delta x_l^i - \sum \frac{\delta T_k^j}{\delta x_l^j} \Delta x_l^j + \Delta\tau^i - \Delta\tau^j +$$

$$\sum \sum \frac{\delta T_k^i}{\delta x_{mn}} \Delta x_{mn} - \sum \sum \frac{\delta T_k^j}{\delta x_{mn}} \Delta x_{mn}$$

$$= \sum \frac{\delta T_k^i}{\delta x_l^i} \Delta x_l^i - \sum \frac{\delta T_k^j}{\delta x_l^j} \Delta x_l^j + (\Delta\tau^i - \Delta\tau^j) + \sum_{m=1}^{M} \sum_n \frac{\delta T_k^i - \delta T_k^j}{\delta x_{mn}} \Delta x_{mn}$$

$$d_k^{ij} = \sum \frac{\delta T_k^i}{\delta x_l^i} \Delta x_l^i - \sum \frac{\delta T_k^j}{\delta x_l^j} \Delta x_l^j + \sum_{m=1}^{M'} \sum_n \frac{\delta T_k^{ij}}{\delta x_{mn}} \Delta x_{mn} \qquad (20)$$

where $\delta T_k^{ij} \equiv \delta T_k^i - \delta T_k^j$ in the final term is the travel time *difference* at station *k* from events *i* and *j*. T_k^{ij} Because the travel path, from both events *i* and *j* to station *k* is shared over most of the path, the difference in travel time within this section of the path is zero, so the sum only covers those *M'* voxels between the two events.

Note that, although d_k^{ij} is the double difference, we solve for the absolute locations of the two events separately. The solution for origin time difference $(\Delta\tau^i - \Delta\tau^j)$ is lost as this difference is set to zero, without significant loss of generality.

For equation (20), the input data is the difference in travel time between events, based on the "picks" of P- and S-wave arrivals. Cross-correlation is a convenient way to improve on the observed travel time difference between events. If the seismograms are aligned by the pick" of the P- or S-wave, then the phase shift identified by cross-correlation provides an improvement to the difference in travel times.

One inversion approach, is to follow equations (15, 16) to get the absolute location of events and initial material parameters, then follow equation (20) to get refined locations and material values between events. These are then held fixed, and the inversion for equation (15, 16) is performed again, then equation (20) again, ect. until conversion for minimum residuals dr_k^{ji} is met. With the locations held fixed, we need a combination of at least seven such pairs with seven stations to solve for the anisotropic parameters in a voxel. This however, separates the simultaneous inversion from the localized isotropic inversion. Further, it is difficult to find enough pairs to get isotropic parameters for a particular voxel

In our inversion approach we solve for earthquake locations, and anisotropic parameters for the whole volume and localized voxels simultaneously. Specifically, we:

(1)perform inversion as shown in equations (15, 16) to get initial earthquake locations and anisotropic parameters; then

(2)identify events and stations that have the geometry that is shown in Figure 2, and obtain the relative travel-time between them;

(3)designate one of the events (closest to the recording station) to be fixed and change it to a "station". This "station" is added to the list of stations for that event.

(4)rerun the inversion with equations (15,16), etc. until convergence.

Accuracy and Resolution

Accuracy and resolution are complimentary properties necessary to interpret the results of earthquake location and tomography studies. We utilize synthetic data to evaluate the relationship between the number of "recording stations and earthquakes" and "accuracy and resolution" (A&R) in our 3D tomography study. Accuracy is the how close an answer is to the "real world". For earthquake locations, we compare our locutions to known synthetic locations. Earthquake location resolution is often expressed as 95% confidence ellipses, where resolution is how small of confidence ellipse one can achieve. In tomography, we similarly test how close tomographic images are to "actual" geology, and how small of confidence ellipse can be achieved.

We have modified SimulPS (Thurber, 1986) in several ways to provide a tools for evaluating A & R. First, we calculate synthetic arrival times from synthetic three-dimensional velocity models and earthquake locations. These are the "real" travel times, velocity models and earthquake locations. Then, travel times are perturbed with noise, the velocity model is approximated as a one-dimensional starting model, and hypocenters are randomly moved to replicate a starting location away from the "true" location, and inversion is performed by each program. We establish travel times with the pseudo-bending ray tracer and use the same ray tracer in the inversion codes. This, of course, limits our ability to test the accuracy of the ray tracer. We also consider likely numbers of actual recording as a function of magnitude in the calculations. We consider earthquakes from magnitude from about -1.0 to 3.0.

As a first order estimation of the number of stations and earthquakes needed to achieve reasonable accuracy and resolutions we examine number of nodes sampled and the degrees of freedom for typical tomographic inversion studies. The degree of freedom (DoF) is number of observation values minus the number of parameters solved for. In general, one wants the DoF to be four times the number of parameters solved for; i.e. twice the number of observations as parameters. In simultaneous inversion for velocity structure and earthquake location the number of parameters solved for is four times the number of earthquakes plus the number of velocity nodes solved for and possibly station corrections. The number of observations is the number of P- or S-waves observed. The relation for DoF is described by the equation:

DoF = number of phases recorded * qfac - number of parameters solved (22)

where, the number of phases (P or S) equals the number of earthquakes times the number of stations, and multiplied by a quality factor (*qfac*) that diminishes this number due to noise and magnitude of the earthquake. We recognize that generally there are more P- than S-waves utilized, so there is a better *qfac* for P-waves than S-waves. Here, we are assuming we will solve for both P- and S- wave model parameters, and that 75% of the P-arrivals are usable and 50% of the S-arrivals are usable, due to SNR and interference; so, *qfac* equals 0.75 and 0.50 for P- and S-waves, respectively. It is not reasonable to evaluate resolution separately for P- or S-wave arrivals because both will help in locating the earthquakes. However, since S-waves are able to obtain a higher resolution because of the lower velocity, but lower resolution because of fewer hits, we call it "even", and evaluate them together as the overall resolution of the study. Figure 1 shows a three dimensional plot of the number of stations, number of earthquakes, and node spacing versus the degrees of freedom for the 6 x 6 x 4 km volume discussed above.

The number of "hits" per node for different scenarios of the inversion study. Here, we are assuming we will solve for both P- and S- wave model parameters, and that 75% of the P-arrivals are usable and 50% of the S-arrivals are usable, due to SNR and interference. We also assume a 6 x 6 x 4 km volume and the micro-earthquakes are distributed randomly between 2.0 and 3.5 km deep within the volume. A node represents a cube volume around the node. Hits per node might be described by:

“hits”/node = (3.5/node-spacing) * (earthquakes) * (stations) * qfac / nodes (2)

where, we are assuming a 3.5 km average ray path, so the first term represents an average of nodes passed through in travel to a station for a particular node spacing. Figure 2 shows hits as a function of node spacing. We are assuming 10 hits per node for high resolution.

Ray Tracers

We utilize the ray tracer Program ANRAY (Psencik, 2009). it is an updated version of program with the same name which has been used in packages ANRAY86 and ANRAY89 written by Gajewski & Psencik [1], [2]. It is designed for ray, travel time and ray amplitude computations. Two ways of approximation of distribution of elastic parameters are available, In the first, "B-spline approximation", elastic parameters in an arbitrary point of a layer are determined by B-spline approximation from values of parameters specified at grid points of a 3-D rectangular network. B-splines with tension by A.K.Cline [3] with additions by L.Klimes [4], are used. In the second way, "isosurface interpolation", elastic parameters are determined by vertical linear interpolation of values specified at interfaces, which represent surfaces of constant values of elastic parameters. Rays can be computed in two modes. In the first one, rays are specified by the point source location and the initial orientation of the slowness vector at the source: initial-value ray tracing. In the second mode, rays are specified by the point source location and a system of regularly or irregularly distributed receivers situated on surface or on an interface or on a vertical profile: two-point ray tracing. The point source can be situated at any point of the model. Polarization vectors, geometrical spreading and reflection, transmission and conversion coefficients may be evaluated along the rays.

Study Area and Data

We apply our analysis to the Enhanced Geothermal System (EGS) demonstration project at the northwest part of The Geysers, California (Figure 3). We examine a 6 x 6 km lateral and 5 km deep volume. Figure 4 shows this study area and locations of seismic recording station

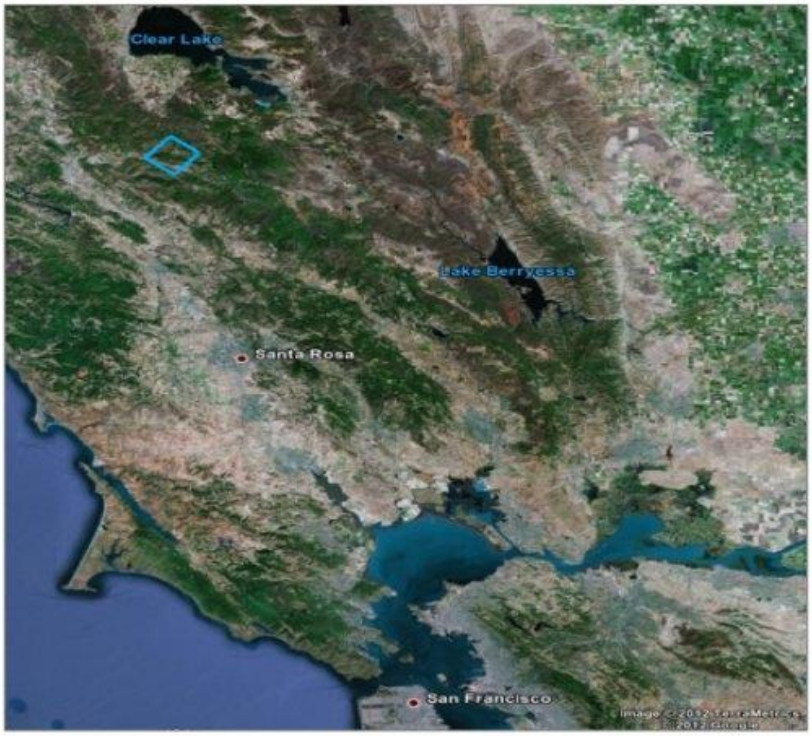

scale |_____| 10 km

Figure 3. The Geysers study area, north of San Francisco, California. Faults are in red.

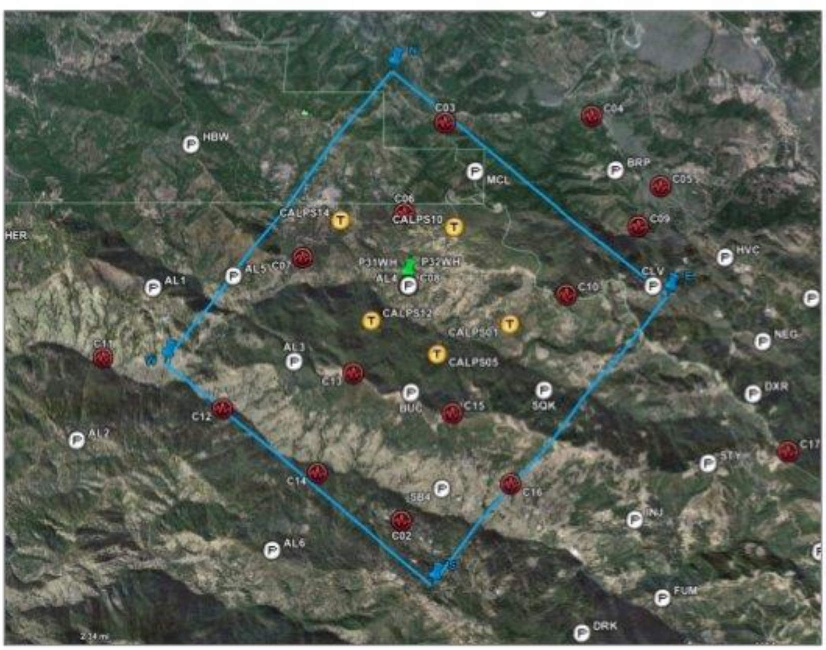

scale |___|___| 2 km

Figure 4. The study area and instrument locations. "white" symbols are permanent LBNL network stations; "yellow" are temporary DOE monitoring sites; and, "red" are supplementary instruments installed by LBNL for the Prati-32 test. Only instruments located within the study area were used for the tomography, except C08 was also used.

The Geysers geothermal field located in the Coastal Ranges, just north of Napa Valley. The region is dominated by the plate boundary motion along the San Andreas Fault (Figure 1). The Geysers is nested between the Southwest-bounding Maacama Fault and the northeast-bounding Collayami Fault, and includes a mixture of strike-slip and thrust faults [McLaughlin, 1981]. The subduction of the Farallon plate beneath the North American plate led to Pliocene-Holocene volcanism, which left enough heat to metamorphose the graywacke of the overlying Franciscan mélange to biotite [Moore and Gunderson, 1995].

The Geysers geothermal reservoir is the world's largest generator of electricity from geothermal energy since 1970. It is a vapor-dominated geothermal reservoir with temperatures reaching 400°C between 2 and 5 km depth, and where significant volumes of waste water are injected in order to fully exploit the resources [Majer et al., 2007]. The reservoir is thought to be created by percolating groundwater through the natively low-permeability Franciscan mélange and along fractures opened due to local faulting, and heated by a large, silicic magma body just north of the steam field [Stimac et al., 1992]. The Geysers was historically fluid-dominated [Sternfeld, 1989; Moore and Gunderson, 1995], but increased fracture volume due to crustal extension has been implicated in the formation and sustained presence of the vapor-dominated conditions that exist today [Allis and Shook, 1999]. A number of steam production wells were drilled into the northwest Geysers in the 1980's, but later abandoned because of uneconomically low natural steam production as well as problems with corrosive non-condensable gases (NCG).

References

Aki, Keitti and Paul G. Richards (2009) Quantative Seismology. Second edition, University Science Books.

Zhang, Haijiang (2003) Double-difference seismic tomography method and its applications. dissertation submitted in partial fulfillment of the requirements for the degree of Doctor of Philosophy(Geophysics), University of Wisconsin-Madison.

Berryman, James G. (2008) Exact Seismic Velocities fro Transverseley Isotropoic Media and Extended Thomsens Formulas fo rStronger Anisotropies. Geophysics, 73, D1-D10.

Cerveny, V. (1972) Seismic Rays and Ray Intensities in Inhomogeneous Anistropic Media. Geophy. J. R. Astro. Soc., 29,1-13.

Chapman, C. H. and R.G. Pratt (1992) Traveltime Tomography in Anistropic Media—I. Theory (1992) *Geophys J Int*, 109, 1-19.

Chapman, C. H. and W. S. Leaney (2012) A New Moment-tensor Decomposition for Seismic Events in Anisotropic Media. *Geophys J Int*, 188, 343-370.

Crampin, S., 1993. A review of the effects of crack geometry on wave propagation through aligned cracks, Can. *J. Expl. Geophys.*, 29, 3–17.

Crampin, S. & Booth, D.C., 1989. Shear-wave splitting showing hydraulic dilation of pre-existing joints in granite, Scientific Drilling, 1, 21–26.

Crampin, S. & Zatsepin, S.V 1995. A new understanding of shear-wave splitting, in EAGE 57th Conference and Technical Exhibition abstract, Glasgow, Scotland, 29 May–2 June.

Elkibbi, Maya, Ming Yang and J. A. Rial (2005) Crack-induced anisotropy models in The Geysers geothermal field. Geophys J Int 162, 1036–1048.

Hulen, J.B. & Nielson, D.L., 1996. The Geysers coring project, in Reseach Summaries-Reservoir Technology, US Department of Energy.

Lou, Min and Jose Rial (1997) Characterization of geothermal reservoir crack patterns using shear-wave splitting. Geophysics, 62, 487-494.

Nielson, D.L. & Nash, G.D., 1997. Structural fabric of The Geysers, Transactions, Geothermal Resources Council, 21, 643–649.

Psencik, Ivan (2009) Program package ANRAY, version 4.61. Institute of Geophysics, Acad.Sci. of the Czech Rep., Bocni II, 141 31 Praha 4, Czech Republic.

Stewart, R.R. (1988) An Algebraic Reconstruction Technique for Weakly Anisotropic Velocity (1988) *Geophysics*, **53**, 1613-1615.

Tsvankin, I. (2001) Seismic Signatures and Analysis of Reflection Data in Anisotropic Media. Handbook of Geophysical Exploration, Seismic Exploration, Vol. 29, editors: Klaus Helbig and Stven Treitel. Institute of Geophysics, Acad.Sci. of the Czech Rep.,Bocni II, 141 31 Praha 4, Czech Republic.

Thomsen, Leon (2002) Understanding Seismic Anisotropy in Exploration and Exploitation. Distinguished Instructor Short Course, Series No. 5, Society of Exploration Geophysicists & Engineers.

Waldhauser, F. and W. L. Ellsworth (2000) A double-difference earthquake location algorithm: method an application to the northern Hayward Fault, California, Bull. Seism. Soc. Am., 80, 1548-1368, 2000.

Wu, Huatao and Jonathan M. Lees (1999) Cartesian parameterization of anisotropic traveltime tomography. Geophys J Int, **137**,64-80.

Appendix 6-1- Abstract for Maity (2013) Dissertation

Integrated reservoir characterization for unconventional reservoirs using seismic, microseismic and well log data

This study is aimed at an improved understanding of unconventional reservoirs which include tight reservoirs (such as shale oil and gas plays), geothermal developments, etc. We provide a framework for improved fracture zone identification and mapping of the subsurface for a geothermal system by integrating data from different sources. The proposed ideas and methods were tested primarily on data obtained from North Brawley geothermal field and the Geysers geothermal field apart from synthetic datasets which were used to test new algorithms before actual application on the real datasets. The study has resulted in novel or improved algorithms for use at specific stages of data acquisition and analysis including improved phase detection technique for passive seismic (and teleseismic) data as well as optimization of passive seismic surveys for best possible processing results. The proposed workflow makes use of novel integration methods as a means of making best use of the available geophysical data for fracture characterization. The methodology incorporates soft computing tools such as hybrid neural networks (neuro-evolutionary algorithms) as well as geostatistical simulation techniques to improve the property estimates as well as overall characterization efficacy. The basic elements of the proposed characterization workflow involves using seismic and microseismic data to characterize structural and geomechanical features within the subsurface. We use passive seismic data to model geomechanical properties which are combined with other properties evaluated from seismic and well logs to derive both qualitative and quantitative fracture zone identifiers. The study has resulted in a broad framework highlighting a new technique for utilizing geophysical data (seismic and microseismic) for unconventional reservoir characterization. It provides an opportunity to optimally develop the resources in question by incorporating data from different sources and using their temporal and spatial variability as a means to better understand the reservoir behavior. As part of this study, we have developed the following elements which are discussed in the subsequent chapters: 1. An integrated characterization framework for unconventional settings with adaptable workflows for all stages of data processing, interpretation and analysis. 2. A novel autopicking workflow for noisy passive seismic data used for improved accuracy in event picking as well as for improved velocity model building. 3. Improved passive seismic survey design optimization framework for better data collection and improved property estimation. 4. Extensive post-stack seismic attribute studies incorporating robust schemes applicable in complex reservoir settings. 5. Uncertainty quantification and analysis to better quantify property estimates over and above the qualitative interpretations made and to validate observations independently with quantified uncertainties to prevent erroneous interpretations. 6. Property mapping from microseismic data including stress and anisotropic weakness estimates for integrated reservoir characterization and analysis. 7. Integration of results (seismic, microseismic and well logs) from analysis of individual data sets for integrated interpretation using predefined integration framework and soft computing tools.

Appendix 6-2- Abstract of Tafti (2013) Dissertation

Integrated Workflow For Characterizing and Modeling Fracture Network in Unconventional Reservoirs Using Microseismic Data

We develop a new method for integrating information and data from different sources. We also construct a comprehensive workflow for characterizing and modeling a fracture network in unconventional reservoirs, using microseismic data. The methodology is based on combination of several mathematical and artificial intelligent techniques, including geostatistics, fractal analysis, fuzzy logic, and neural networks. The study contributes to scholarly knowledge base on the characterization and modeling fractured reservoirs in several ways; including a versatile workflow with a novel objective functions.

Some the characteristics of the methods are listed below:

1. The new method is an effective fracture characterization procedure estimates different fracture properties. Unlike the existing methods, the new approach is not dependent on the location of events. It is able to integrate all multi-scaled and diverse fracture information from different methodologies.

2. It offers an improved procedure to create compressional and shear velocity models as a preamble for delineating anomalies and map structures of interest and to correlate velocity anomalies with fracture swarms and other reservoir properties of interest.

3. It offers an effective way to obtain the fractal dimension of microseismic events and identify the pattern complexity, connectivity, and mechanism of the created fracture network.

4. It offers an innovative method for monitoring the fracture movement in different stages of stimulation that can be used to optimize the process.

5. Our newly developed MDFN approach allows to create a discrete fracture network model using only microseismic data with potential cost reduction. It also imposes fractal dimension as a constraint on other fracture modeling approaches, which increases the visual similarity between the modeled networks and the real network over the simulated volume.

Appendix 8-1- 2011 Geothermal Technologies Peer Review

U.S. DEPARTMENT OF ENERGY | Energy Efficiency & Renewable Energy

Reviewer Comments and Principal Investigator Responses

Review: 2012 Geothermal Technologies Program Peer Review
ID: EE0002747
Project: Characterizing Fractures in Geysers Geothermal Field by Micro-seismic Data, Using Soft Computing, Fractals, and Shear Wave Anisotropy
Principal Investigator: Aminzadeh, Dr. Fred
Organization: University of Southern California
Panel: Seismicity, Fluid Imaging & Reservoir Fracture Characterization

RELEVANCE/IMPACT OF RESEARCH

Reviewer 23471

Score: 3.0

Comment: This project is relevant to GTP goals in that it can map the distribution of seismic anisotropy at depth (a potential indicator of fracture alignment) and facilitates time-dependent mapping of hypocenters for defining structures and seismic tomography for defining variations in fluid pressure/saturation at depth. However, the presentation contained numerous physical interpretations/conclusions that were poorly justified, as noted below. Thus, more attention needs to be paid to model validation and the physics on which these interpretations are based in order for these results to have the desired impact on GTP goals.

PI Response:

Three independently derived indicators are used to validate the model of fracture network and its propagatation into the high temperature zone. Those include fractal dimension of 2.6 for microseismic distribution which is the same as the nucleation and growth of fractures in random media, significant movement of microseismic fuzzy clusters in high temperature zone and correlation between velocity anomalies with this movement Cross validation of these phenomena would give us a high level of confidence of the ture fracture network model and the areas with higher densities. Also results have been cross validated with other authors like Elikibbi about fracture density.

Reviewer 23583

Score: 3.0

Comment: The goal of this project is to develop better understanding of the mechanisms for the stimulation of existing fractures in the northwest portion of the Geysers field. If the project's goals are achieved, notable progress and impact toward accomplishing GTP's broad EGS mission "...to improve performance, reduce cost, and facilitate technology validation and deployment…" will be realized. A better understanding of mechanisms to activate existing fractures at The Geysers will notably reduce EGS hydraulic fracturing knowledge gaps and further the deployment of permeability-enhancement technologies in general. This project's goals, as stated, will definitely improve understanding of how to lower current EGS reservoir creation technology barriers (reduce costs and boost performance) by providing a better understanding of the mechanisms for fracture activation.

PI Response:

agree

Reviewer 23412

Score: 2.0

Comment: It has been the intent of operators at The Geysers of use the MEQ data to define structure and connection to injection and production activities. The project results graphics vaguely made any conclusion. The most important part of the project was the Auto picker algorithm and is a deliverable.

PI Response:

With the specific limits of slides, it is our best to present most out of our accomplishment. In our future publications at GRC, and AGU we will issue your concern. The autopicker development has progressed substantially with studies on fuzzy segmentation and neuro-fuzzy autopicker implementation under progress.

Reviewer 23641

Score: 3.0

Comment: Relevant research in MEQ approaches to characterize fractures. Several useful outcomes with near term application to MEQ fracture characterization including auto picker, fractal analysis, time lapse velocity tomography, anisotropy mapping.

PI Response:

Thanks

SCIENTIFIC/TECHNICAL APPROACH

Reviewer 23471

Score: 2.0

Comment: This project employs a clever phase picking algorithm, which is then used for improved earthquake locations and to produce maps of P- and S-wave velocities as a function of time, with mapping out of shear wave splitting/anisotropy a work in progress. Other than this, the interpretations of b values, fractal dimension, and stress regime indicators were presented without sufficient physical explanation or justification, and were unconvincing. What, for example, is the physical basis by which one can infer hydrostatic and extensional stresses from P- and S-wave velocities alone? Also, b values ranging from 1.1 to 1.4 were cited by the speaker as evidence that these earthquakes were induced, yet no discussion was presented on key issues widely recognized to be important in b-value analyses, such as magnitude of completeness and the related issue of variation in b values with earthquake magnitude range. Finally, the fractal dimension in and of itself has little physical significance, and in future work I encourage these investigators to explicitly relate fractal dimension to more meaningful parameters related to the fracture population or earthquake frequency-magnitude relations.

PI Response:

We have posted our results and all physical meaning of b-values and Fractal Analysis into our last year annual report to DOE which is avalilable to the public. With the limited slides we were not able to cover all of them. We have also cover most of b- value and fractal part in our previous presentations.

Reviewer 23583

Score: 2.0

Comment: The scientific/technical approach consists of several tasks to better exploit MEQ data at The Geysers: develop a new autopicker using hybrid neuro-fuzzy logic techniques, map fractal structure of network using induced seismicity, develop a Kriged velocity model to observe time-dependence of fracture network and infer stress and rock properties from tomographic inversion results and, finally, verify and fine-tune velocity anomaly maps using anisotropy mapping and fractal results.

This scientific/technical approach is a little disjointed. Why develop a new autopicker? There are many out in the literature, devising a new one for this project was not justified when the goal was to understand fractures. Also, analysis of data to support claims made about its capabilities being better were not offered. Motivation to perform fractal analysis and correlate with b values at The Geysers was not discussed not easy to infer from the materials presented. Determining whether or not the seismicity was triggered versus induced is important but the background for such a statement was not revealed; does 2.6 D really mean induced? What about 2.5D? Finally, Kriged, time-dependent velocity models and inferred rock properties and stresses are important but very little discussion of how the tomography was accomplished and very little interpretive discussion on what the results might mean.

Key technical barriers to achieving the project's objectives such as better descriptions of fracture activation mechanisms were not presented in any detail necessary for evaluation. All in all, there are significant weaknesses and noteworthy areas for improvement in the design of the approach as presented. It is hard to judge the scientific rigor employed in the analyses presented when very little information is provided to evaluate the claims made, furthermore, verification and validation results were not presented, so the overall sense of the presentation did not build confidence in the conclusions. The R&D research plan is not as well thought-out as it could be, the description of, and logical connections between, these different analyses to the overall goal of the project is missing in the presentation, certainly in the interpretation of the results. The project, as presented, will contribute to progress in overcoming stimulation barriers/knowledge gaps.

PI Response:

The development of a new autopicker was considered vital in getting the best possible inversion results. This was to minimize the error that propagates (as a result of picking errors) into subsequent processing steps. The use of the new autopicking algorithm has shown substantial improvements in results, particularly for noisy datasets. The Fractal value is not exact. 2.5 or 2.6 is not make difference about induced sesimicity. Although we comparing the value of 2 with these numbers which is significantly lower. The background of this statement has beed revealed in our last year annual report and our publication at GRC. Tomography part has not been done internally by USC people, we only use velocity models generated by LBNL scientist in our innovative workflow and show how to use these valuale data. The full interperation of velocity models have been published in three different conference paper and will be available in our final report to DOE. with limited slides and time of presentation, we can not fully include our result and interpretation.

Reviewer 23412

Score: 2.0

Comment: After the auto picker development the project should have been considered complete.

PI Response:

Agree

Reviewer 23641

Score: 4.0

Comment: Impressive scientific/technical approach that has yielded useful advances in MEQ fracture characterization as well as techniques (autopicking) to facilitate and lower cost of this type of work.

PI Response:

Thanks

ACCOMPLISHMENTS, RESULTS, AND PROGRESS

Reviewer 23471

Score: 1.0

Comment: The project has made reasonable progress in achieving its stated goals, with phase-arrival autopicker and fractal/b-value analyses already completed. Anisotropy mapping and time-lapse velocity tomography are in progress and are to be completed later this year. The velocity tomography results presented for The Geysers are promising, and appear to show low velocities associated with injection of cold fluids (although I could not tell which velocities, P or S, since the figures were not labeled). However, the physical interpretation of many of the other results presented was questionable, as noted elsewhere in this review, and was presented in a black box fashion, with little obvious attention paid to statistical uncertainties, uniqueness of interpretation, or the physics of the processes being addressed. Unfortunately, two of the papers listed in the Publications and Presentations section of the report are submitted for publication, and the other products consist of titles or abstracts only. Thus, it was not possible for me to investigate further the scientific quality of the work that has been performed under this contract to date (all I could find to look at was a very short AGU abstract written in 2010, which was not very helpful).

PI Response:

We included all of our b-vlaue and fracal result in our last year DOE annual report. We will also publish our result on velocity tomography in GRC this year which the full paper will be availbe online. We have different convinving logic behind our interpretation of velocity models which will be presented in our next year report as well as one of USC student PhD thesis.

Reviewer 23583

Score: 3.0

Comment: As stated in the presentation and summary, the project accomplishments include: a new, validated neural network first arrival auto-picker for MEQ data using a neuro-fuzzy approach, confirmed the induced nature of seismicity at the Geysers field from the b values and the fractal dimensions of MEQ's, based on LBNL velocity inversions developed Kriged velocity, stress, and rock property fields and analyzed the changes with time to establish the impact of high temperature fluid movement in the rocks on the velocity field.

The accomplishments as presented are minor when compared to addressing the goal of the project, and, in summary, do not justify the claims made concerning progress. For example, in future directions work planned slide 14; many of the tasks proposed do not address the goal of the project. They might be interesting things to do, but do not shed light on the fracture mechanisms at The Geysers. Furthermore, the quality and significance of the technical accomplishments and results are not equal to the resources expended and technical progress towards project objectives—there is significant room for improvement. In addition, the productivity in work underway and future work, and the value of the accomplishments compared to the schedule and costs, reveals that much more progress needs to be made.

PI Response:

Reviewer 23412

Score: 3.0

Comment: With the development of the auto picker completed, the project has accomplished a deliverable.

PI Response:

Agree

Reviewer 23641

Score: 4.0

Comment: Impressive results in several areas with useful accomplishments ranging from practical aid (autopicker) to new imaging apporach (time lapse velocity changes).

PI Response:

Thanks

PROJECT MANAGEMENT/COORDINATION

Reviewer 23471

Score: 4.0

Comment: This project appears to be well managed and is proceeding according to schedule. This project is also very inexpensive for DOE, and yet is receiving matching funds from USC, LBNL and Calpine. Partnerships are listed as having been established between the lead investigators at University of Southern California (USC), Calpine and LBNL. However, it was hard for me to figure out what other members of the partnership were doing scientifically, since the four publications/talks listed had the same first three authors, all of whom are at USC and only one non-USC person is listed on any of the pubs/talks. Given the low cost of this project, I do not consider this to be a real concern, but something that should be clarified in future presentations.

PI Response:

Reviewer 23583

Score: 2.0

Comment: The PI claims the project is on budget, scope and schedule. However, if only 15% of the budget is left and many of the analyses are not completed (see the future work list) then it looks like the project is over spent to the scope. Considerable time and effort has been made but project goals have not been reached. Prospective future plans are of adequate quality and may be effective in meeting the project's goals but so much work for 15% of the budget.

The inclusion of appropriate and logically placed decision points that effect the future direction of the work were discussed but only briefly and the PI claims coordination of activities with collaborators and stakeholders is very effective. Better management practices are desirable in getting the project on to the original overall goal as well as speed-up the productivity.

PI Response:

Reviewer 23412

Score: 3.0

Comment: The completion of the auto picker has been the goal of this project.

PI Response:

Agree

Reviewer 23641

Score: 3.0

Comment: Results are indicative of a well managed project.

PI Response:

Thanks

STRENGTHS

Reviewer 23471

Comment: The earthquake location algorithm results are interesting and show some promise for identifying time-variations in P- and S-wave velocities and shear-wave anisotropy within The Geysers geothermal field, as well as defining the seismogenic structures at depth.

PI Response:

The final project deliverables include improved understanding of the fracturing as well as a better understanding of the flow pathways and their time - variant devalopment. Results involving fracture zone identification and integrated analysis involving shear wave splitting studies provide promising results. Some results will be shared at the GRC annual meeting this year.

Reviewer 23583

Comment: As envisioned, this project will definitely improve understanding of how to lower current EGS reservoir creation technology barriers (reduce costs and boost performance) by providing modeling tools to accelerate EGS implementation. The scientific/technical approach consists of several tasks to better exploit MEQ data to better understand fracture mechanisms at The Geysers. As stated in the presentation and summary, there have been several project accomplishments such as: a new auto-picker for MEQ data, and time-dependent, Kriged velocity, stress, and rock property maps.

PI Response:

Thanks

Reviewer 23412

Comment: The strength of this project is that it has finished the auto picker.

PI Response:

Work on a more complex hybrid autopicker using a neuro-fuzzy approach is still in progress.

Reviewer 23641

Comment: Mix of practical tools and approaches with bigger picture, more speculative technique development.

PI Response:

Thanks

WEAKNESSES

Reviewer 23471

Comment: The physical significance of several of the interpretations presented is unclear, especially the claim that b values determined at The Geysers were indicative of an induced origin for the seismicity and that P- and S-wave velocities could be used to infer attributes of the in-situ stress state (i.e., extensional vs hydrostatic stress). The b-values fell in the recognized range of values observed for tectonic events elsewhere, with no discussion of statistical uncertainties or variation in b value with earthquake magnitude range. Also, the stress interpretations based on seismic velocities were poorly justified, and should have been validated against more widely recognized means for inferring the in-situ stress state, such as earthquake focal mechanisms.

PI Response:

We have posted our results and all physical meaning, Interpretation of b-values and Fractal Analysis into our last year annual report to DOE which is avalilable to the public. The stress and velocity models has been cross validated with other phenamena like shear wave splitting and fuzzy clustering.

Reviewer 23583

Comment: This scientific/technical approach is a little disjointed. There was no discussion of how the tomography was accomplished and little interpretive discussion on what the rock properties maps might mean with regards to fracture mechanisms. The accomplishments as presented are minor when compared to addressing the goal of the project, and, in summary, do not justify the claims made concerning progress. The project has had minor achievements compared to project goals and considering resources expended.

PI Response:

Tomography part has not been done internally by USC people, we only use velocity models generated by LBNL scientist in our innovative workflow and show how use these valuale data.

Reviewer 23412

Comment: The weakness of this project is the other interpretation of MEQ.

PI Response:

Reviewer 23641

Comment: None.

PI Response:

IMPROVEMENTS

Reviewer 23471

Comment: Reviewer did not provide comments for this criterion.

PI Response:

Reviewer 23583

Comment: Better management practices are desirable in getting the project on to the original overall goal as well as speed-up the productivity. Interpretation of results with regard to fracture mechanisms is needed.

PI Response:

Reviewer 23412

Comment: The improvement to this project is that it is complete.

PI Response:

Reviewer 23641

Comment: None

PI Response:

Appendix 8-2- External Publications

- Fred Aminzadeh, Debotyam Maity, and Tayeb A. Tafti, 2013, An integrated methodology for sub-surface fracture characterization using microseismic data: A case study at the NW Geysers , Computer and Geosciences 54, 39-49.
- Tayeb A. Tafti, Muhammad Sahimi, Fred Aminzadeh, and Charles G. Sammis, 2012, Using Microseismicity to Map the Fractal Structure of the Fracture Network at The Geysers Geothermal Field in California, Bull. Seism. Soc. Am., submitted for publication.
- Tayeb A. Tafti and Fred Aminzadeh, 2011, Application of high-resolution passive seismic tomographic inversion and estimating reservoir properties, AGU Fall Meeting, San Francisco, CA
- Tayeb A. Tafti and Fred Aminzadeh, 2011, Fracture characterization at the geysers geothermal field using time lapse velocity modeling, fractal analysis and microseismic monitoring, Geothermal Resources Council Transactions, Vol. 35, pp. 547-551.
- Fred Aminzadeh, Debotyam Maity, Tayeb A. Tafti, and Friso Brouwer, 2011, Artificial neural network based autopicker for micro-earthquake data, In: SEG Annual Meeting. pp. 1623-1626. Link: http://library.seg.org/doi/pdf/10.1190/1.3627514.

Our Geysers papers include:

- Characterizing Fractures in Geysers Geothermal Field by Micro-seismic Data Using Soft Computing, Fractals, and Shear Wave Anisotropy
- Characterizing Fractures in Geysers Geothermal Field using Soft Computing
- Analysis of Microseimisicty using Fuzzy Logic and Fractals for Fracture Network Characterization
- Integrated Workflow for Characterizing Fracture Network in Unconventional Reservoirs using Microseismic Data
- Characterizing Fractures in the Geysers Geothermal Field by Micro-seismic Data, Using Soft Computing, Fractals, and Shear Wave Anisotropy
- Artificial Neural Network based Autopicker for Microearthquake Data
- Reservoir Characterization of an Unconventional Reservoir by Integrating Microseismic, Seismic, and Well Log Data
- Framework for Time Lapse Fracture Characterization using Seismic, Microseismic & Well Log data
- Fracture Network Interpretation Through High Resolution Velocity Models: Application to the Geysers Geothermal Field

- Use of Microseismicity for Determining the Structure of the Fracture Network of Large-Scale Porous Media
- Integrated Reservoir Characterization for Unconventional Reservoirs using Seismic, Microseismic and Well Log Data
- Integrated Fracture Characterization And Associated Error Evaluation Using Geophysical Data For Unconventional Reservoirs
- Fracture Characterization in Unconventional Reservoirs Using Active and Passive Seismic Data With Uncertainty Analysis Through Geostatistical Simulation
- Dynamic Characterization of Fracture Network Using Seismic, Microseismic & Well Log Data
- An Integrated Methodology for Sub-Surface Fracture Characterization using Microseismic data: A Case Study at the NW Geysers
- A New Approach Towards Optimized Passive Seismic Survey Design With Simultaneous Borehole And Surface Measurements
- A Geomechanical Approach for Microseismic Fracture Mapping

Link: **http://digitallibrary.usc.edu/cdm/ref/collection/p15799coll3/id/294857**